MPHIL

Validation and Improvement of Current Automotive Cooling Systems

Mitra, Pratoy

Award date:
2022

Awarding institution:
University of Bath

MPhil Thesis (corrected)
Validation and Improvement of Current Automotive Cooling System: Steady-State and Transient Analysis

Pratoy Mitra
Student Number: 189470478

Supervisors:
Professor Sam Akehurst
Dr Andrew Lewis

Department of Mechanical Engineering, University of Bath
Bath, United Kingdom

October 2022

Copyright Notice

Table of Contents

Abstract

Current research in the field of automotive thermal heat rejection systems is limited. The advancements in high-performance vehicles and electrification fields haven't been considered yet, and studies carried out for aggressive testing conditions are limited. Less than half of the studies reviewed throughout the course of this research tested under high-performance and aggressive testing. Many of these studies were for niche applications such as in-cycle radiators or finned-tube evaporators. Therefore, there is a need to test heat the ejection of automotive radiators under high-performance systems. This would not only improve the thermal heat rejection systems' efficiency but also indirectly improve emissions.

A modular and mobile rig with a length of 7-8m was constructed (depending on the test case). The heat rejection and airside pressure loss were then measured by changing the flow rate from 30-180lpm and airflow velocity from 2-10m/s. These graphs were then plotted, and delta HR plots (comparing two different cases) were then analysed for 14 other cases with varying angles, fan configurations and blockages.

The LTR was modelled using the ε-NTU method to provide a base for further testing. Due to limitations in data, an NTU of 3 was assumed, which correctly predicted the heat rejection within a 4% margin. For the HTR case, the air velocity significantly affected the heat rejection, whilst the coolant flow rate effect was much smaller. Higher coolant flow rates showed that the heat rejection was 19% higher for an air velocity of 2m/s when comparing the 180lpm case to the 30lpm case. However, this was 76% higher for the 10m/s case. The average heat rejection at 180lpm only showed an overall improvement of 51% over that of the 30lpm case. This is possibly due to the radiator's sizeable effective surface area, which enhances the heat rejection rate.

Fan operation generally improved the heat rejection; however, a fan did not show much change at 8m/s and 10m/s when the fan at 13.6V and fan at 0V cases were compared for the 90° case. This could imply that the fan acted as a blockage for air velocities of over 6m/s.

Although angled configurations of 15° and 25° showed slight improvements in heat performance, the 35° case showed an improvement of about 14kW for air velocities of the 8m/s and 10m/s cases. A possible reason for the enhancement of heat rejection in only the 35° case would be the additional direct convection caused by the inner geometry of the radiator, which would be the louvres in this case.

When the 1m blockage, 13.6V case, was compared with the baseline case, it was found that the average heat rejection for 180lpm was 15.4kW more than that of the baseline case. The same averaged heat rejection was more than 15kW(for 180lpm) for the 1m blockages, with no fan case compared to the baseline case. The effects of the fan were pronounced for the 10m/s air velocity case, as a fan showed an average increase of 4.5kW in heat rejection. The same heat rejection for a 0.5m blockage was 14.1kW without a fan at 180lpm and 16.4kW with a 13.6V fan. Hence, a 1m blockage without a fan provided better heat rejection (by 0.4kW at the highest point). However, with a 13.6V fan, this changed as 0.5m blockage showed better heat rejection (by 1.5kW at the highest point) with the fan on compared to the 1m blockage case.

For the angular 35° case, the airflow was accelerated over a smaller area, and the adverse effects of the blockage were more pronounced, while the 35°, 1m blockage case saw a heat

rejection decrease of 2.7kW, this was brought down to 1.9kW when a fan was used. Like the 0.5m blockage case, heat rejection decreased from 4.7kW (no fan) to 1.9kW (with 13.6V fan).

Thus, a comprehensive analysis of automotive thermal systems was completed with certain limitations, such as non-uniformity of airflow and lack of temperature control. This leaves avenues for future work on the rig, which could include using an auxiliary heater to maintain the desired temperature, CFD analysis to get a better idea of turbulence intensity and modifying the wind tunnel to enable closed-loop testing, as it would allow for more uniform airflow.

Lists of Figures

List of Tables

Nomenclature

AC- Alternating Current

AOI- Angle of Incidence

CAC- Charge Air Cooler

CAD- Computer Aided Design

CFD- Computational Fluid Dynamics

COP- Coefficient Of Performance

DC- Direct Current

HTR- High Temperature Radiator

LMTD- Logarithmic Mean Temperature Difference

LTR- Low Temperature Radiator

WCAC- Water Charge Air Cooler

NTU- Number of Transfer Units

PID- Proportional Integral Derivative

Re- Reynolds Number

TCU- Temperature Control Unit

w.r.t- with respect to

1 Introduction

Automotive cooling systems are essential to the performance of a vehicle.

There is a need for an automotive engine to reach its operating temperature as soon it is started to avoid any energy losses. Studies [1][2][3] have found that having reached the operating temperature slowly can add to frictional losses, driving patterns can hurt thermal performance, and an increase of 20°C can increase fuel consumption by more than 10%. Additionally, with the call for the adoption of renewables and the need for curtailing emissions and improving fuel efficiency, hybrid/battery electric vehicles must be a prospect for the future. However, research in improving battery range, reducing battery size (typically weighing about 200kg), and thermal management of battery systems is accelerating. [4] Working on cooling systems is a crucial component to consider for improving current vehicle technology. With the advances in electrification and vehicle technology, an automotive engine has become more complicated; hence, a better cooling system is imperative to achieve better fuel efficiency and reduced tailpipe emissions.

To do so, it is imperative to define a conventional automotive thermal heat rejection system.

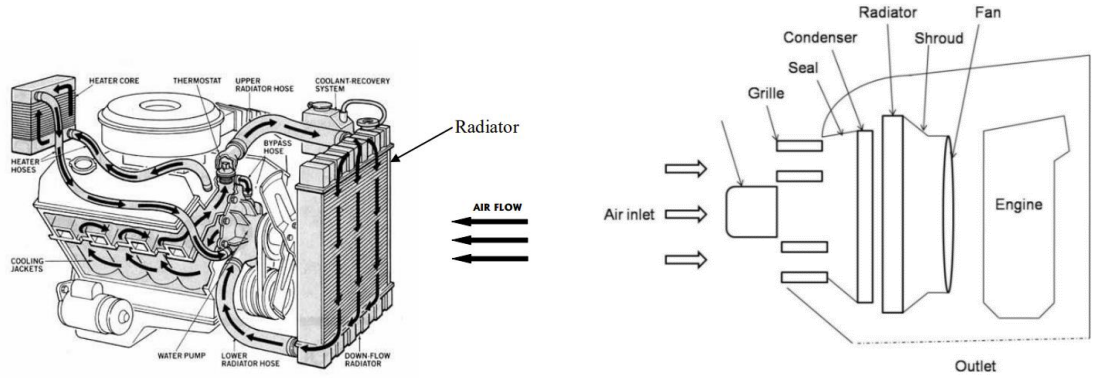

Figure 1-1: Automotive Thermal Heat Rejection System and Front End Assembly[1]

A conventional IC engine car uses a radiator assembly to dissipate heat generated in the engine effectively. The air inlet in Figure 1-1 allows ram air to be blown across the face of the front end of the assembly, which cools the radiator. The radiator lowers the temperature of a coolant-water mixture based on engine load and temperature. The fins in a radiator increase the effective surface area, thereby improving the cooling provided by the ram air, and the fan assists with further cooling. This cooled mixture is then passed through the engine to cool the engine temperature and bring it within a specific operating temperature range. Additionally, a charge air cooler (CAC) takes compressed hot air from the turbocharger and feeds it back into the engine after cooling it to improve engine efficiency. An air conditioning condenser converts refrigerant from a warm gaseous phase to a cool liquid state; this allows the cabin to be cooled to a desirable temperature. These three pieces of equipment form a conventional automotive cooling system. The scope of this study will focus on a low-temperature charge air cooler and a high-temperature radiator.

Predicted trends for Passenger LDV sales, seen from the IEA 2010 report and Figure 1-2, state that in the next 30 years, a majority of the light-duty vehicles on the street will be part-

[1] Figure taken from Deepblue.lib.umich.edu. n.d. [online] Available at: <https://deepblue.lib.umich.edu/bitstream/handle/2027.42/57958/?sequence=1>

electric and to compete with the demanding market of the future and with calls for improvement in fuel efficiency and emissions, it is crucial that these vehicles of the future are as efficient as possible.

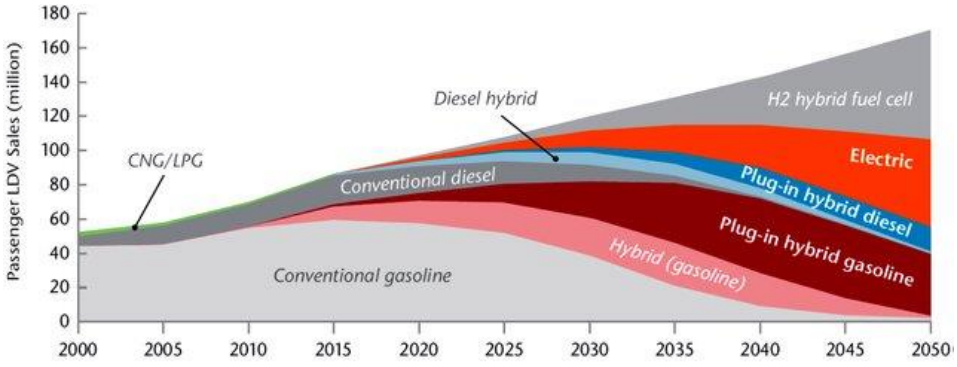

Figure 1-2: Passenger Light-Duty Vehicle Sales [5]

As seen in Figure 1-2(which shows the Euro emissions limits), since Euro 3, the standards have been getting more stringent. The most recent Euro 6 emission standard calls for stricter emissions regulations and considers Real-World Driving Emissions (RDE).

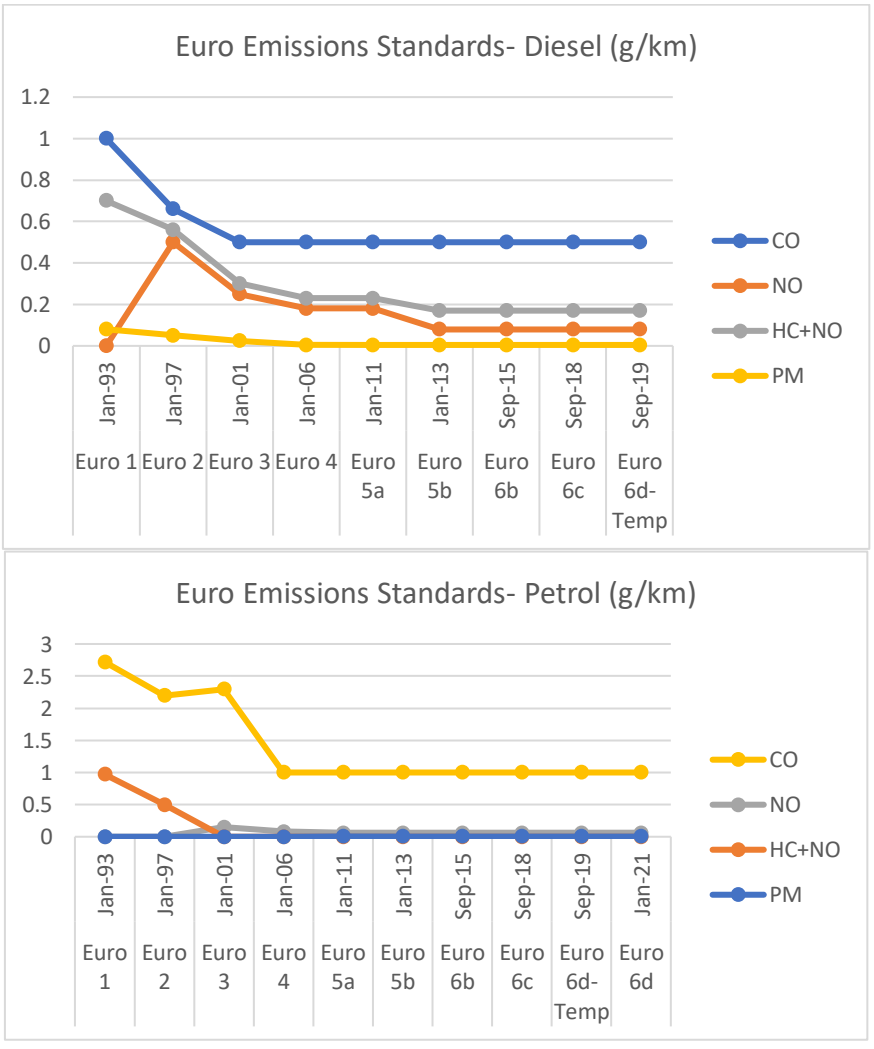

Figure 1-3: Euro Emissions Standards (g/km)

Better thermal management in automotive systems can provide better and more stable operating temperatures. Automotive engines today have an operating temperature of about 100°C. Hence, the coolant has to have a maximum operating temperature of around 120°C (under high load) to avoid engine knocking.[6] This, in turn, can help reduce cold start emissions and frictional losses, thereby indirectly increasing the efficiency while reducing the emissions. The calls for that and increased power and efficiency have put several constraints on automotive cooling systems. With the need to downsize an engine, a car's thermal heat rejection systems are required to be more efficient than ever.

1.1 Aim and Objectives

Given the advancements in thermal heat rejection systems and the advent of electric vehicles in cars, redefining automotive heat rejection systems is essential. Newer high-performance vehicles and electric vehicles do not share the same configurations as conventional internal combustion engine cars. Hence, this study aims to quantify the performance of radiators that current studies do not consider, i.e., measuring heat performance for high-performance vehicles with different angular and non-uniform configurations. The objectives of the study are as follows:

1.1.1 To design a mobile and modular rig that would provide for high-temperature and high-performance evaluation of thermal heat rejection systems. The rig's modular nature would allow for various configurations, including angular blockage and fan testing. An initial set of baseline tests would then assess the rig.

1.1.2 Evaluate heat rejection of a high-temperature, high-performance radiator with different angular configurations. This will be done for a range of coolant flow and air mass flow rates in the radiator.

1.1.3 Evaluate heat rejection of a high-temperature, high-performance radiator with different blockage configurations. This will be done for a range of coolant flow and air mass flow rates in the radiator.

1.1.4 Assess the effects of a radiator fan on the high-temperature radiator’s heat rejection and pressure drop.

1.1.5 Study the combined effects of the three – angular configurations, blockage and fan.

1.1.6 Predict low-temperature radiator heat rejection by using Effectiveness-NTU modelling techniques.

1.1.7 Provide a basis for future testing, which could include testing newer cooling systems such as those used in electric and fuel cell vehicles.

1.2 Structure

The structure of the report is as follows:

- Abstract summarising the report along with important conclusions
- Introduction to the topic of the automotive radiator, defining the need for high-performance thermal heat rejection systems and objectives for the study
- Literature review where wind tunnel construction, various heat exchangers, and heat transfer will be examined
- Methodology describing the testing method and experimental rig
- Forming results obtained by experimental testing for the high-temperature radiator and Effectiveness-NTU modelling for the low-temperature radiator
- Discussions around the results facilitated by Delta Heat Rejection (HR) plots which measure the difference in heat rejection between two plots
- Conclusion and direction of future work which could address the limitations of the given rig caused by the modularity of the rig

2 Literature Review

Several topics were investigated to form a base for this thesis, which helped develop a study structure. The different types of wind tunnels were studied to construct a functional wind tunnel, and the rig's wind-tunnel was constructed accordingly. Several probes and sensors were considered to determine the best method for measuring velocity for the rig, and the best option was chosen based on the reviews. Since the thermal performance of heat exchangers and charge air coolers is determined, concepts regarding heat exchangers and methods to assess heat transfer were investigated. As part of the test plan, baseline tests, blockage tests, angle of incidence tests, transient tests and the use of the Effectiveness-NTU model were considered, and appropriate literature was chosen for each topic.

2.1 Current Automotive Cooling Configurations

To understand the current cooling system needs, it is vital to understand the environmental conditions within an automotive environment. Operating temperatures for different areas in a car are listed in Table 2-1. [2]

Table 2-1: Automotive Environment - Operating Temperatures

Component	Operating Temperature (°C)
Driver Interior	-40°C to 85°C
Underhood	-40°C to 125°C
On-engine	-40°C to 150°C
In the exhaust/Combustion areas	-40°C to 200-600°C
Electronic Systems	-30°C to 175°C (depending on ECU location)

Typical temperatures for the front of a car can also be seen in Figure 2-1. [2]

[2] Taken from Johnson, R.W. et al. (2004) "The Changing Automotive Environment: High-temperature electronics," IEEE Transactions on Electronics Packaging Manufacturing, 27(3), pp. 164–176. Available at: https://doi.org/10.1109/tepm.2004.843109.

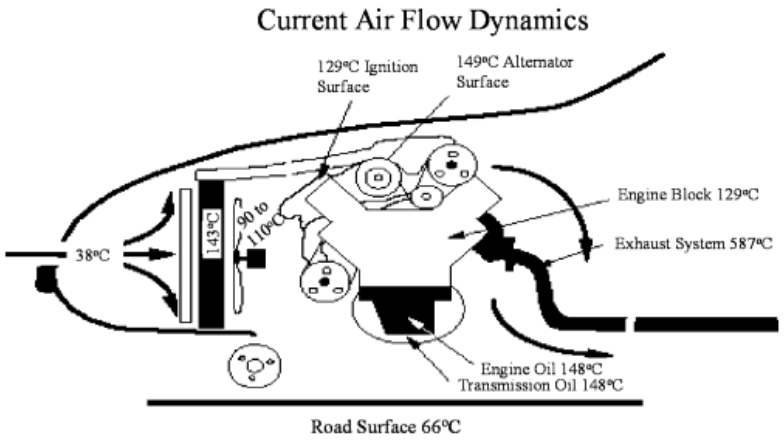

Figure 2-1: Car Temperatures with Air Flow Dynamics

Heat transfer coefficients for various automotive components/areas were also studied. Heat transfer coefficients tend to be higher for higher vehicle velocities, and the magnitude varies depending on the working surface area, fins, and temperature. These have been detailed in Table 2-2.[3]

Table 2-2: Automotive Heat Transfer Coefficient

Component/Area	Heat Transfer Coefficient (W $m^{-2}k^{-1}$)
ECU	5-10
Automobile cabin	8-50
Lithium Ion Battery	10-25
PEM Fuel Cell	8-44
Combustion Chamber - IC Engine	1000-2000

The present scope of work is limited to developing high-performance internal combustion engines. However, going forward, it is vital to investigate cooling systems for electric vehicles and fuel cell electric vehicles. Energy-dense high-voltage batteries have a limited temperature range in which they can perform; a difference in operating temperature can significantly reduce the battery life of an electric vehicle [7]. Hence, radiator configurations for other vehicles need to be investigated to further develop the required testing capabilities of the rig [8][9][10][11][12].

The I12 powertrain (depicted in Figure 2-2 used in the BMW i8 uses high-temperature and low-temperature cooling circuits. The two cooling circuits are used to maximise efficiency and for component protection. Depending on the heat dissipation requirement and operating temperature, a specific circuit cools the component. The high-temperature circuit utilises a single large radiator, whereas three smaller radiators are used in the low-temperature cooling circuit. The low-temperature circuit uses two 80W coolant pumps (denoted by B and D in the figure) to effectively distribute the coolant to cool the high-voltage components (excluding the battery) and auxiliary components. The I12 powertrain uses active flap control by controlling the ram air through the vehicle grille.

[3] Taken from Engineering ToolBox, (2003). Overall Heat Transfer Coefficients. [online] Available at: https://www.engineeringtoolbox.com/overall-heat-transfer-coefficient-d_434.html

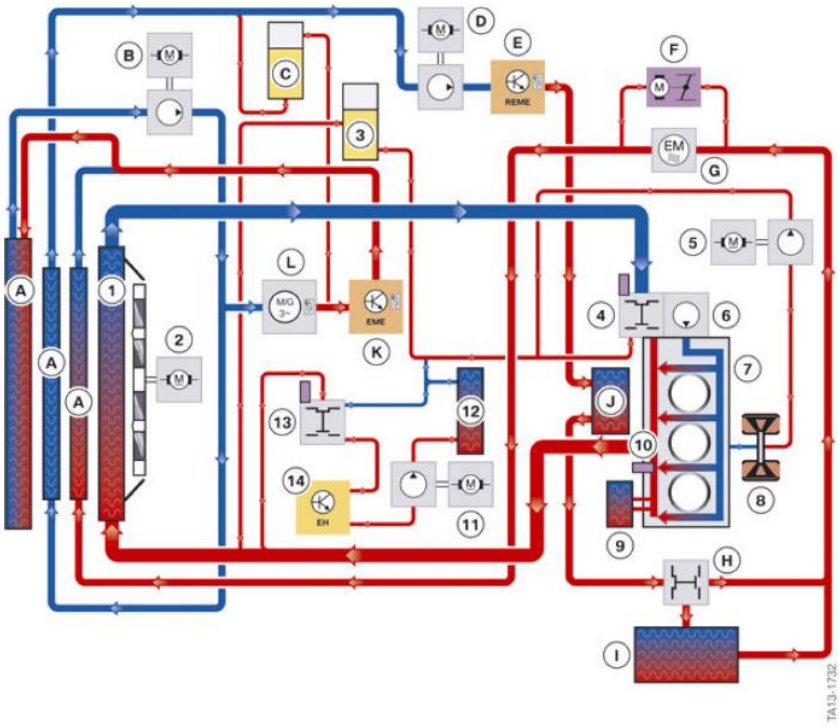

Figure 2-2: I12 powertrain high-temperature radiator (1) and low- temperature radiator (A) circuits

The blue lines indicate a cooler temperature, whereas the red indicates a higher temperature of coolant flow. At start-up, the combustion engine is started by a high-voltage starter motor generator.

The front end of the cooling system comprises three low-temperature radiators (denoted by the letter A), a high-temperature radiator placed behind them (denoted by 1 in Figure 2-2 and 13 in Figure 2-3), an electric fan (denoted by 2 in the first diagram and 12 in the second) and a condenser.

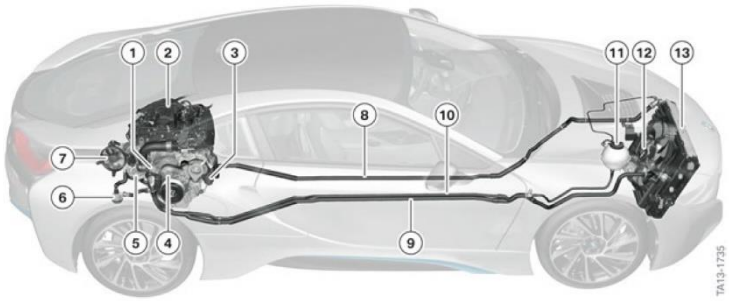

Figure 2-3: High-temperature cooling circuit for the I12 powertrain

Figure 2-3 shows the high-temperature cooling circuit for the I12 powertrain. The front assembly is at an angle with a 2.3L cooling tank at its bottom. To study the cooling system performance, it would be essential to consider these factors.

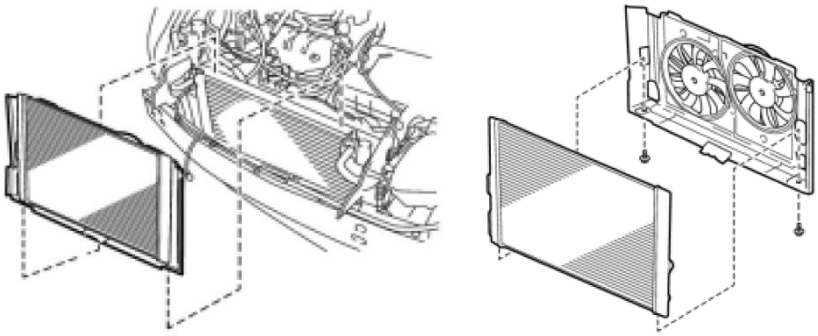

Figure 2-4: Toyota Prius: Radiator and Fan shroud assembly

As seen in Figure 2-4, the radiator assembly in the Toyota Prius is somewhat similar to the i8. It consists of a front-end assembly with the bumper acting as an upstream blockage. The fan shroud consists of two slightly askew fans mounted to the back of the radiator. It is also important to note that the radiators used in these assemblies are crossflow radiators, whereas the current testing is being carried out for downflow radiators. Improvements of additional testing capability would involve modifying the rig for crossflow radiator testing capabilities.

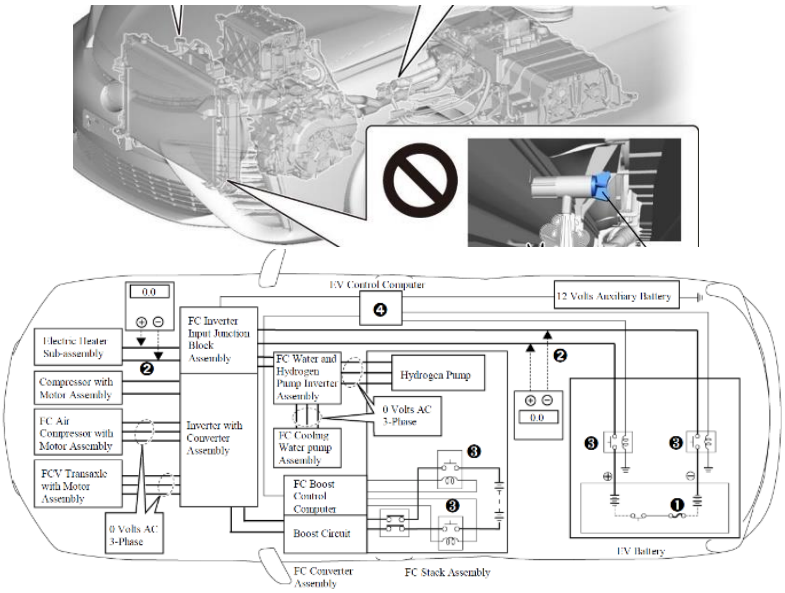

Figure 2-5: Front-end assembly and EV/FCV assembly for the Toyota Mirai

When looking at fuel-cell vehicles like the Toyota Mirai, as depicted in Figure 2-5, a different set of aspects must be considered. A 12V auxiliary battery supplies power to the low-voltage devices, whereas a 245V battery pack acts as the main battery for the vehicle. Additionally, a cooling system is needed for the fuel cell stack. As Polymer Electrolyte Membrane (PEM) fuel cells operate at 60-70C, dealing with low-temperature heat rejection, the cooling circuit still uses liquid cooling systems. However, the coolant itself should be deionised for extreme weather testing. Effects such as transients of the radiator might also come into play as it operates at a lower temperature. [13] The radiator has a few components, namely the electric heater and compressors downstream of it, and they are followed by an inverter assembly and the fuel cell stack. To assess the heat rejection of the Mirai, the balance of fuel-cell/electricity/charging states needs to be considered for five cases along with its state of charge (SOC)- once the car is started, when it is in the normal driving state, while accelerating, while decelerating, and while stopping.

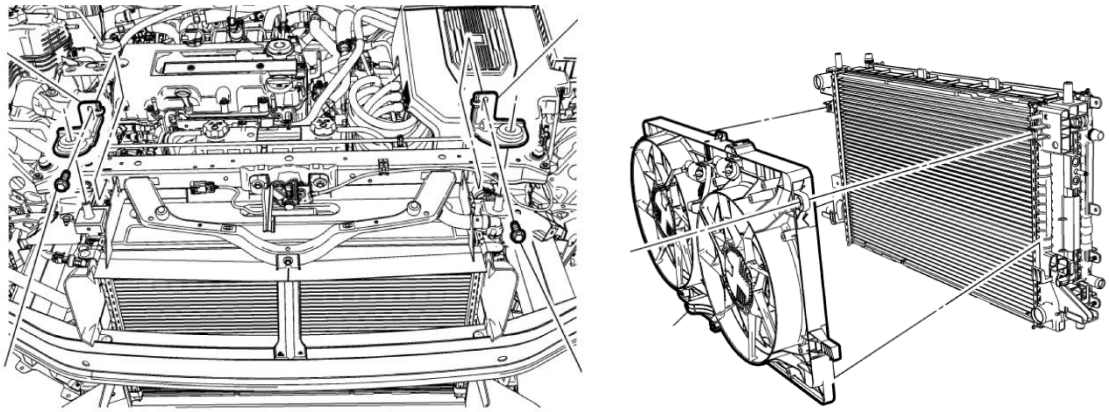

Figure 2-6: Chevrolet Volt Front-End and Radiator Assembly

The Volt has a complex front-end assembly, as seen in Figure 2-6, where each cooling circuit has its radiator. It has four cooling circuits:

- the engine-radiator cooling circuit, which cools the main gasoline engine and occasionally acts as a source of cabin heat,
- the electric drive unit cooling circuit, which uses a transaxle cooler to cool the transmission, axle and differential assembly,
- the high voltage battery cooling circuit, which uses a three-way coolant circuit to divert coolant flow onto the Lithium-ion battery pack depending on temperature and load at a given point,
- the power electronics cooling circuit is responsible for the battery and uses a 12V electric coolant pump to pump coolant into a charger-cooling radiator-power inverter-pump assembly.

The complex circuit and assembly would therefore require understanding the impact of cascading the radiator. Thus, blockage testing needs to be a priority for further testing.

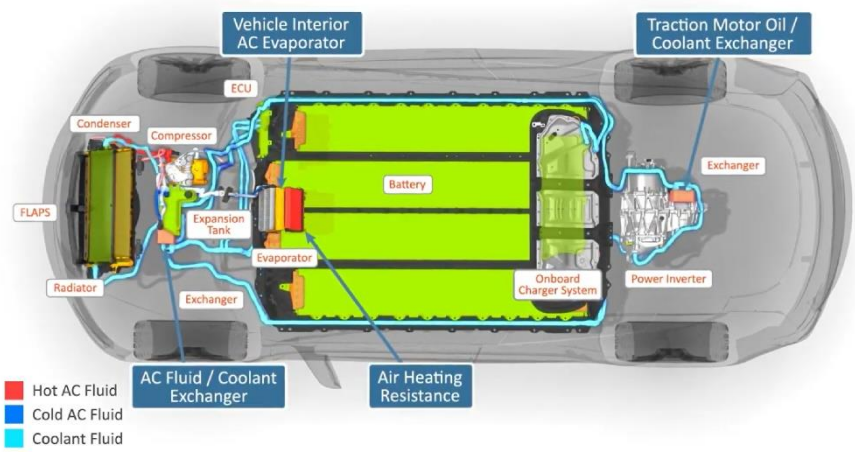

Figure 2-7: Tesla Model 3 cooling system

The Model 3 does not use a fan shroud downstream of its radiator; however, it uses ram air cooling. As seen in Figure 2-7, the coolant enters the motor and cools the stator assembly; the Tesla Model 3 has two cooling loops and can divert the flow based on these parallel or series loops. Depending on the load, it can cool the electronics via the coolant or the battery pack using the cooler.

Range-extender configurations improve an electric vehicle's range by using an auxiliary power source and are becoming more prominent in electric cars. Further analysis of the same also needs to be considered in this study. Pischinger et al. [14] studied a V2 engine concept in combination with two generators. In the case of thermal management for the cabin, the residual heat generated by the range extender can be used as a source of heat to maintain a suitable cabin temperature, if needed. For an electric vehicle, cabin heating would be done electrically, taking energy from the main battery and reducing the available range. Hence, using a range extender, one can conserve the battery's State of Charge, thereby increasing its range. The location of the range extender within the vehicle architecture needs to be considered; it is not always located in the front of the vehicle, like traditional ICE vehicles and is also used for auxiliary power; therefore, studying the transient performance is essential. Analysis of transient coolant temperatures would accurately characterise these heat rejection systems depending on the coolant used (Range Extender or Electronics).

Advanced Engine Cooling Systems have similar performance criteria wherein it is required to optimise the operation and combustion characteristics while maintaining a high-efficiency auxiliary power source and minimising frictional losses [15].

A vehicle coolant control strategy can often prove challenging as it must cope with a wide variety of conditions, such as heavy accelerations, hill climb (slow, high load) idling, frequent braking, and cruising at low speeds. [15] Hence, as a part of future work, transient coolant control strategies could be studied under aggressive load conditions. Modelling of the circuit can also provide insights into metal-coolant interactions. This can be facilitated by analysing the radiator design and studying the material/fin/louver structures. To study combustion effects such as knock set by lower temperature set points, this rig could be used to support combustion simulation work taking boundary conditions into account.

2.2 Electric Vehicle and Fuel Cell Electric Vehicle Cooling

A study conducted by NREL, USA, determined the electric motor system and energy storage system thermal performance by carrying out bench testing for electric vehicles [16]. A single liquid coolant system was put through a UDDS/ double HWFET drive cycle test (45%/55%). The temperature vs time graphs and drive cycle profiles for the study are shown in Figure 2-8.

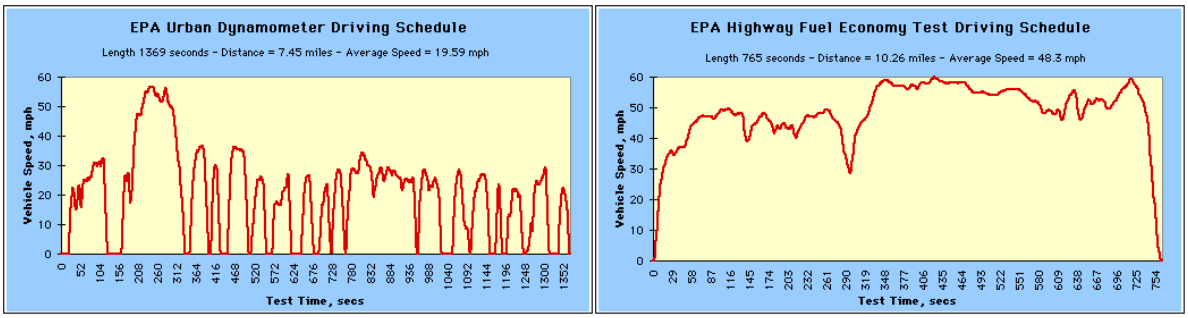

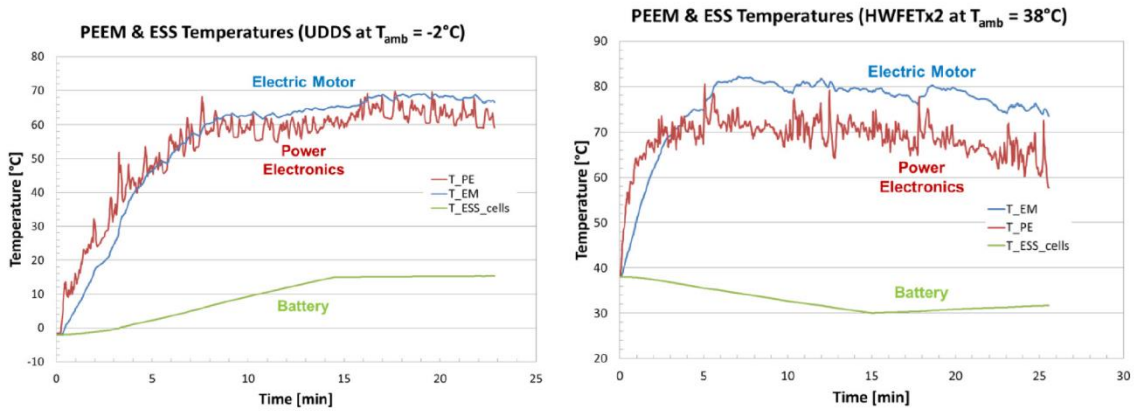

Figure 2-8: Component Temperatures vs Time- NREL study [17]

The study mapped the thermal performance based on the given drive cycles. The study examined a range of ambient temperatures (in 5°C increments) to account for extreme weather conditions while also simulating cabin conditions such as additional cabin heat provided by the sun. Whilst it might not be possible to recreate similar conditions with the current rig, similar simulation work (possibly based on real-world testing, e.g., measuring the increase in cabin temperature in a car on a sunny day) might aid a comprehensive testing setup which would specifically benefit thermal analysis of Electric Vehicles as battery temperature is a critical factor in the performance of such vehicles.

To study the effects of an aggressive transient drive cycle on the thermal performance of electric vehicles, a study was conducted at Arizona State University [18]. The effects of a US06 drive cycle were studied on an electric vehicle, and the thermal performance was measured for three cases:

- No Coolant
- Liquid Coolant with a Simple Thermostat
- Liquid Coolant Controlled cases

The results of heat generation in a battery with the three setups can be seen in Figure 2-9.

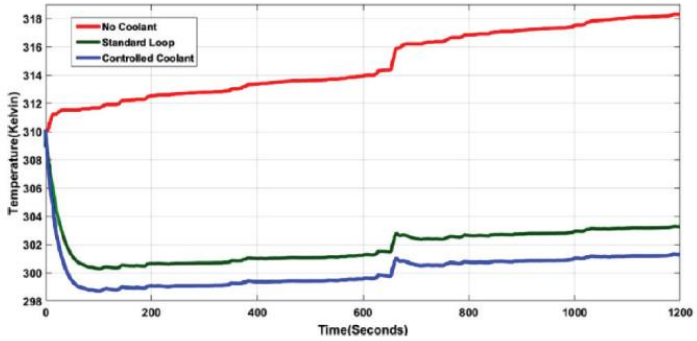

Figure 2-9: Heat generation (Battery Temperature vs Time) with time for 3 different coolant flow conditions [19]

Hence, it was seen that the third case with the controlled coolant provided brought down the temperature for the stack by the most. The study also called for different temperature ranges, coolant rates and drive cycles to be studied to measure EV thermal performance. Hence, real-world testing could be carried out in the rig being built, and better PID control of the valves can enable us to control the parameters for more aggressive transient cycles.

A mathematical model was developed [20] to study the coolant flow rates and stack thermal performance for fuel cells using a lumped capacitance model for Polymer Electrolyte Fuel Cells using heat transfer and pressure loss data for a fuel cell. Transient thermal performance was then obtained using this model, and the effects on the coolant flow rate and airside flow rate were observed, as shown in Figure 2-10. Fuel Cells have auxiliary cooling requirements (required for the electric components) along with the standard fuel cell stack cooling. Here, a simple model was taken in which a radiator with a fan assembly had coolant passing through a pump into a fuel cell stack system back into the radiator.

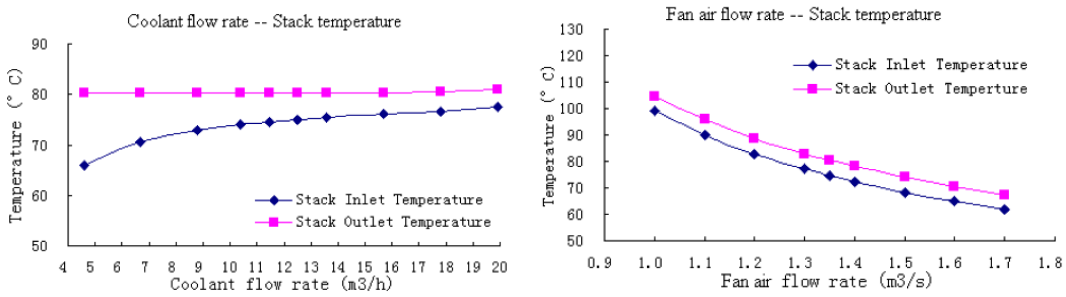

Figure 2-10: Temperature plots against Coolant flow rate and air flow rates [21]

As with the case of IC engines, the airflow in a stack was shown to have more of an effect on the temperature than the coolant flow rate. As the lumped capacitance model takes the pressure loss and heat transfer into account, the airflow results are to be expected. The transient tests showed that the stack material and materials were crucial to improving thermal performance; however, further testing was called for to get more accurate results and to study the effects of variables such as fan structure and performance into account.

As can be seen from these studies, the testing conditions can be encompassed in the current rig capabilities. With minimal changes to the coolant flow rate, airflow, and further radiator material/inner geometry analysis, the rig can render and model accurate results for configurations similar to the ones above. Hence, the rig can be further expanded to get heat rejection data from several varied configurations.

2.3 Hea exchanger review

Heat exchangers can be characterised by either open/closed nature, flow or construction. Closed radiators involve the coolant is passed through the heat exchanger at a higher operating temperature. In contrast, open radiators involve the coolant being renewed in the actual environment by mixing.[4] Based on construction, they can be shell and tube, plate and frame type, extended surface and regenerative. The extended surface can be subcategorised into plate and tube fin heat exchangers. These are depicted in Figure 2-11.

[4] From Nasrabady, S., 2008. [online] Open Heat Exchanger For Improved Energy Efficiency In The Heating Of Hot Spas. Available at: <https://orkustofnun.is/gogn/Orkusjodur/Orkusjodur-55-Open-heat-exchanger.pdf>

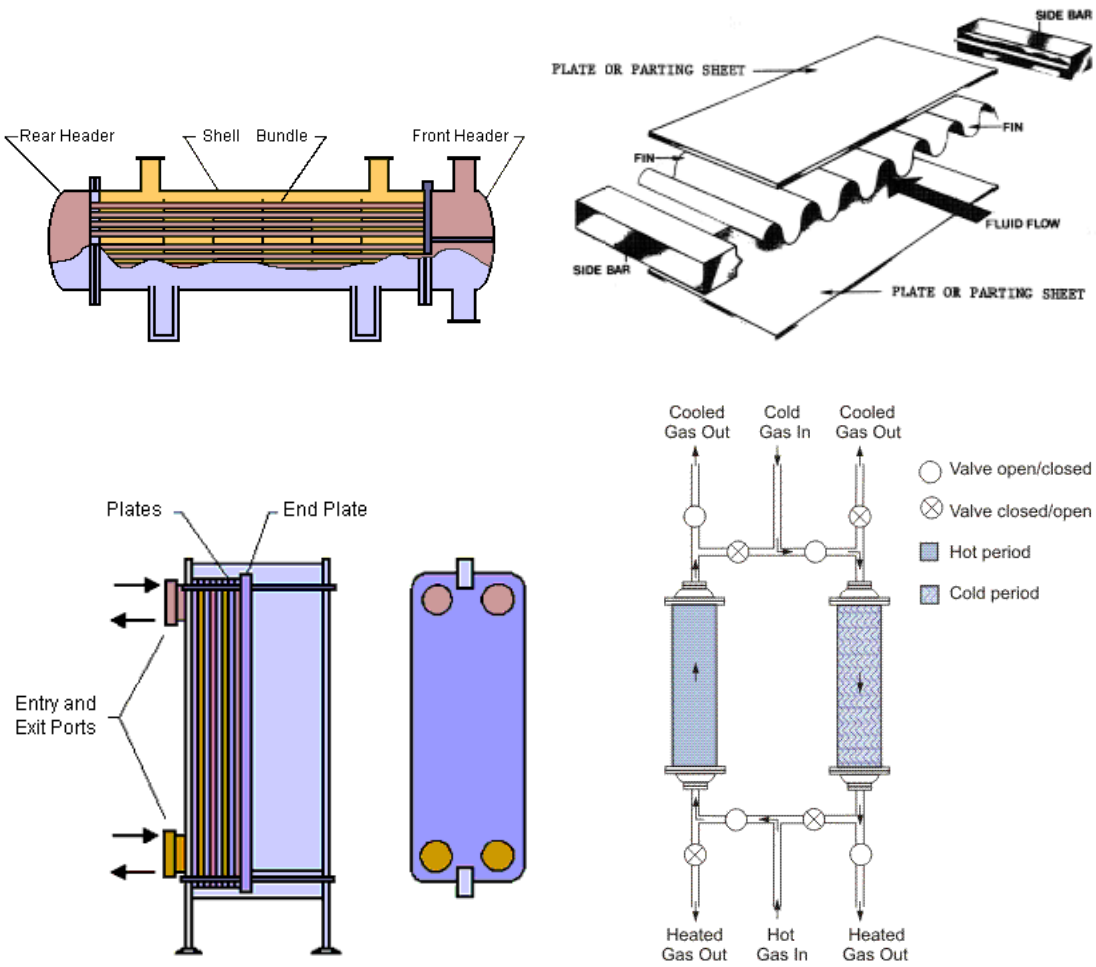

Figure 2-11: Shell and Tube, Plate and Frame Extended Surface and Regenerative Heat Exchanger[5]

A plate-fin heat exchanger (extended-surface) is one of the most extensively used in the industry. It consists of a corrugated sheet sealed between two flat plates, several of these stacks are placed together and made into a radiator. Plate-fin heat exchangers can be further subdivided into sub-categories based on the types of louvres.

Louvres can be fabricated onto the radiator by pushing elements from the base and are responsible for providing different flow directions and arrangements in a radiator.

Several types of corrugation types are also available for this type of radiator- plain, perforated, herringbone and serrated. Plain corrugations are simple straight channels, and perforated corrugations are the same as plain ones but have holes. Herringbone corrugations have channels resembling continuous waves, and serrated corrugations have channels in a staggered configuration. An advantage of a herringbone corrugation is the increased heat rejection characteristics/ better heat dissipation. These corrugation types are depicted in Figure 2-12. [6]

[5] Figure taken from Brogan, R., n.d. HEAT EXCHANGERS. A-to-Z Guide to Thermodynamics, Heat and Mass Transfer, and Fluids Engineering,.

[6] Figure taken from: Gregory, E., n.d. Plate Fin Heat Exchangers. A-to-Z Guide to Thermodynamics, Heat and Mass Transfer, and Fluids Engineering,.

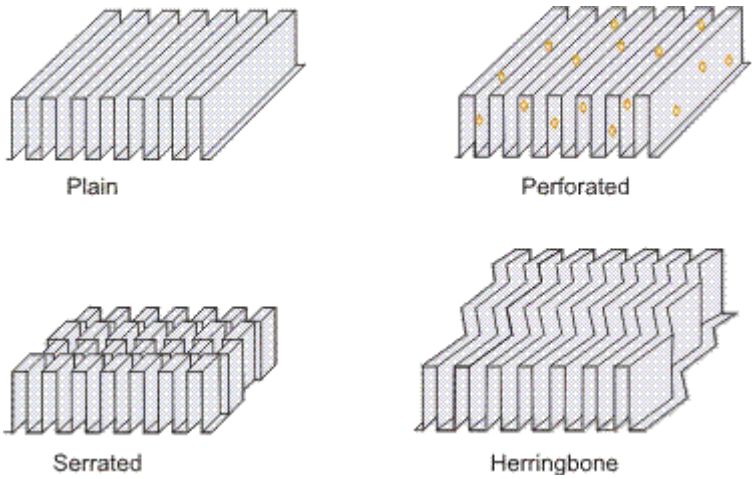

Figure 2-12: Different Radiator Corrugations

Flow can also be used to characterise different radiator types. Typically, heat exchangers have two tanks on either end- an inlet tank and an outlet tank. Coolant at a high temperature passes from the inlet to the outlet. The surface of the radiator, which is covered in louvred fins, enables the heated coolant to be cooled down and recirculated.

Based on the direction of flow, heat exchangers can be classified as parallel-flow, counter-flow or cross-flow. The flow directions for each of the configurations can be seen in Figure 2-13. Parallel-flow heat exchangers are fluid-fluid heat exchangers in which the hot and cold fluids flow in the same direction. Due to the convective heat transfer between the two fluids, the temperature gradient at the inlet in such a heat exchanger is larger than the gradient at the outlet (the outlet temperatures are close to each other).

A counter-flow heat exchanger is also a fluid-fluid heat exchanger in which the hot and cold fluids flow in the opposite direction. The hot fluid passes through one end of the heat exchanger whereas the cold fluid passes through the other. This heat exchanger is generally more efficient and can provide a better heat transfer coefficient than a parallel-flow heat exchanger.

Heat exchangers are commonly used in cars as radiators, charge air coolers and in air conditioning evaporator coils. The principle behind such heat exchangers is that the hot fluid (typically water or, coolant or, coolant in the case of an evaporator coil) passes through the tubes of a radiator and is cooled by the cooler fluid (typically ram air) that flows perpendicular to the surface of the radiator hence, forming a cross-flow configuration. Due to spatial constraints in an automobile, a cross-flow heat exchanger can also be a down-flow heat exchanger. The only difference between the two is the placement of the heat exchanger (horizontally for cross-flow and vertically for down-flow). Gravity aids the flow of coolant in a down-flow radiator.

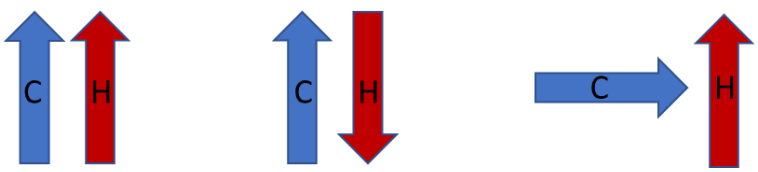

Figure 2-13: Parallel, Counter and Cross flow directions in radiators, respectively

Zhan et al. [22] tested and compared M-cycle radiators depicted in Figure 2-14 (which run on an indirect evaporative cooling cycle, which effectively distributes air flow using a smart geometrical arrangement [23]). The study compared counter-flow and cross-flow M-cycle radiators for cooling performance in buildings. The study found that although the cooling capacity was more significant for counter-flow radiators, cross-flow radiators had a better energy efficiency (COP). For automobiles, energy efficiency would be more crucial than the system cooling capacity. Hence, cross-flow heat exchangers prove to be better.

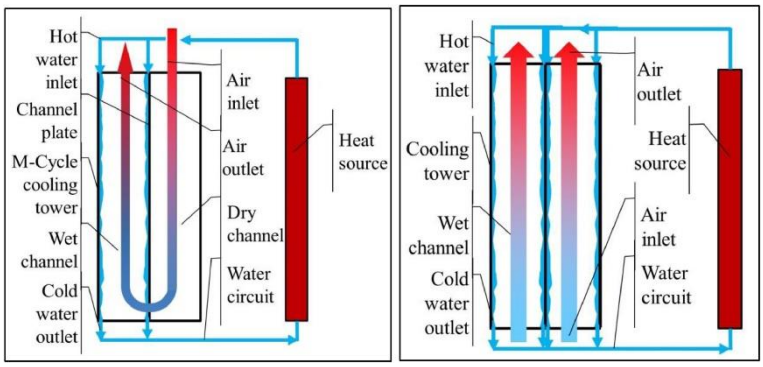

Figure 2-14: M-cycle cooling tower (Left) and Traditional Cooling Tower (Right)[7]

Gorman et al. [24] compared heat transfer and pressure drop for louver and plain finned radiators and found that with an increasing Reynolds number, the change in fluid velocity affected the pressure drop more than it affected the heat transfer rate. The results of this study are seen in Figure 2-15.

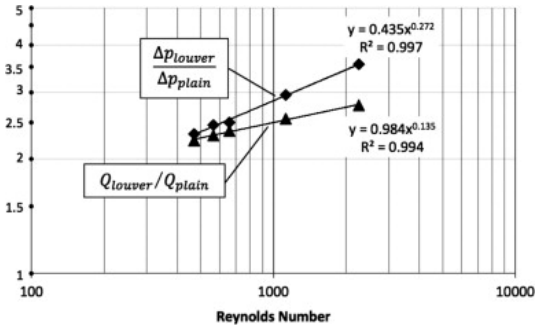

Figure 2-15: Findings of Gorman et al. study

A comprehensive review carried out by Erbay et al. [25] also found that 2D analysis was insufficient to determine the heat transfer coefficient for louvred fin radiators. A 3D analysis was found to be more apt.

A few studies [26][27] have simulated the effects of corrugation angles on heat transfer coefficients. They have found that although the heat transfer coefficient generally increases with the increase in the corrugation angles, experimental research in the field is still required. Moreover, both studies considered the laminar flow of a relatively low (<10000) Reynolds number; hence, there is a need for carrying out turbulent testing.

A summary of the findings can be found in Table 2-3. As can be seen, the studies considered for this project were only found to be for niche applications and for low Re, laminar flows. Hence, there is a need for more aggressive testing in the area.

[7] Figure from: Pandelidis, D., Drąg, M., Drąg, P., Worek, W. and Cetin, S., 2020. Comparative analysis between traditional and M-Cycle based cooling tower. International Journal of Heat and Mass Transfer, 159, p.120124.

Table 2-3: Summary of Heat Exchanger Review

Study	Findings	Limitations and Future Research
Zhan et al	Cross-flow radiators had a better COP than counter-flow	Only studied a niche radiator (M-cycle) with its applications in cooling for buildings
Gorman et al	With an increasing Reynold's number, Change in fluid velocity affected the pressure drop more than it affected the heat transfer rate	Effects for Re>10,000 were not studied
Erbay et al	2D analysis would be insufficient to measure heat transfer coefficient	3D analysis for determining the heat transfer coefficient
McNab et al/Erbay et al	Heat transfer coefficient increases with an increase in corrugation angles	Only considered laminar flows

2.4 Incidence angle testing review

Several studies have carried out incidence angle testing; however, each has its own limitations. This was done to ensure the rig was designed to meet objective 1.1.2. The setup has been defined in Figure 2-16.

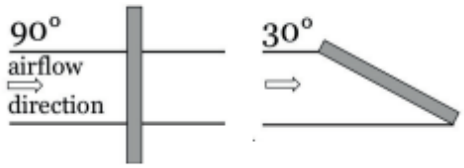

Figure 2-16: Angle of Incidence Testing for Heat Exchangers [28]

Higher mass flow rates were analysed in Henriksson et al. [28] and Larsson et al. [29], where heat rejection and pressure drop were measured. Conclusions from studies verified CFD data by following them with experimental testing. The study established that the heat transfer rate increased for the 30° case by 26% compared to the 90% case. Increases were also seen in the 10° case. These are depicted in Figure 2-17.

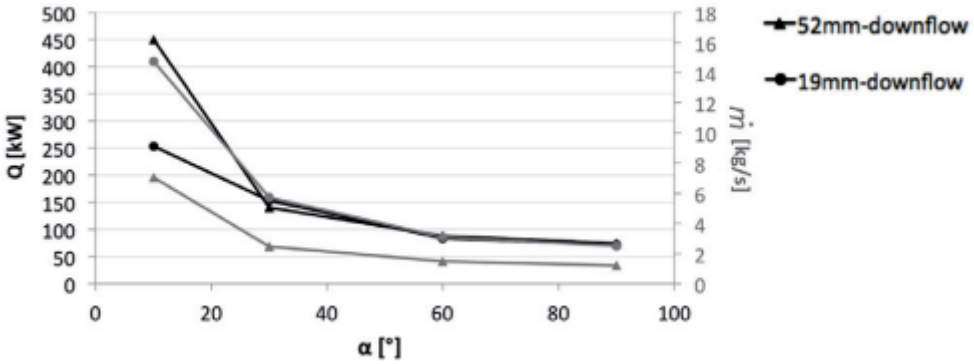

Figure 2-17: Results from Henriksson et al. study showing an increase at 30° case at a dP of 100Pa [28]

Achaichia and Cowell [30] tested and mapped the mean airflow w.r.t the Reynolds number (as shown in Figure 2-18). The characteristic length here is defined as the hydraulic diameter of the setup.

Since the coolant temperature was constant and the only difference was the angle, the heat rejection and heat transfer coefficient obtained followed similar curves for the studied angles. They found that a small louvre pitch with a small louvre angle produced non-desirable effects.

A drawback is that they only considered flow with low Reynolds number, and it would be beneficial to test the system for higher Reynolds numbers.

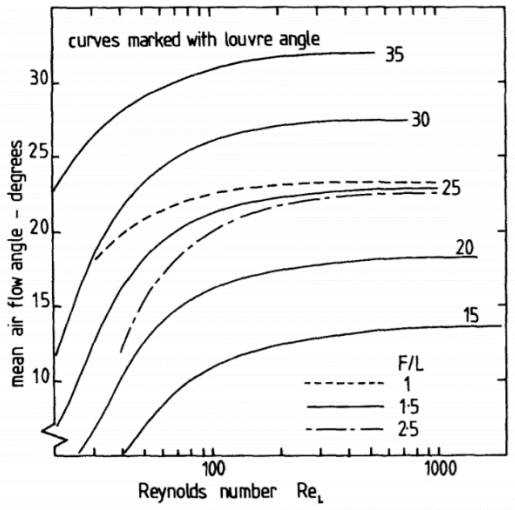

Figure 2-18: Incidence angle airflow results [30]

Similar results can be seen in a study conducted by Sadeghianjahromi et al.[31], ; although they studied a larger range of velocities and Reynolds numbers and found that the effect wasn't pronounced, the range was still low (maximum velocity is 6.5m/s, equivalent to a Re of 8100). For a high-performance vehicle, a more comprehensive study is required as real-world driving conditions require more robust conditions than those exhibited by these Re values. Higher Reynold's numbers cannot be obtained using a simple Navier-Stokes Equation because of the different mixing lengths that arise from the turbulent flow. A modified approach such as the Reynolds-Averaged Navier-Stokes (RANS) approach is adopted to account for this. Averaged time eliminates the need for time derivates, providing a better system for highly turbulent cases. [32]

Webb and Trauger [33] demonstrated that at 20°-30°, the flow efficiency increased with an increase in the Reynolds number value because of forced convection caused by the louvre angles. This would also mean an increase in heat transfer performance. However, their estimates for flow separation were not found to comply with their experimental results. Also, as seen with previous studies, they only considered a maximum Re of up to 4000. Hence, the study calls for more extensive and aggressive research.

Nuntaphan et al. [34] studied the heat rejection for several angles for water at 40°C-80°C.

Figure 2-19 for inclination angles greater than 45° showed a sharp drop in the heat rejection performance. This was preceded by a sharp increase in the heat rejection performance data at angles between the 30°-40° range. A similar range would yield the best insights.

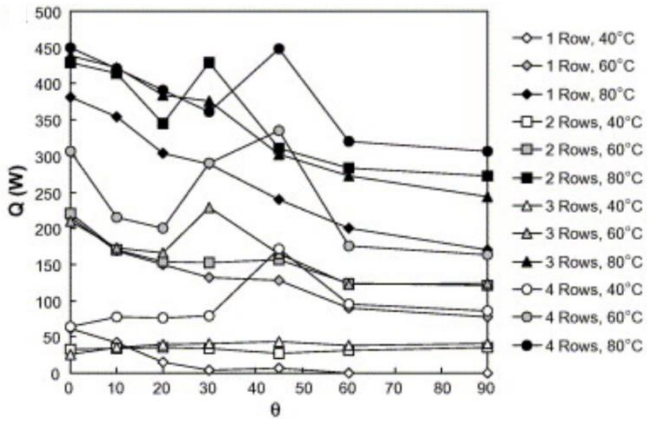

Figure 2-19: Findings from the Nuntaphan et. al. study [34]

The results from the studies are summarised in Table 2-4.

Table 2-4: Summary of Incidence Angle Testing

Study	Findings	Limitations and Future Research
Henriksson and Larsson	Found increased heat transfer rate for 10-30 degrees case	Only studied plate-fin heat exchangers
Achaichia and Cowell	Small louver pitch with a small louver angle produced non-desirable heat transfer effects	Effects for higher Reynolds numbers were not studied
Sadeghiana jahromi et al	A larger range of air velocities were considered; however, the effect of Re wasn't pronounced	Only air velocities of up to 6.5m/s were considered
Webb and Trauger	Needed more robust testing	Only considered laminar flows
Nuntaphan et al	Sharp decrease in heat rejection for angles greater than 45 degrees	Heat Exchangers considered only used water at 40-80°C

As evident from the literature review in this field, more robust testing conditions (higher air flow rates and coolant temperatures) need to be considered to study the full effects of incidence angle on the heat rejection of a radiator. Angles of up to 30°-40° should be studied as heat rejection may drop off at greater angles and a radiator is often aligned at those angles in a typical engine bay.

2.5 Blockage and Fan testing review

A significant amount of research [35][36] has been carried out to study the effects of the engine bay as an upstream blockage w.r.t the radiator fan. To ensure these effects were incorporated into the rig design and appropriate variables were chosen, this was done to meet the requirements of objectives 1.1.3 and 1.1.4.

With an upstream blockage on a radiator face, the airflow is expected to be reduced on the face of an automotive heat exchanger; hence, depending on the area of the blockage, a decrease in the heat rejection.

Datta et al. [37] studied the effects of non-uniformity using different blockages. They studied heat rejection under a side blockage (half of the face was blocked), a peripheral blockage

(sides were blocked), a uniform blockage (uniform grille over the face), and a middle blockage (middle blocked off). Depending on the flow profile, the blockage and area covered had different effects on heat rejection. A larger portion of the face covered did equate to a decrease in performance; however, a side blockage showed a significant reduction in heat rejection when compared to a peripheral blockage. As seen in Figure 2-20, the study considered low air mass flow rates (<1kg/s); hence, it could be beneficial to study higher flow rates and look at different upstream distances from the face of the radiator. The layouts are depicted in Figure 2-21.

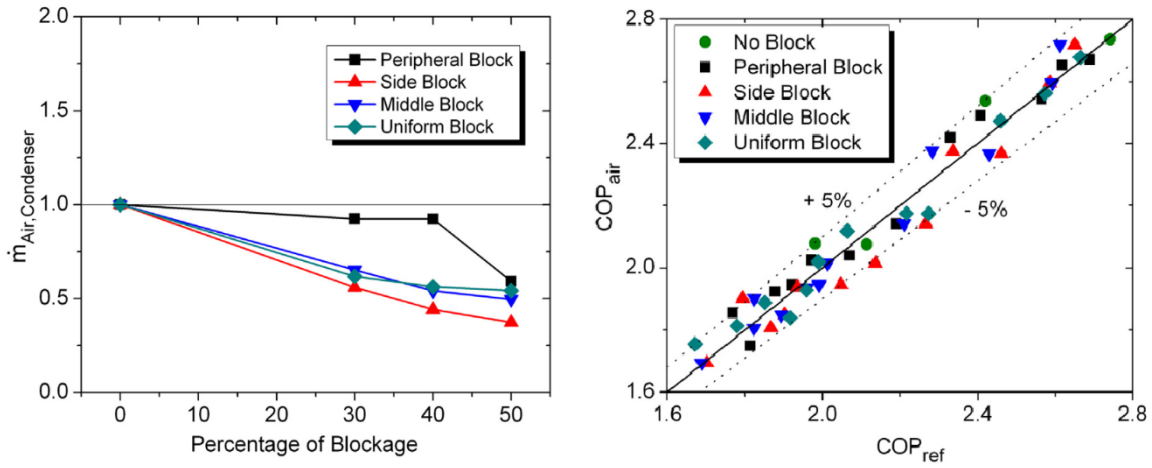

Figure 2-20: Results from Datta et al. study [41]

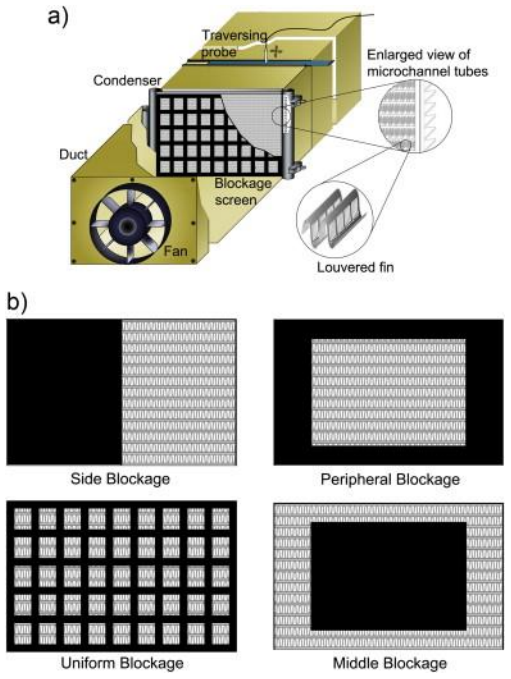

Figure 2-21: Blockage Layouts from Datta et al. study [38]

Similarly, Baskar and Rajaraman [39] studied the effects of blockages on the uniformity of flow. These blockages and the associated partial results are depicted in Figure 2-22. The study found that other characteristics, such as the type of blockages, also affected the uniformity, with specific blockages providing a more uniform airflow distribution than others. Uniformity for vertical and horizontal blockages was much higher than the side to centre

blockages. Partial results shown in Figure 2-22 also indicate low-velocity zones in the corners in the baseline case, which were not as prevalent with a blockage in place.

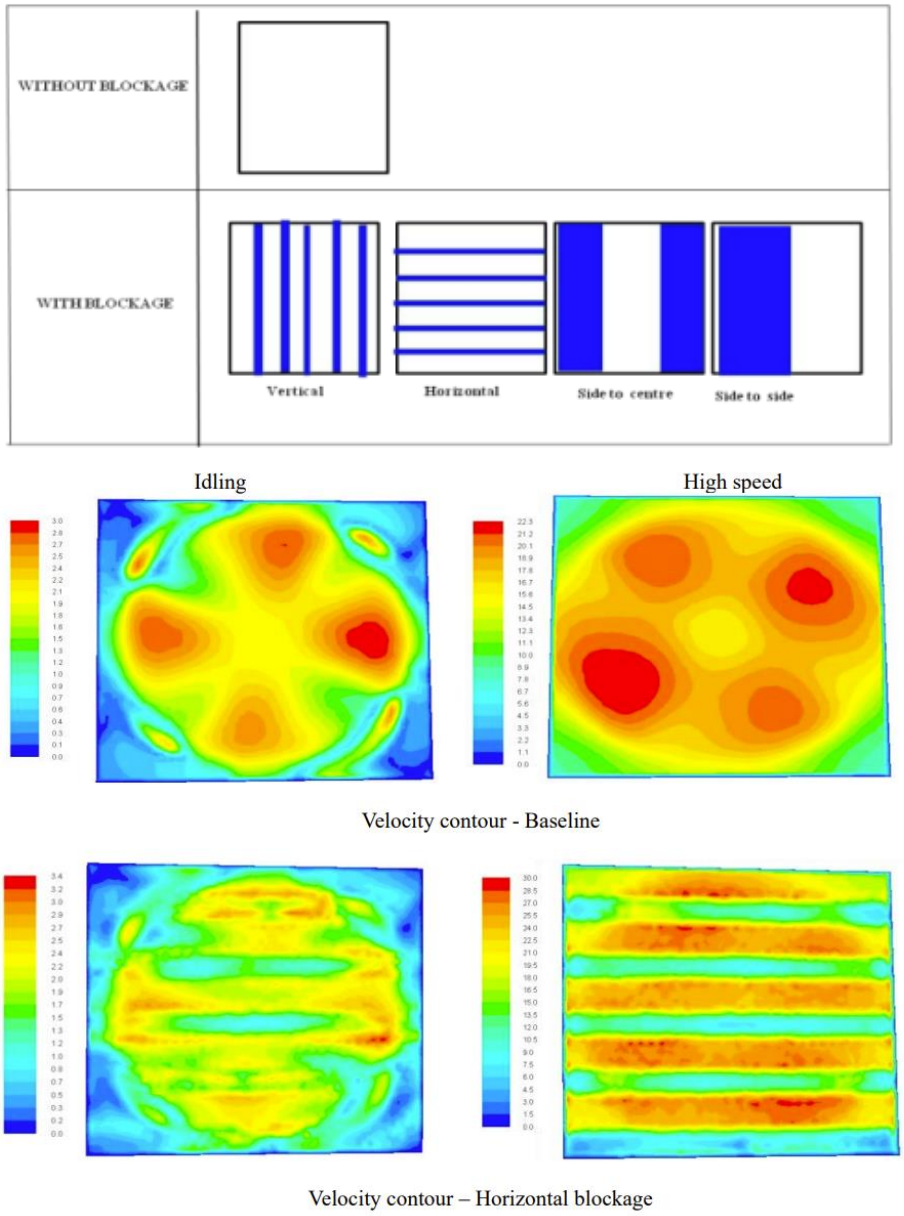

Figure 2-22:Blockages used in Baskar and Rajaraman study (top) and partial results (bottom) from the study

Choi et al. studied [40] the effects of maldistribution on the cooling capacity of a finned-tube evaporator. They found that a non-uniform airflow could lead to a 6% decrease in the cooling capacity.

Mao et al. [41] compared the effects of a uniform flow with that of a non-uniform parabolic, saddle-like and linear velocity profile. Like the Choi study, it was found that a non-uniform air flow gave up to a 6% decrease in heat rejection and up to a 34% decrease in pressure drop.

Blockage effects were also analysed in a vehicle grille by Kim et al., as grille commonly have blockages which affect the flow of ram air. [42] The position of the blockage and the mass flow rate of the ram air is seen in Figure 2-23.

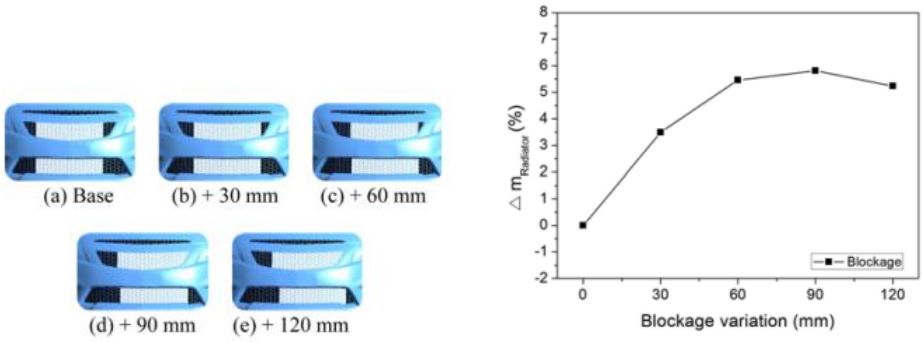

Figure 2-23: Blockage positioning and Mass flow rate based on blockage variation in Kim et al

The mass flow rate steadily increased until the blockage variation was +90mm. However, it decreased at +120mm. The added drag coefficient in the +120mm case.Table 2-5 summarises the literature review process for blockage and fan testing.

Table 2-5: Summary of Fan and Blockage Testing

Study	**Findings**	**Limitations and Future Research**
Datta et al	Larger blockage does not equate to a decrease in heat rejection; side blockage showed a reduction in heat rejection compared to the peripheral case.	Only low air mass flow rates considered
Baskar and Rajaram an	The type of blockages affected the uniformity; side-to-centre blockages were less uniform than horizontal and vertical blockages.	Heat transfer effects were not studied.
Choi et al	Non-uniform airflow led to a 6% decrease in the cooling capacity of an evaporator.	Only a finned-tube evaporator was considered.
Mao et al	Non-uniform parabolic air flow effects were studied, and a decrease of 6% was seen in the heat rejection.	Only a finned-tube evaporator was considered.
Kim et al	The mass flow rate increased until +90mm and then decreased at +120mm.	Simulation will need to be verified by experimental results.

As seen with these studies, it is observed that the testing conditions are not intended for robust real-world driving conditions. Hence, a more comprehensive analysis of the effects on automotive heat rejection systems is required. As seen from the literature review, aspects such as positioning and type of blockage would also need to be considered to get a holistic overview of radiator thermal performance.

2.6 Conclusion

The literature review thus proved that further research is still needed to quantify high-performance automotive thermal heat rejection systems. Heat exchangers have been only studied for niche or low-performance (low Reynold's numbers) flow. The high-performance characterisation of automotive radiators is still inadequate to meet the needs of such automotive thermal heat rejection systems. Similarly, angled configurations only studied low temperatures and air velocities, and blockages and fan testing only considered low air mass flow velocities and simulated results. Thereby, there is a need for testing high-performance, robust thermal automotive heat rejection systems.

3 Methodology

Given the aims of the thesis and the requirements to test different configurations of incidence angles and blockages, it was essential to develop a rig with modular mobile sections capable of having its ducts replaced to provide an optimum configuration to measure heat rejection.

3.1 Test Rig – wind tunnel

Computational Fluid Dynamics (CFD) deals with computer programming and analysis of data structures to model fluid mechanics. Simulations are generated using mathematical equations, and fluid flow is modelled to study objects within certain boundary conditions. Equations such as conservation of mass and momentum can be applied to systems modelled in CFD, enabling a wide variety of flows to be modelled by this method. [46] Although CFD analysis is a cheaper and more straightforward (no physical setup is needed) alternative to real-world testing, accurate results would be needed to be verified by experimental testing.

Test benches are relatively (when compared to wind tunnels) simple sets of instrumentation capable of simulating real-world test conditions in a chamber or other controlled environment. While it is more cost effective and allows for experimental testing, it is most beneficial for testing components. [43] More aggressive forms of testing would require a more elaborate setup.

Wind tunnels are large tubes or connected lengths of ductwork which consist of a fan or a pump to blow air through them, a working section through which the air travels and a test section whereby measurements are taken to quantify the performance of a given element. The front-end ram airflow through an automotive grille is simulated for testing automotive radiators.

The upstream flow is essential to estimate the mass flow rate of the air through the radiator [44]. It should also be noted that due to the grille and other upstream blockages, the air going through the radiator is not the actual velocity of the automobile.

As subsonic (Mach number <0.8) speeds are used to simulate on-road conditions, wind tunnels of this kind can be open-return or closed-loop return [45].

An open return wind tunnel (as seen in Figure 3-1) consists of a fan blowing air through its length and is open at both ends. The air is blown from the fan into the test section and, after that, is recirculated back into the room. The construction of such a wind tunnel is cost-effective and relatively simple.

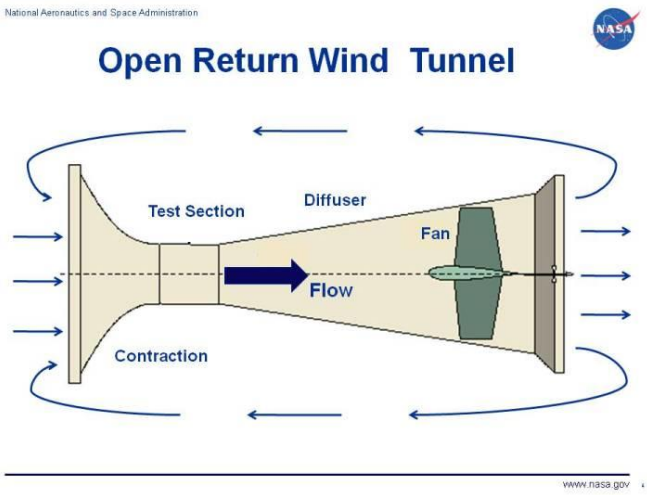

Figure 3-1: Open return wind tunnel [56]

A closed return wind tunnel (as seen in Figure 3-2) recirculates the air from the test section back through the fan. This ensures uniformity and better control of airflow [47].

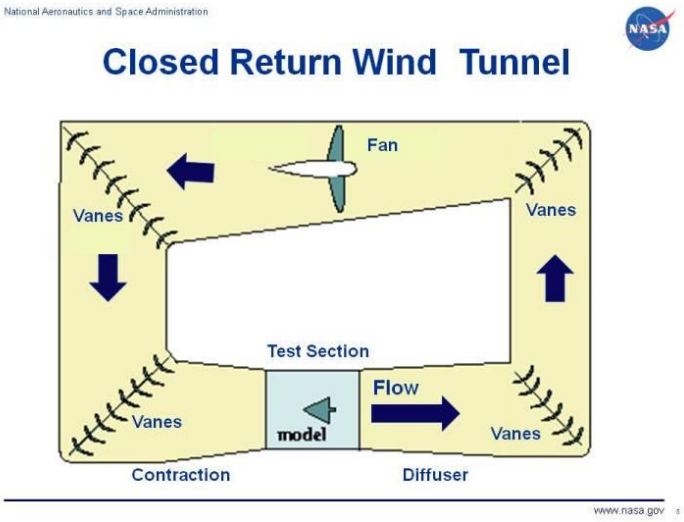

Figure 3-2: Closed return wind tunnel [47]

A comparison of the various methods is given in Table 3-1.

Table 3-1: Summary of wind tunnels and alternatives

Methods	**Complexity**	**Costs**	**Accuracy of Results**	**Need for verification of results**
CFD	Low	Low	Low	High
Test Bench	Medium	Medium	Medium	Medium
Open return wind tunnel	High	High	High	Low
Closed return wind tunnel	Very High	Very High	Very High	Low

Even though the costs and complexity of wind tunnels tend to be high, given the high accuracy of the results and low/no need for verification of results, wind tunnels provide advantages if more aggressive testing is needed.

3.2 Velocity measurement techniques

Aerodynamic and thermal performance in wind tunnels is measured using the average air velocity in the working section. Velocity allows for air mass flow rate calculation, which determines heat rejection. Air velocity is measured by pressure probes or transducers that measure the dynamic and static pressures. A wide range of differential pressure transducer options are available. These make use of devices such as orifice plates, venturi tubes/ nozzles pitot-static tubes to create a pressure drop coupled with a transducer. Finer and more precise methods, such as hot-wire anemometry, are used to measure small and instantaneous changes in velocities using thermal sensors and transducers.

An orifice plate consists of a circular steel plate with a hole in the middle, inserted between flanges between two ductwork sections. Pressure tappings could be made on either side of

the plate. Although it is inexpensive and easy to install and operate [48][49], the permanent pressure loss makes this an unviable option.

Venturi nozzles/ tubes are an alternative wherein the pressure loss can be recovered by using a pipe that consists of a convergent inlet followed by a divergent outlet which gradually converges/ diverges at certain angles. Despite the improvement in pressure loss, the required length and cost of such a sensor make it unfeasible for this application.

Pitot-static tubes are inserted into the ductwork. They are narrow steel tubes which are positioned to face the flow. As there is fluid movement inside the pipe, the airflow generates a dynamic pressure on one side of the pitot-static tube, which in turn generates a stagnation pressure on the other side of the tube. The pressure difference is then measured by the change in the diaphragm placed inside a tube. The principle is shown in Figure 3-3.

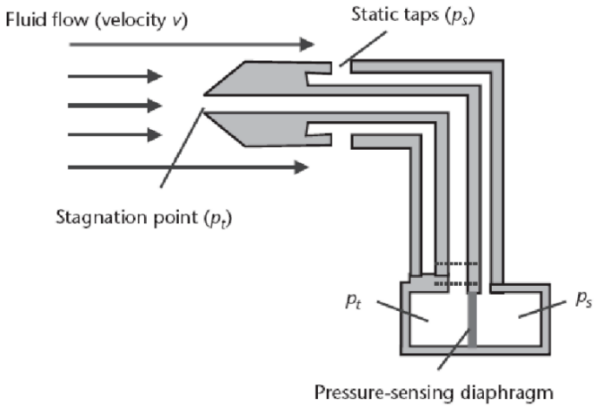

Figure 3-3: Pitot-static tube- construction and principle [50]

According to ISO 3966:2008[30], to accurately measure velocity using a pitot-static tube, an array is required, and an average needs to be taken off the pitot array.

Standard array setups for pitot-static tubes are shown in Figure 3-4. For the given setup, an array of 25 pitot tubes would be required to get an accurate air-speed velocity, or a few pitot tubes would be needed to be traversed across the face of the working section. Besides being incredibly complex, an array of this size would result in a significant pressure drop and add to the airflow's non-uniformity. Given the spatial restrictions associated with the rig, a pitot-static array would not be feasible.

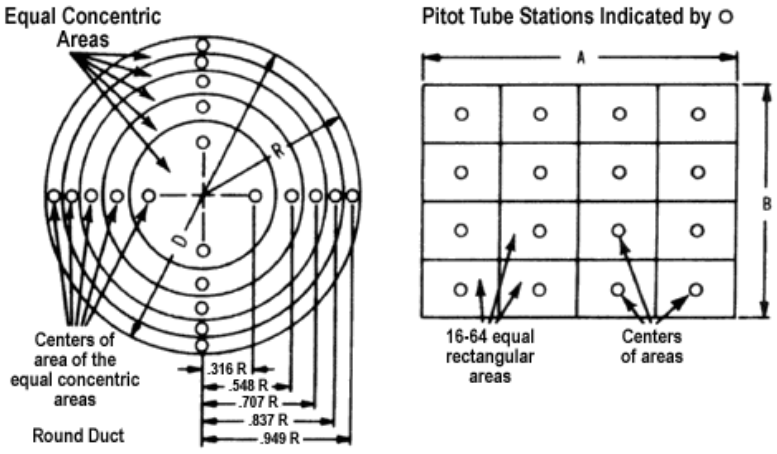

Figure 3-4: Measurement of velocity using a pitot-static array

An averaging pitot tube, shown in Figure 3-5, is a multiport tube which consists of an inner channel and an outer channel; the holes are placed in a log-linear position on the outer channel. The pressure sensors are at the holes where the upstream pressure is averaged, after which the pressure is taken at the internal chamber to lend more accuracy to the measurement.

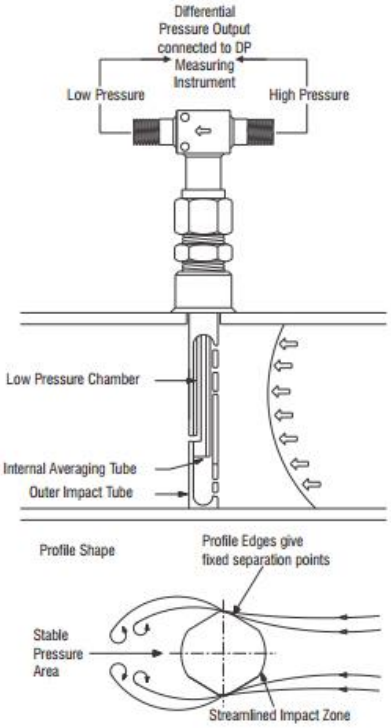

Figure 3-5: Averaging pitot tube

Due to its high-frequency response and accuracy at lower air velocities, hot-wire anemometry is another method which has been frequently used in research [51][52][53].

Hot-wire anemometry passes a current through a taut tungsten, gold or platinum wire, causing it to heat up. The operating principle is shown as a circuit diagram in Figure 3-6. As air flows over the wire, it lowers the wire's temperature. Hot-wire probes can be operated under constant current or constant temperature configuration. Under a constant current, it can be challenging to effectively cool down a wire due to overheating issues or excessive cooling [54][55]. Hence, constant temperature hot-wire anemometry which is based on the principles of a Wheatstone bridge, is chosen for its advantages over its counterpart. The resistance, in this case, directly relates to the change in temperature.

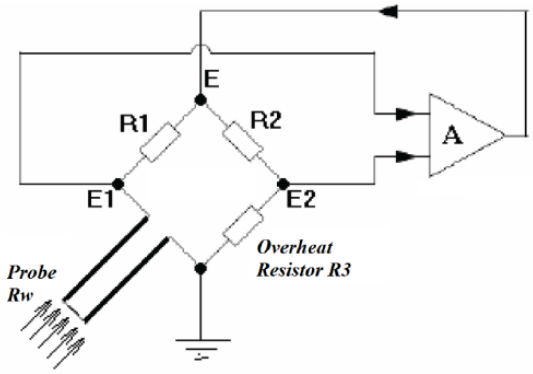

Figure 3-6: Constant temperature hot-wire anemometry [56]

Comparisons of each differential pressure method are shown in Table 3-2. Although averaging pitot tubes are not the most cost-effective and simple option, they have the lowest permanent pressure loss (caused by the equipment). Hence, they offer a distinct advantage when testing under aggressive conditions by providing highly-accurate results without causing excessive pressure loss.

Table 3-2: Summary of Velocity Measurement Techniques

Methods	**Complexity**	**Costs**	**Accuracy of Results**	**Permanent Pressure Loss**
Orifice Plates	Low	Low	Medium	High
Venturi Nozzles	Medium	Low	Medium	Medium
Pitot-static tubes	Very High	Very High	Very High	Medium
Averaging Pitot Tubes	Medium	Medium	High	Low

3.3 Rig Construction

An open return wind tunnel (Figure 3-7 and Figure 3-8) was chosen over a closed return wind tunnel for this research project for the following reasons:

- Relatively inexpensive construction
- Simple design which can be completed in a limited time frame
- No requirements for additional heat exchangers, which would have been required in a closed return wind tunnel
- Space constraints

Figure 3-7: Wind tunnel and the Cooling circuit, respectively

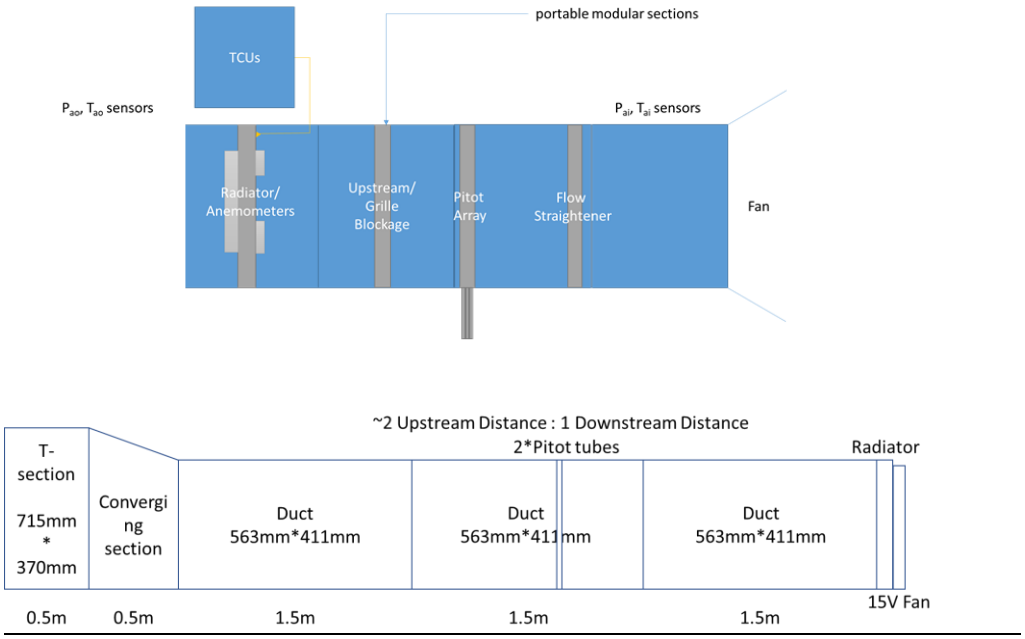

Figure 3-8: Wind-tunnel layout and Rig Schematic, respectively

A centrifugal pump was chosen to pump air into this wind tunnel because it operates with acceptable stability over a large range of airflows and does not produce much noise while operating under a high load. An alternative would have been an axial fan; however, as seen from Figure 3-9, centrifugal pumps are more suited for high-performance applications.

A standard fan performance curve (Figure 3-9) maps the pressure and flow in a graph and determines a pump's efficiency and operating region. The fan performance curve for our pump needs to match the performance data for our testing conditions. As the aim of the experiment is to measure heat performance in aggressive testing conditions, a centrifugal pump is more suited to this.

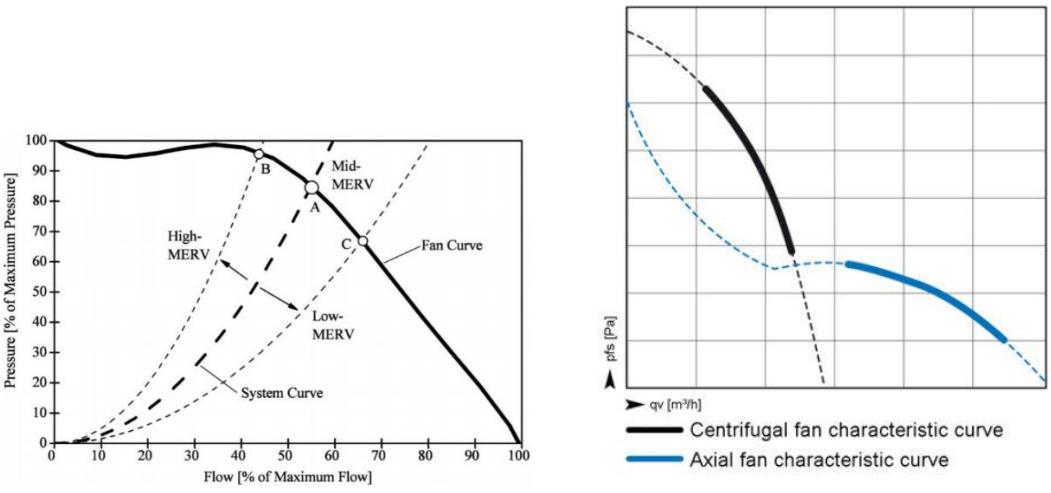

Figure 3-9: Fan-performance curve [57] and Typical Fan-performance curves for Axial and Centrifugal fans [58]

For reasons mentioned in the literature review, a suitable centrifugal pump was chosen for its air mass flow rate/ pressure drop and was connected to a working duct section. Filter papers were used as flow straightening devices, and appropriate design considerations from the

DW144 [59] (industry design standard for ductwork) were considered when designing the ductwork.

For the ease of installation and simplicity of the system, an array of averaging pitot tubes is used in the rig. As the rig needs to be portable, every section of ductwork can be replaced with ease, and for testing different blockages/ angles, different configurations of the rig are essential.

It is important to note that the supplier of the pitot tube recommended that a 2D:D ratio be maintained (upstream and downstream, respectively) for accurate flow measurement in the working section.

Here, D is the hydraulic diameter and can be defined by:

$$D = \frac{2hw}{w+h} \qquad (1)$$

Where h is the height of the rectangular working section and w is the width.

Reynold's number calculations are made according to this, and a correction factor (k) is also determined using this hydraulic diameter and Reynold's number.

As the dimensions of the low-temperature radiator are smaller than the high-temperature radiator, a further contraction is needed to go down from the high-temperature radiator working section to the low temperature charge air cooler section, allowing for transient testing.

Two thermocouple sensors are used in the duct to measure the airflow temperature. An average of the two is used as a measure of the ambient air temperature. Temperature sensors were measured in different locations within the working section, and uniformity in temperature was observed; hence the temperature probes were placed in the section just before the flow straighteners.

By studying expected pressure drops, suitable pressure sensors are chosen with a minimal error rate (as shown in Figure 3-10). To measure the differential pressure, one end of the air-side pressure drop sensor is connected to the top of the pitot tube array (a pressure tap was made between the two pitot tubes). In contrast, the other end of the sensor measures the atmospheric pressure.

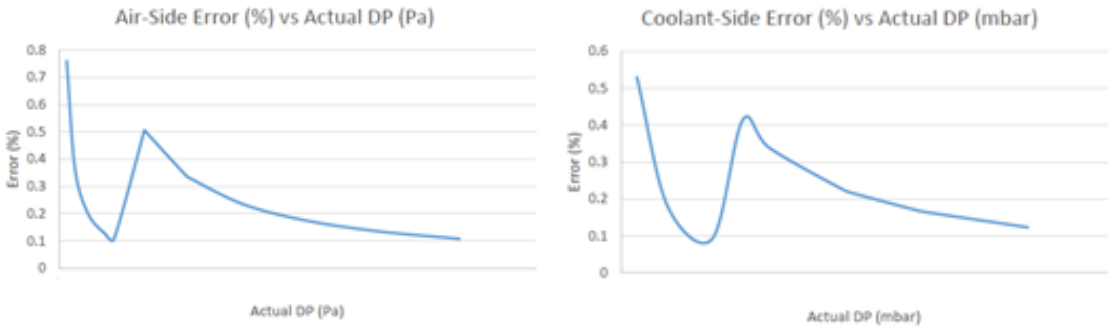

Figure 3-10: Selection of suitable pressure sensors for expected flow conditions

The exact location of the pressure sensor changes depending on the configuration of the rig, whereas the location of the coolant-side pressure sensor remains unchanged. The differential pressure is measured between the coolant's inlet and outlet pressure while it flows through the radiator.

Differential pressure sensors were used to estimate air velocity and are defined by Bernoulli's principle, which is based on the conservation of energy; it states that the change in the velocity of a fluid is inversely proportional to the change in the static pressure.

For an incompressible flow wherein the density of the fluid does not change, this can be represented by the equation,

$$\frac{v^2}{2} + gh + \frac{p}{\rho} = constant \qquad (2)$$

In this equation, v is the velocity of the fluid, g is the constant acceleration due to gravity, h is the height above the plane of reference, p is the pressure, and ρ is the density of the fluid.

When the differential pressure is considered in a closed flow/ pipe case and it is further simplified, then the velocity can be defined as,

$$v = \sqrt{2 * \frac{dP}{P_{static}}} \qquad (3)$$

The two techniques that were employed to measure the air speed velocity in the given wind tunnel were:

- Measuring air velocity by using a set of averaging pitot tubes
- Constant temperature hot-wire anemometry

A hot-wire system is chosen to measure the flow velocity on the face of the radiator. A slot is made in a section of the duct, and with a couple of DC stepper motors, the probe is traversed across the face of the radiator, shown in Figure 3-11. This was needed to verify and provide a correctional factor for the averaging pitot tube measurements as uncertainties in flow were found (simple flow straighteners could not correct these).

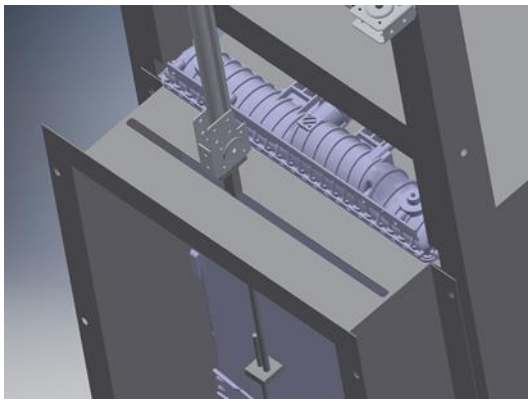

Figure 3-11: CAD drawing of the hot-wire probe and traversing system

Ambient temperature and atmospheric pressure on the day were measured; simple flow straighteners could not correct these although these parameters remained mostly unchanged (minor differences were observed) throughout the experiment. These changes were not expected to cause major changes to the experiment results.

As shown in Figure 3-12, the cooling circuit for the rig serves both the high-temperature radiator circuit and the low-temperature charge air circuit. Depending on which circuit is being used, appropriate piping and valve alterations are made. Temperature Control Units (TCU) are responsible for bringing the temperature of the coolant up to a desired 95°C; this is then

passed through the circuit. The high-temperature and low-temperature radiators used in this study are louvred-fin downflow radiators with herringbone fins.

For the high-temperature circuit, the two temperature control units provide heated coolant to the flow circuit. They have individual valves to control them, and a PID is set for the same. The heated coolant flows through the circuit as the valves in the red are shut (low-temperature circuit); the coolant flows through the circuit into the high-temperature radiator, which is then cooled by airflow from the centrifugal fan and passes through a flow meter, thereafter. The inlet and outlet for the low-temperature radiator are closed off in this rig, and the low-temperature radiator itself is disconnected.

For the low-temperature circuit, the valve going into the high-temperature radiator is closed, and all the red valves are open. A separate liquid-liquid heat exchanger controls the temperature of the coolant flowing through the charge air cooler. Cooling water is passed through the heat exchanger, lowering the coolant temperature. This is then pumped into the hotter coolant, which flows through the high-temperature radiator coolant circuit (as the radiator is not connected). Valves control the mixture of the hot and cold coolant providing decent control for dynamic temperatures. The inlet and outlet for the high-temperature radiator are closed off in this rig, and the high-temperature radiator itself is disconnected.

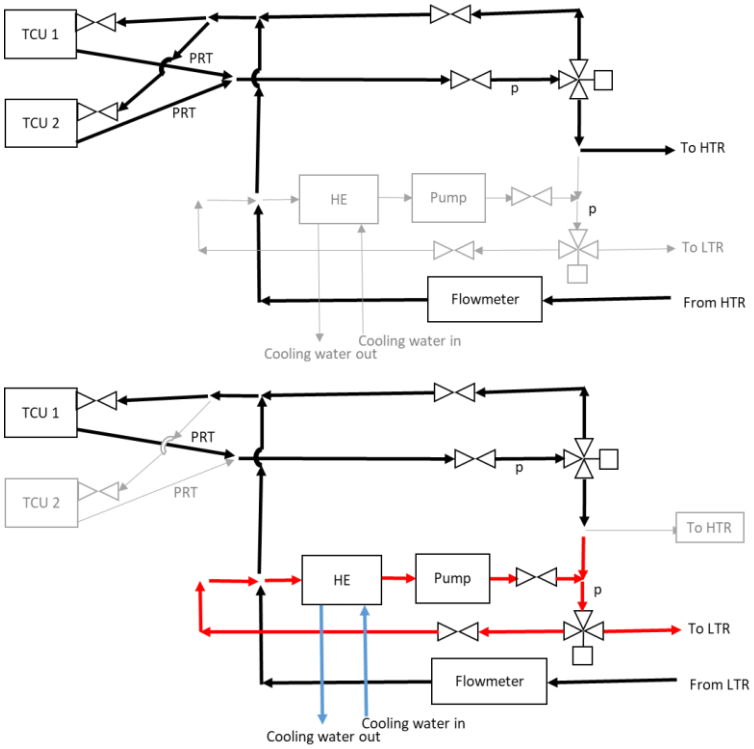

Figure 3-12: Cooling circuit for HTR (top) and LTR (bottom)

The current rig capabilities are defined in

Table 3-3. Room for expansion of the rig has been factored into the rig as the variable parameters (coolant temperature, coolant flow rate, TCU power and airflow) are additional capacity for more aggressive testing.

Table 3-3: Current Rig capabilities

Parameter	Value
Max Coolant Temperature	120°C
Max Coolant Flow Rate	200lpm
Temperature Control Unit (TCU) Power	2x 75kW
Max Airflow	$3m^3/s$

The high-temperature radiator configurations tested are tabulated below in Table 3-4. As seen in the literature review section, these aspects of the radiator have a pronounced effect on heat rejection. They can be incorporated into the design and placement of an automotive radiator. Hence, these are analysed within the scope of this study; other aspects of the radiator, such as the fin configuration, depth and length, would involve cross-sectional analysis and changing the physical attributes of the radiator itself. Thus, only the incidence angle, blockage and fan effects were studied as part of this thesis. As a variety of air and coolant flow rates are to be tested to get a comprehensive understanding of automotive thermal heat rejection systems, coolant flow rates of 30-180lpm (with 30lpm increments) and airflow velocities of 2-10m/s were considered for this thesis (with 2m/s increments). This ensured that high-performance/more aggressive heat rejection was measured for the high-temperature radiator.

Table 3-4: HTR Testing configurations

Tests/Conditions	**Angle**	**Blockage**	**Fan**	**Illustration**
Baseline configuration				
Baseline HP - 90Deg	No	No	No	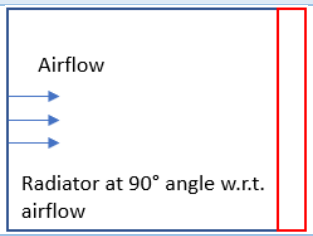
Angled configurations				
HP - 15Deg	15 Deg	No	No	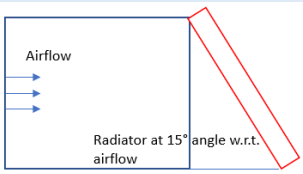
HP - 25Deg	25 Deg	No	No	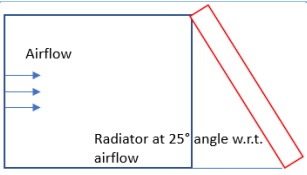
HP - 35Deg	35 Deg	No	No	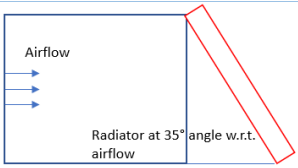
Fan configurations				

HP - 13.6V fan	No	No	13.6V	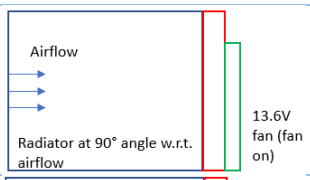
HP - 0V fan (fan mounted on the radiator but not operational)	No	No	0V	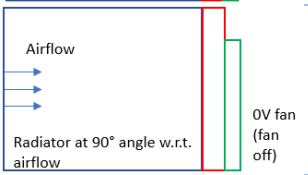
Blockage configurations				
HP - 0.5m	No	0.5m	No	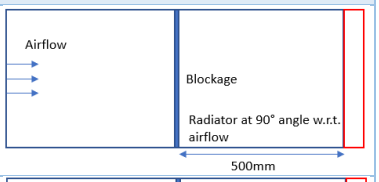
HP - 1m	No	1m	No	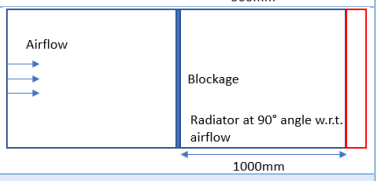
Combined configurations				
Case 1	No	0.5m	13.6V	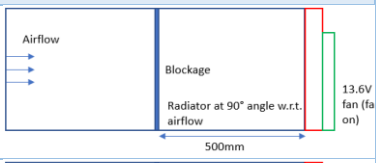
Case 2	No	1m	13.6V	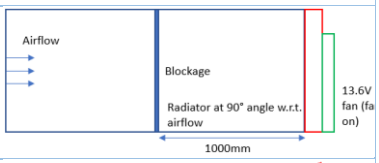
Case 3	35 Deg	0.5m	No	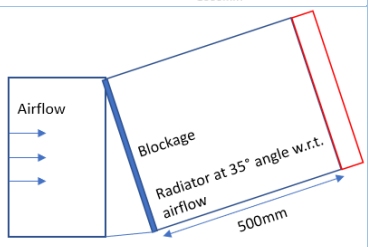
Case 4	35 Deg	1m	No	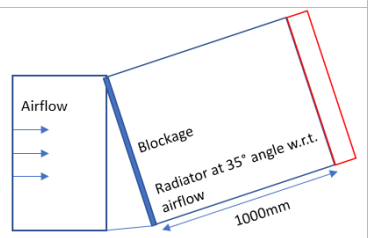
Case 5	35 Deg	0.5m	13.6V	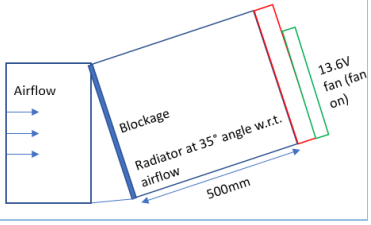

Case 6	35 Deg	1m	13.6V	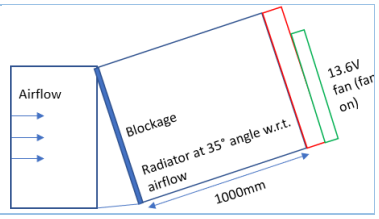

Various testing configurations were tested wherein the angle of the taper, positioning of the blockage and position/voltage of the fan was varied. The heat rejection was studied for each case, and the results were analysed and discussed using delta plots.

Errors for the experimental rig are mentioned below.

- Equipment Error (this includes various sensors and pitot tubes): 2%
- Ambient air temperature measured: ±1.5°C
- Coolant temperature measured: ±1°C
- Hot-wire anemometer error: 2% for ±1°C change in ambient air temperatures

Given the measurement errors, the error in heat rejection can be predicted to be 2.5% (at lower air velocities) - 5% (at higher air velocities).

3.4 Heat Transfer Calculations

A thermodynamic system within a simple radiator is described in Figure 3-13. A difference between the two enthalpies gives heat rejection. Heat flowing from the hotter fluid (normally coming in from the inlet) is transferred to the cooler fluid (normally going out through the outlet). This change can be depicted as the following.

$$Q = H_1 - H_2 = m(h_1 - h_2) \quad (4)$$

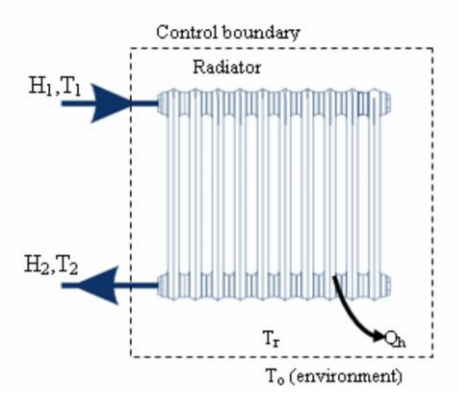

Figure 3-13: Thermodynamic System for An Automotive Radiator[8]

For steady-state testing, the heat transfer can be defined by . A simple energy balance equation can be used [62].

$$Q = \dot{m} C_p dT \quad (5)$$

Here,

[8] Figure taken from Konjusha, E. and Krasniqi, F. (2007) 'Exergy analyses of heating systems with radiators', Annals of DAAAM & Proceedings,, 383+, available: https://link.gale.com/apps/doc/A177174655/AONE?u=anon~90a3a70c&sid=googleScholar&xid=dc4f4538

Q is the total heat rejection, ṁ is the mass flow rate (kg/s), Cp is the specific heat capacity (kJ/kg/°C), and dT is the difference in temperatures before and after being passed through the heat exchanger.

As certain parameters, such as the specific heat capacity, tend to vary for transient testing, different methods can be used to estimate the heat transfer.

As mentioned above, the energy balance equation is to be used to calculate heat transfer. It can be rewritten as:

$$dQ = UAdT \quad (6)$$

Here,

A is the area, and U is the general heat transfer coefficient.

For automotive heat exchangers, this heat transfer coefficient can depend on coolant and air flow rates, coolant properties and the overall geometry of a heat exchanger. When assuming one-dimensional flow, the overall heat rejection/heat transfer coefficient should be defined by the overall convection (between air and radiator) and conduction (within the radiator itself). A general one-dimensional flow diagram is shown in Figure 3-14, where t_i to t_1 and t_2 to t_o are stages of convection, whereas t_1 to t_2 is the conduction stage.

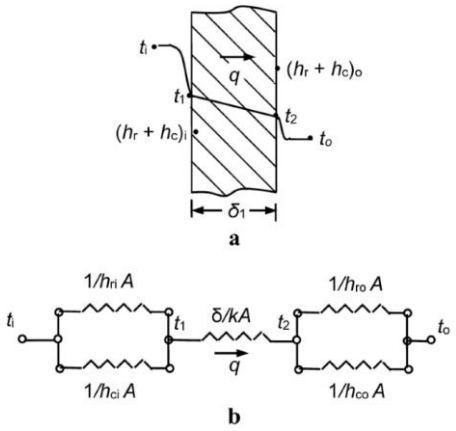

Figure 3-14: Convection and Conduction within a Heat Exchanger[9]

A modified approach to the Efficiency-NTU method has been used to study transient heat transfer effects in a previous study. [60] Hence, an approach tailored to the current testing configuration could be effective when considering the aforementioned method.

This can then be integrated into the Epsilon (efficiency) equation. For crossflow radiators, Gnielinski [64] devised the following equation for the Efficiency-NTU method.

$$\varepsilon = 1 - exp\left(\frac{(NTU^{0.22}.(exp(-C^*.NTU^{0.78})-1)}{C^*}\right) \quad (7)$$

Where, C* can be defined by the following equation.

[9] Figure taken from Bhaskaran, R. and Collins, L., n.d. Introduction to CFD Basics. [online] Dragonfly.tam.cornell.edu. Available at: <https://dragonfly.tam.cornell.edu/teaching/mae5230-cfd-intro-notes.pdf>

$$C^* = \frac{Cmin}{Cmax} = \frac{(m.C_p)min}{(m.C_p)max} \qquad (8)$$

This efficiency value can then be used to calculate the outlet temperature of the coolant (and, if needed, the air outlet temperature) using the inlet temperatures and corresponding specific heat capacity at constant pressures of both the coolant and air.

$$T_{coolant,out} = T_{air,in} - \varepsilon.\frac{C_{min}}{C_{air}}.(T_{coolant,in} - T_{air,in}) \qquad (9)$$

This method was used to calculate the coolant's transient outlet temperature in the LTR.

3.5 Testing Matrix

The following matrix (Table 3-5) of testing points was considered to compare several data points.

Table 3-5: Table used for Data Comparisons

Point	Coolant flow rate	Velocity
	lpm	m/s
1	180	2
2		4
3		6
4		8
5		10
6	150	2
7		4
8		6
9		8
10		10
11	120	2
12		4
13		6
14		8
15		10
16	90	2
17		4
18		6
19		8
20		10
21	60	2
22		4
23		6
24		8
25		10
26	30	2
27		4
28		6
29		8
30		10

Heat rejection (kW), heat dissipation (kW/m^2/°C) and airside pressure drop (Pa) were the parameters which were used to quantify the heat rejection of the thermal heat rejection system.

4 Results and Discussion

4.1 LTR-Transient Testing and Modelling

To ensure that objective 1.1.6 would be met, the transients in this study were to be analysed using the ε-NTU method. McLaren Automotive provided the required drive cycle, and, it simulated on-track conditions. A model was then made that replicated the real outlet temperatures with a good level of fit.

The duration of the drive cycle was 79s, and it was characterised by the graphs in Figure 4-1.

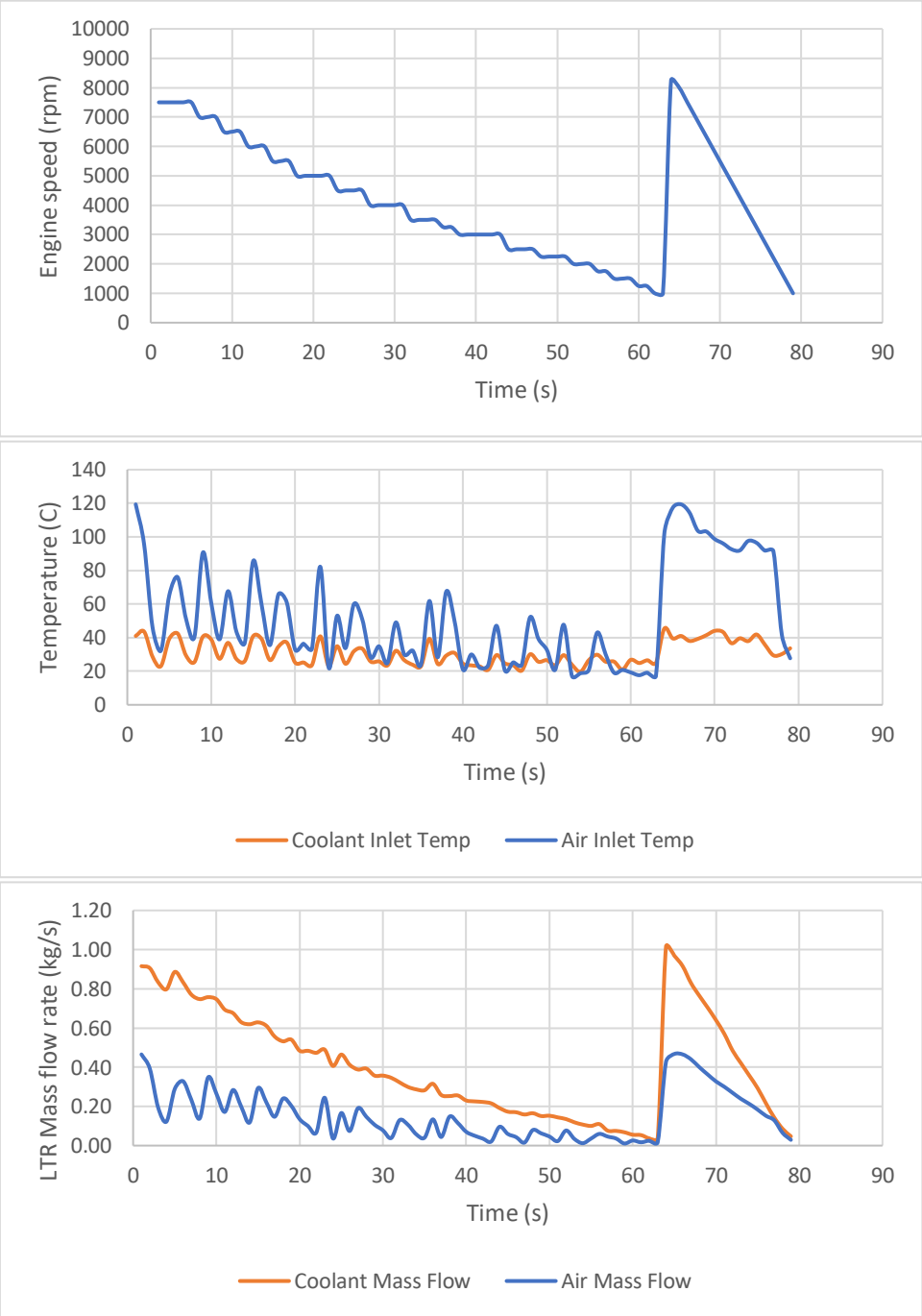

Figure 4-1: Transient drive cycle characteristics

The data was obtained from McLaren for their low-temperature radiator, as physical tests were not possible within the project's timeframe with the resources provided. The steady-state results of this study's low-temperature radiator were then mapped against the transient drive cycle characteristics of the McLaren low-temperature radiator. Other values, such as engine load, were not available. The data provided was then processed and the logic diagram (Figure 4-2) denotes the process used.

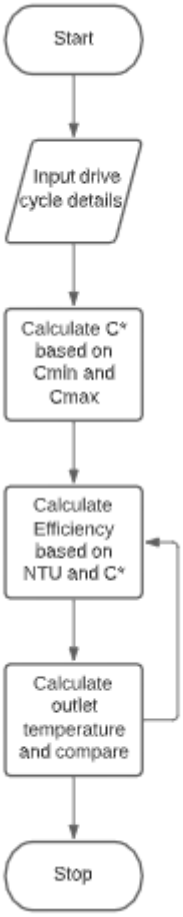

Figure 4-2: Process Flowchart

Due to restrictions in testing, steady-state testing for the LTR-simulated WCAC circuit could not be carried out. Hence, an alternative approach was taken to estimate the NTU values.

In order to calculate NTU values, the overall heat transfer coefficient was needed. This can be denoted by a simple 1D following equation and denoted in Figure 4-3.

$$1/U = \left(\frac{1}{h_1} + \frac{\delta}{k} + \frac{1}{h_2}\right)^{-1} \qquad (10)$$

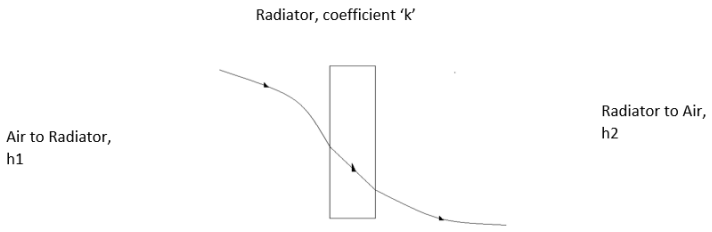

Figure 4-3: 1D heat transfer flow

Where h1 and h2 are the convective heat transfer coefficients for air, and δ and k are the LTR's thickness and conductive heat transfer coefficients. The heat transfer coefficient for Aluminium is fixed.

For the current system, taking the minimum possible value for the unknown heat transfer coefficient, we get NTU values of 1.5-2 (this would be the value obtained when heat is being transferred when air and radiator temperatures would be the same at $t \to \infty$) for the more aggressive testing conditions at the start and the end of the test and values of 3+ for the other testing points.

The value for C^* obtained approaches zero. As can be observed from Figure 4-4, the efficiency for any NTU value above 2 is about 90%, and the differences in NTU values do not make much of a difference in estimating outlet temperatures due to minimal changes in efficiency. Hence, we can take the NTU for the given rig to be 3 (the actual value of NTU would be between 2 and 3, which could not be correctly predicted because of the limited data available, however, given the near identical effectiveness, 3 was deemed appropriate). To predict heat rejection, a difference between the two did not yield results that were too dissimilar. However, future testing could involve determining exact values to yield more accurate results.

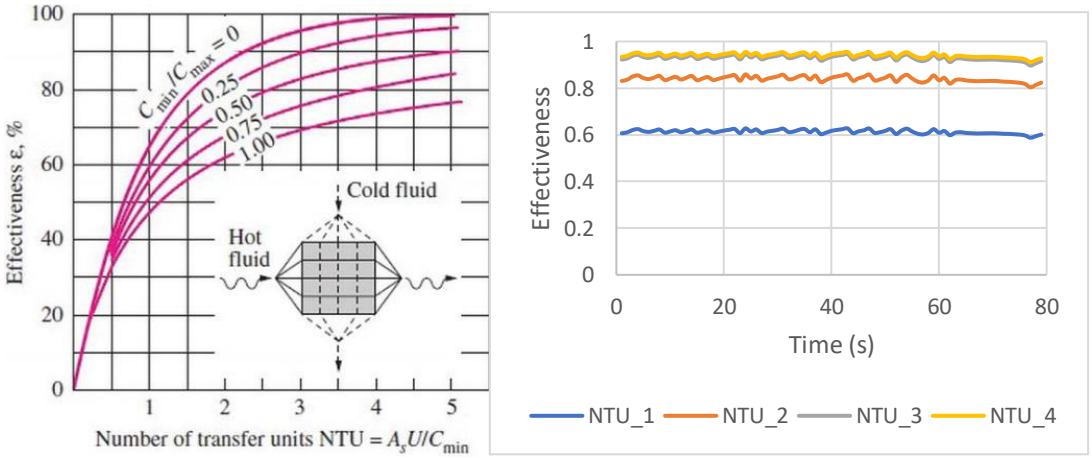

Figure 4-4: NTU graphs for crossflow radiators [61] and Efficiency for Different Number of Transfer Units

Given the conditions, the heat rejection was calculated.

As can be seen from Figure 4-5, the model for transient testing fits the actual data well. Hence, the transient temperature was predicted with reasonable accuracy (the average difference between the two readings is only 4%). The calculated heat rejection is limited by the NTU model as this doesn't offer a high standard of accuracy; this is particularly visible in cases with high changes in heat rejection rates as the difference between the two readings increases to 10% in these cases.

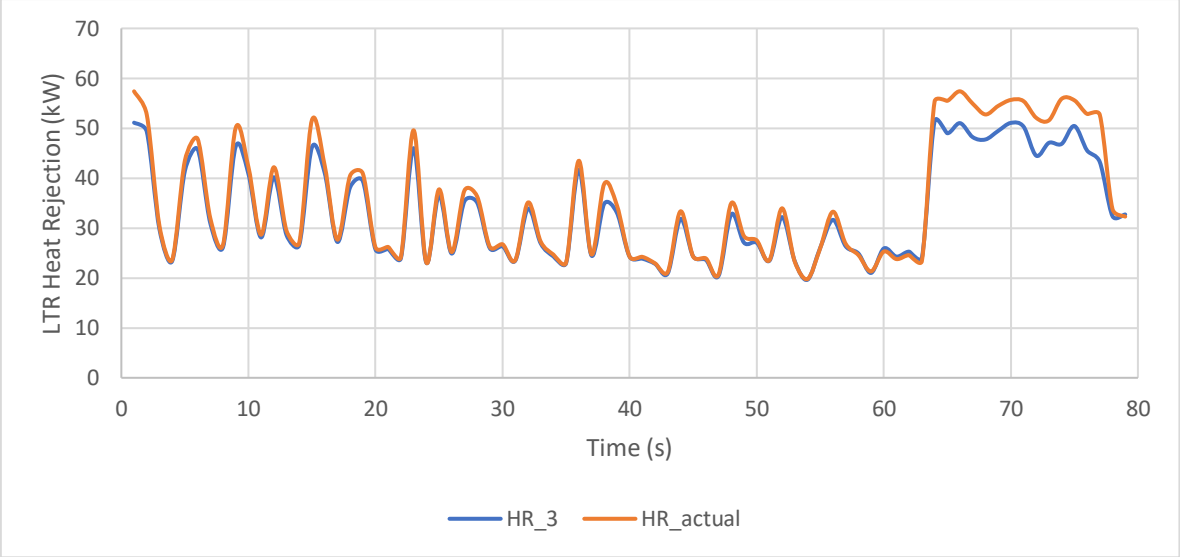

Figure 4-5: Comparison of Calculated Heat Rejection with NTU=3 and Actual Heat Rejection

Hence, although the results can be improved for the more aggressive testing conditions, the current NTU method limits the option.

4.1.1 Limitations and Future Work

As only a limited amount of data was available, certain assumptions were made. The purpose of this chapter was to only provide a base for future work to be conducted. Hence, the limitations observed did not strictly impede the progress of the LTR research for this thesis.

- Steady-state data was available for a low-temperature radiator; however, McLaren's transient cycle data might not have been completely compatible with the data.
- The value of NTU was assumed to be 3 due to the lack of data and an inability to verify it.
- To improve upon the current results, further steady-state and transient tests would need to be carried out, and the model would be required to be optimised for several (different) transient drive cycles.
- Using the lumped capacitance model rather than an NTU model, thermal inertia could also be obtained.

4.2 HTR- Baseline testing results

Preliminary testing (as stated in objective 1.1.1) was carried out for the baseline (no inclination, no fan and no blockage case). Based on the literature review and appropriate industry standards, an array of air and coolant flow rates was chosen, and the heat rejection data was measured.

Figure 4-6 denotes the measured parameters.

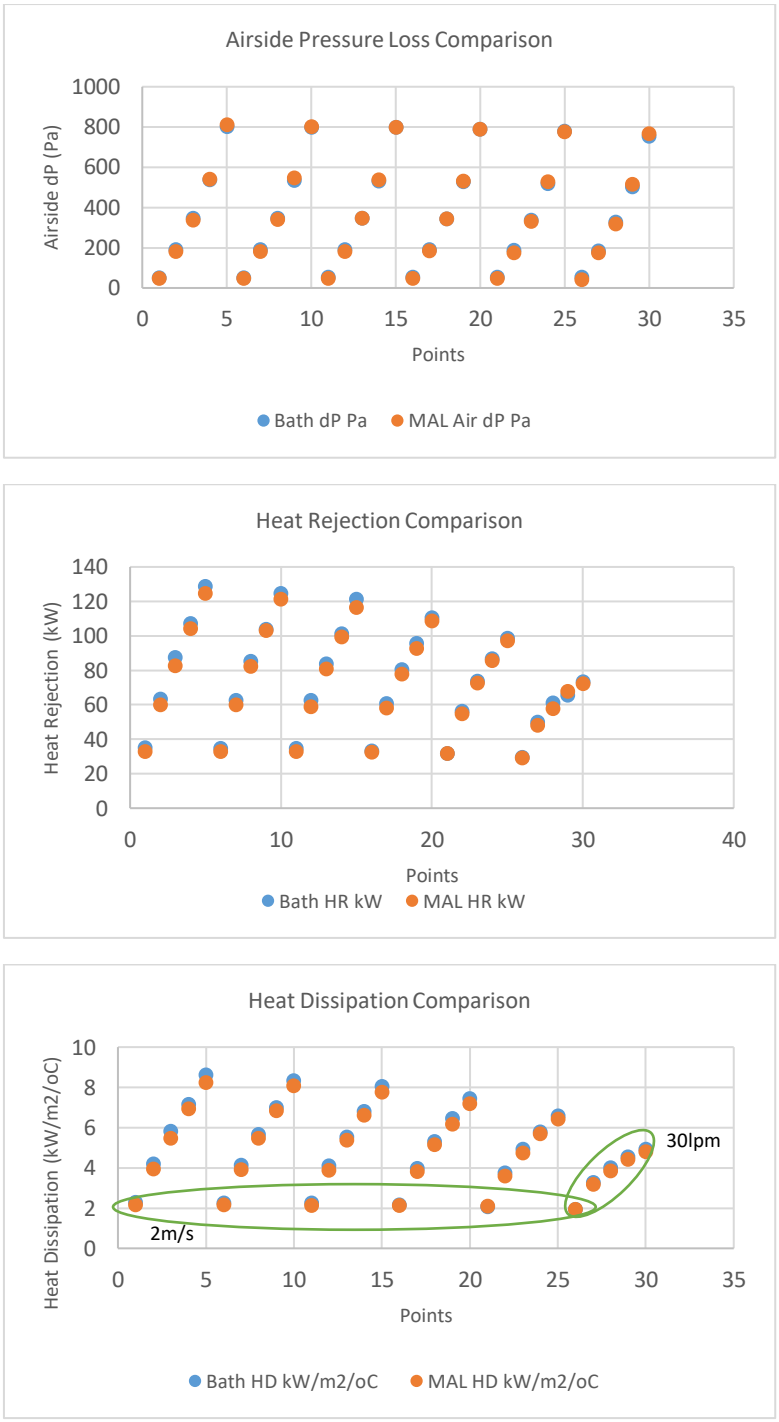

Figure 4-6: Heat rejection data for the Baseline case

As seen from the table and the figure, the heat rejection data has been calculated. It was compared against McLaren baseline (MAL) data for flow rates of 30-180lpm and air velocities of 2-10m/s. The results were in accordance; hence, the rig was running successfully. Points 1-5 (2-10m/s at 2m/s intervals) were for 180lpm, 6-10 were for 150lpm and so on. As seen in the figure, for constant coolant flow rates (column-like shapes in the figure), heat rejection shows an increase with an increase in air velocity. For constant air velocity (row-like shapes in the figure), heat rejection is almost constant for lower air velocities. Increases in heat rejection are prominent with an increase in coolant flow rates for higher air velocities (exceeding 6m/s).

Baseline tests were performed in order to validate the current mobile wind tunnel setup. The results for the MAL testing were obtained from McLaren, who contracted a test house to undertake wind-tunnel testing for the same. Airside pressure loss was compared and was found to be a near-identical match. Heat Rejection and Dissipation data (McLaren's term for the heat transfer coefficient) were plotted for 10m/s (the largest deviation from MAL data was seen here) and compared in Figure 4-7.

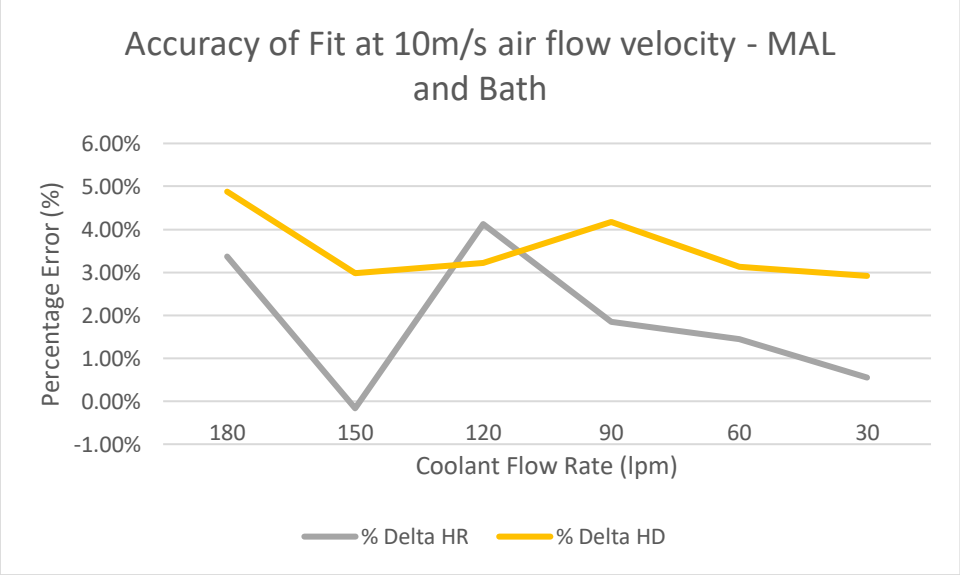

Figure 4-7:Accuracy of Fit – MAL and Bath Comparison at 10m/s airflow velocity

It was observed that the level of fit did not drop below 95%. Hence, this rig was deemed acceptable. This, therefore, ensured that objective 1.1.2 was met.

Delta Plots were also compared where the Difference between two Heat Rejection rates was plotted, and the results were studied to determine which case had a higher rate of heat rejection.

The syntax for the subsequent comparisons made is as follows.

$$HR_1 - HR_2 = Heat\ Rejection\ for\ Case\ 1 - Heat\ Rejection\ for\ Case\ 2 \qquad (11)$$

To provide for ease of comparison, each graph plotting heat rejection and pressure drop for 30 points is accompanied by delta plots, allowing for comparing heat rejection in two different testing cases.

4.3 HTR- Angle of incidence testing

To ensure the angle of incidence effects were studied and objective 1.1.2 was met, appropriate angles (15°, 25°, and 35°) were selected for the testing based on the literature review carried out and they were cross-referenced against the most common radiator configurations used in the industry which were then used for the purposes of this study. Baseline tests were carried out for the 90° case where the radiator was placed perpendicular to the flow. These angled tests ensured that objective The alignment of the radiator w.r.t airflow can be seen in Figure 4-8.

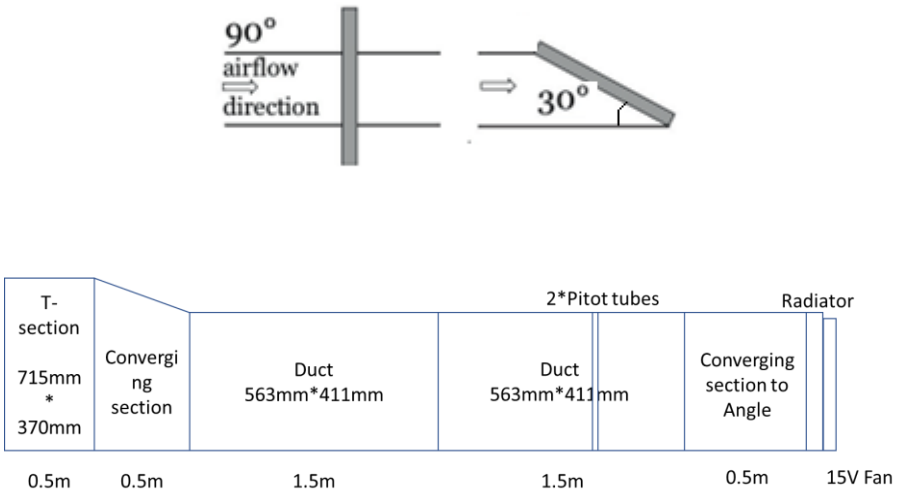

Figure 4-8: Example of Angle of Incidence Setup

In all three cases (15°,25° and 35°), heat-rejection (Figure 4-9) and airside dP (Figure 4-10) were plotted against the air velocities, and it was observed that the flow rates themselves only had a marginal impact on the pressure loss. The pressure loss only increased by 1% for the 15° case, 3.6% for the 25° case, and 6% for the 35° case, with the increase in coolant flow rate (from 30-180lpm). However, when the air velocity was increased (from 2-10m/s), the pressure loss increased by 19 times for the 15° case, 17 times for the 25° case and 16 times for the 35° case (Baseline 90° case also showed a 17-fold increase in pressure loss).

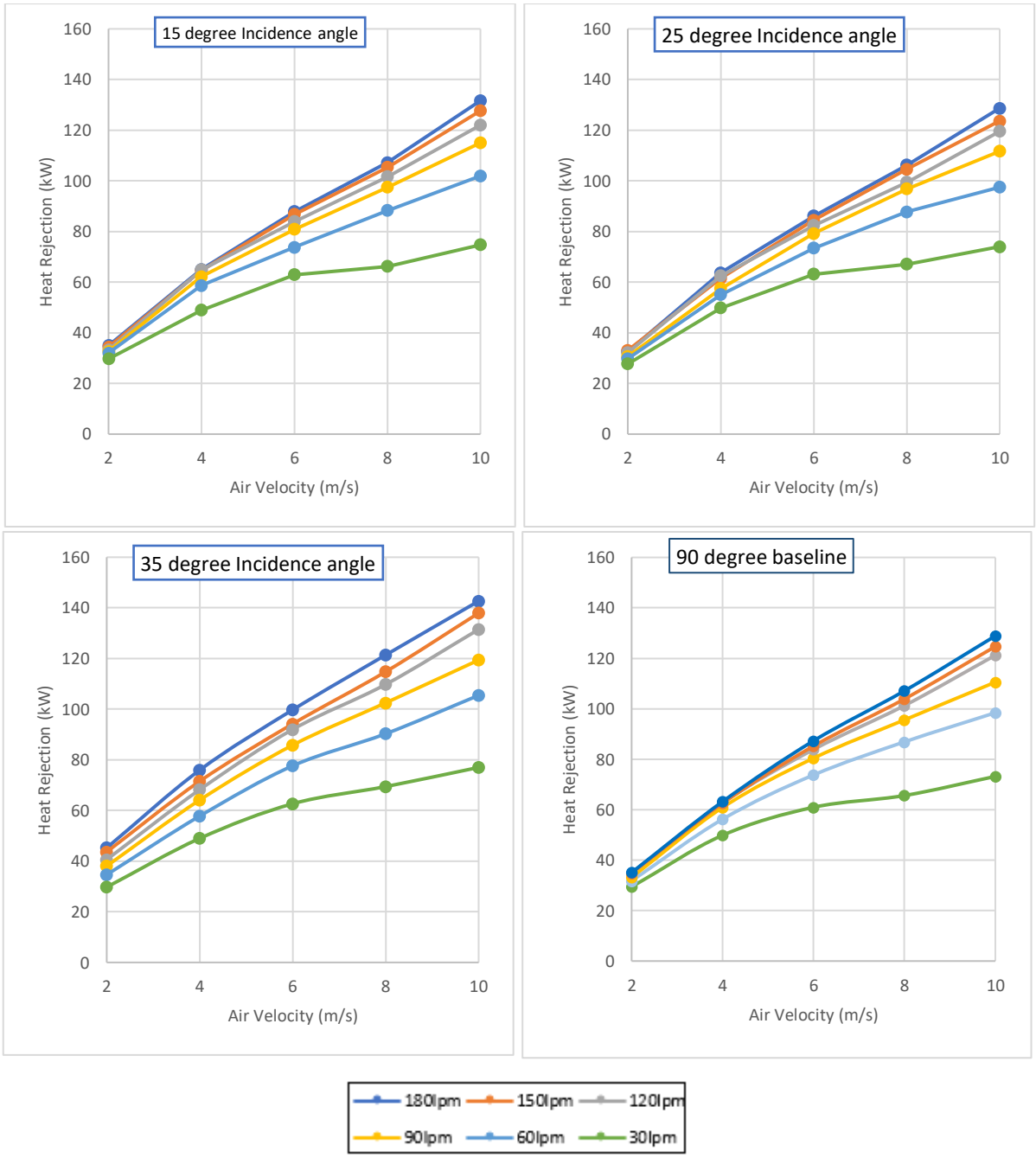

Figure 4-9: Heat Rejection against Air Velocity for Coolant Flow Rates

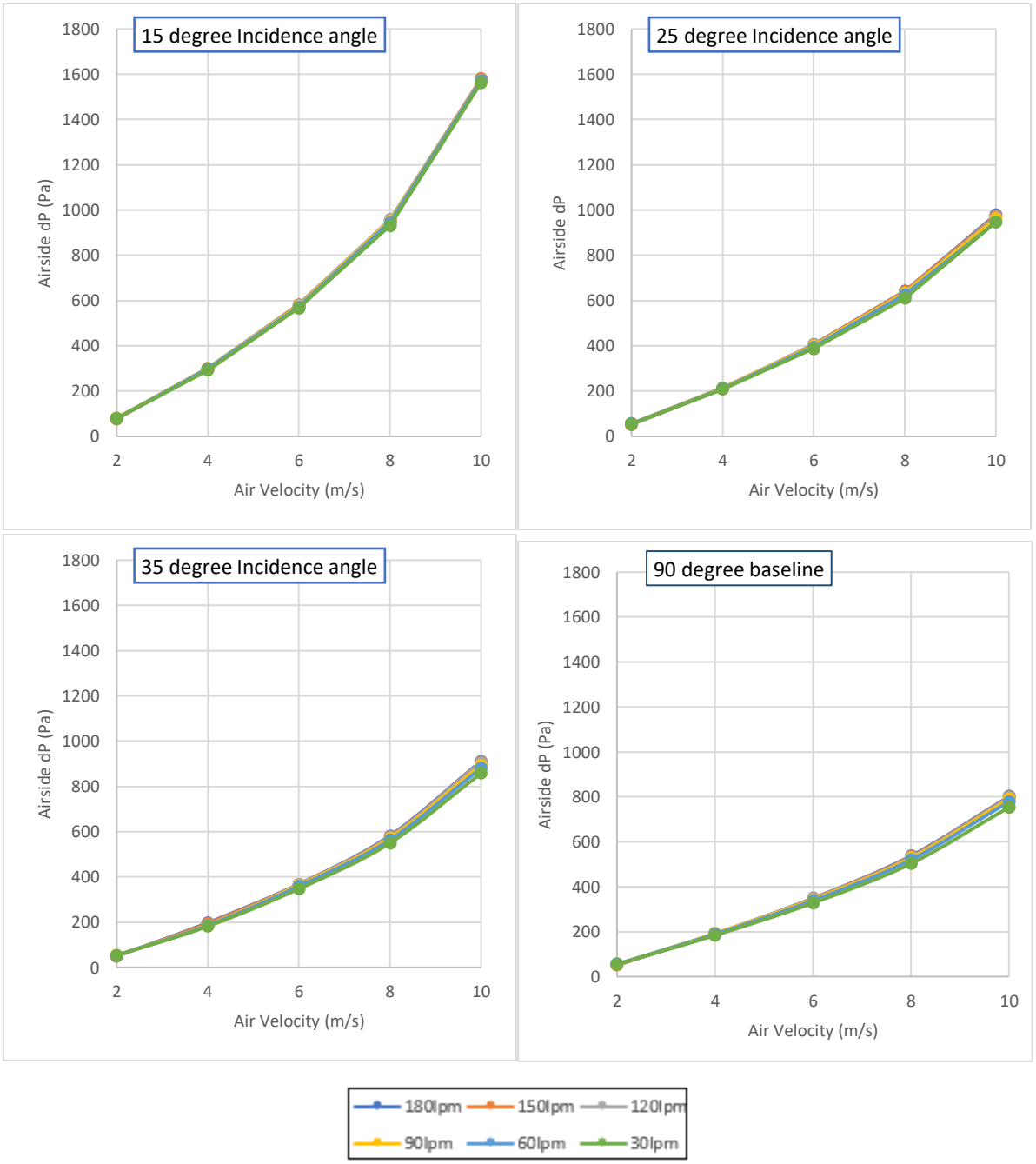

Figure 4-10: Airside dP against Air Velocity for Coolant Flow Rates -

Compared to the baseline tests, the maximum pressure loss increased by 107% for the 15° case, 25% for the 25° case and 10% for the 35° case. It was seen that the 15° and 25° cases had similar heat rejection and dissipation values due to the acute angle of the airflow on the face of the radiator. However, the 35° case showed better heat rejection than the other two cases indicating that forced convection might come into play, in that case, allowing for the louvres to divert flow effectively. To get a better idea of heat rejection characteristics for the angled configurations, delta plots show the differences in heat rejection between the angled cases and the baseline case.

4.3.1 Delta Plots - Angled Comparison

As seen in the plots in Figure 4-11, for the 30lpm case, the delta heat rejection doesn't show much variation for air velocities of less than 6m/s. However, there is a distinct difference between the 35° case and the other angles for higher air velocities.

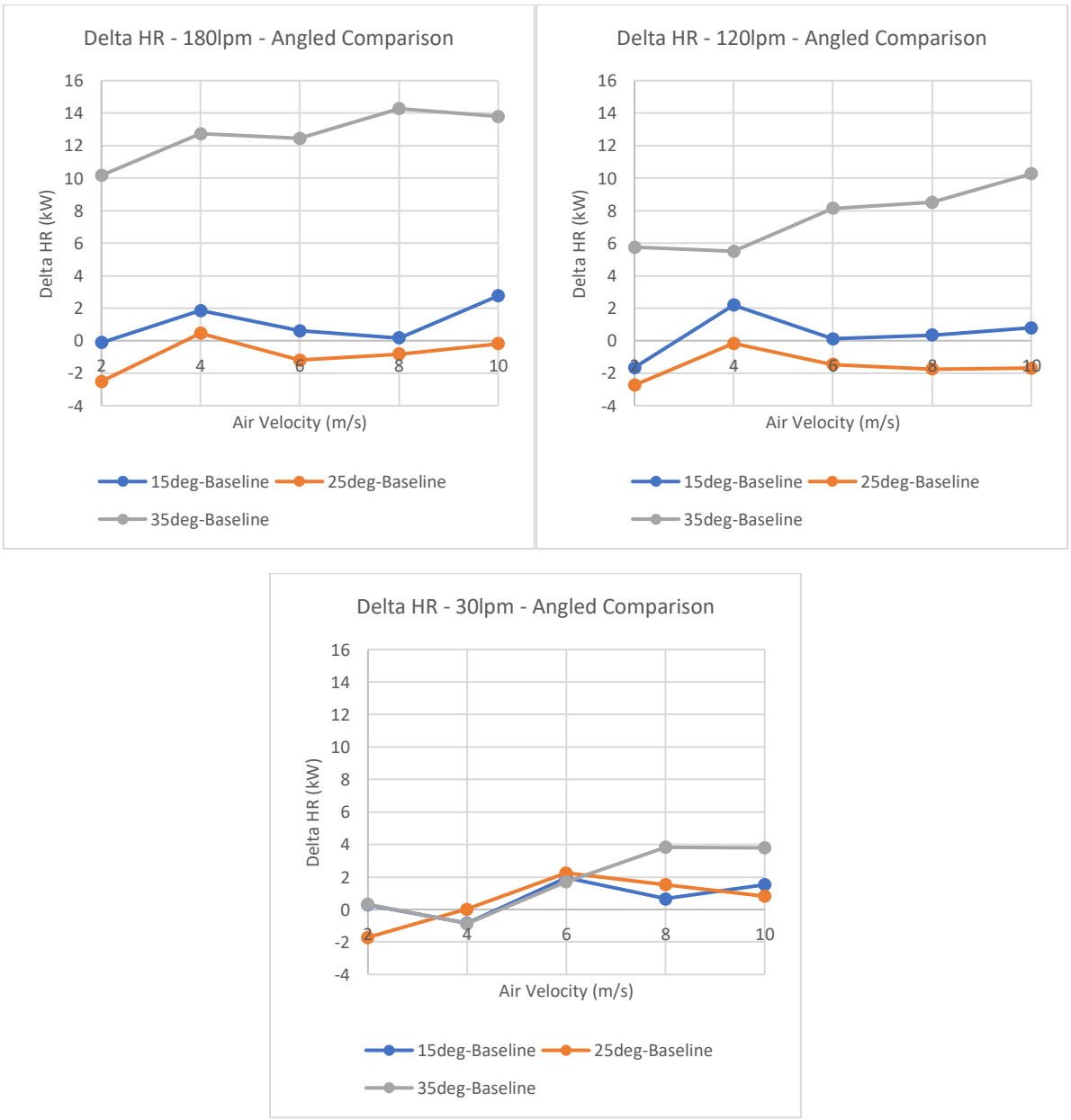

Figure 4-11: Delta HR Plots - Angled Comparison

For the 120lpm and 180lpm cases, the differences were more pronounced. The 15° and 25° cases did not see a great deal of deviation from the baseline case. The differences between the 35° and baseline case were much more prominent. A definite increase in heat rejection was seen, and this further increased with the higher air velocities. For the 180lpm, the 35° case showed an improvement of about 14kW for air velocities of the 8m/s and 10m/s cases. Again, the louvred fins are believed to enhance the heat rejection for the 35° case. A possible reason for the enhancement of heat rejection in only the 35° case would be the additional direct convection caused by the inner geometry of the radiator. Further analysis could be carried out by examining the cross-section of the high-temperature radiator; this would involve cutting a similar radiator in half to study the dimensions and characteristics of the radiator,

such as the fin length, depth, height and so on. Additionally, increases could be attributed to the increased airflow generated in a tapered section of the rig.

4.4 HTR- Blockage and Fan Testing

As mentioned in the literature review, blockages need to be considered to get a holistic analysis of the effects of non-uniformities due to spatial constraints. These represent the layout of the components upstream of the face of the radiator rather than debris or rust caused by the operation of a vehicle. Blockages represented by this testing include underhood components depicted in Figure 4-12. To ensure that objectives 1.1.3,1.1.4, and 1.1.5 were met, the heat performance was measured when blockages upstream of the radiator were used, when a radiator fan was used, and when a combination of all non-uniformities was tested.

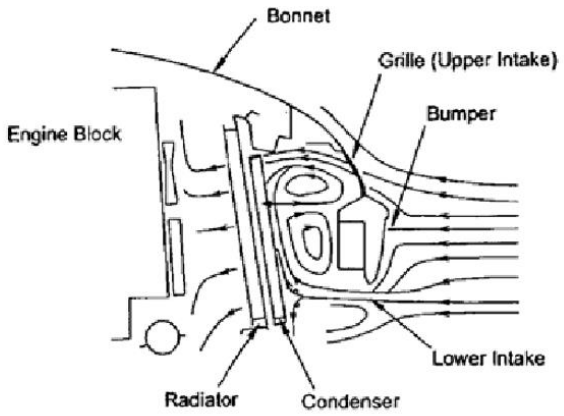

Figure 4-12: Conventional automotive underhood assembly, which would need to be simulated by blockages[10]

A suitable blockage (criteria depicted in Figure 4-13) with an open area of 70-80% was selected, and a millimetre thickness, as per McLaren Automotive's specifications and as they planned to place the radiators in front of the rear wheels, blockages were considered for the baseline 90° and 35° cases. This was then placed in several different locations, and the radiator's heat rejection was measured thereafter.

[10] Figure taken from Ng, E., Watkins, S. and Johnson, P., 2004. New pressure-based methods for quantifying radiator airflow. Proceedings of the Institution of Mechanical Engineers, Part D: Journal of Automobile Engineering, 218(4), pp.361-372.

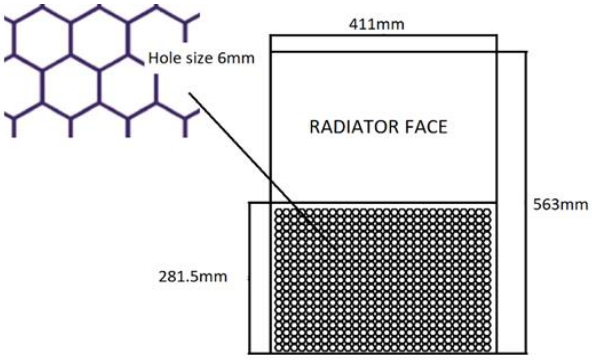

Figure 4-13: Blockage criteria

The performance was measured with and without an axial fan supplied by McLaren. This was attached to the back of the radiator, and a constant voltage of 13.6V was supplied to it (15V fan). The fan's performance data, as supplied by the manufacturer Comex, is shown in Figure 4-14. Maximum rated power is estimated at 150W, given a current of 10A.

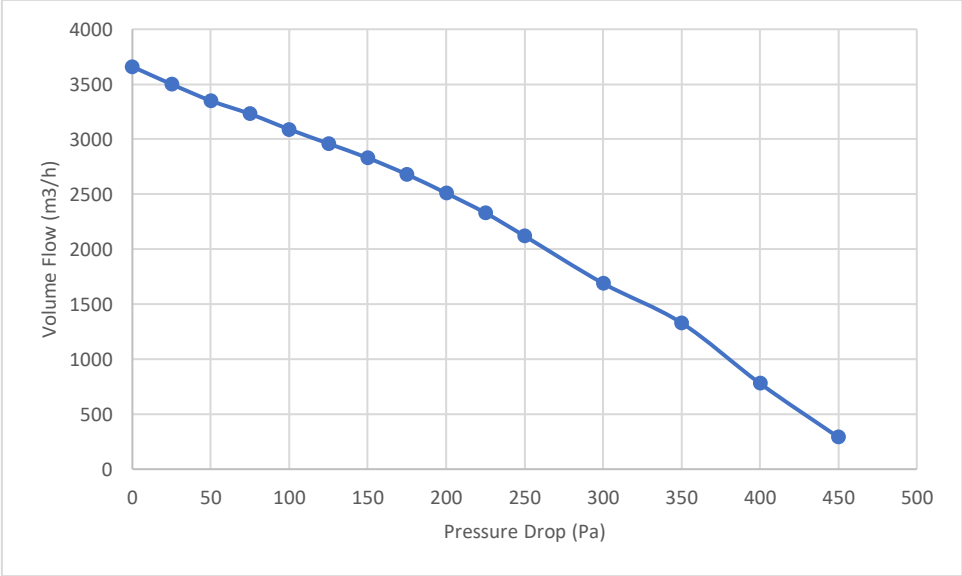

Figure 4-14: 15V Fan performance curve

The non-uniformities (blockages and fan) were then tested at different configurations, and the heat rejection performance was analysed.

4.4.1 90° testing

The baseline 90° tests were thereafter carried out with the addition of non-uniformities in the form of blockages, fan and converging bell mouths. These were then compared against the baseline cases and each other.

4.4.1.1 Fan Testing

A 15V fan supplied by McLaren was attached downstream of the radiator (Figure 4-15). It was placed in such a way that the way fan covered the lower half of the radiator. For safety reasons, a voltage of 13.6V was applied to the fan. A test with 0V (fitted but turned off) going to the fan was also considered.

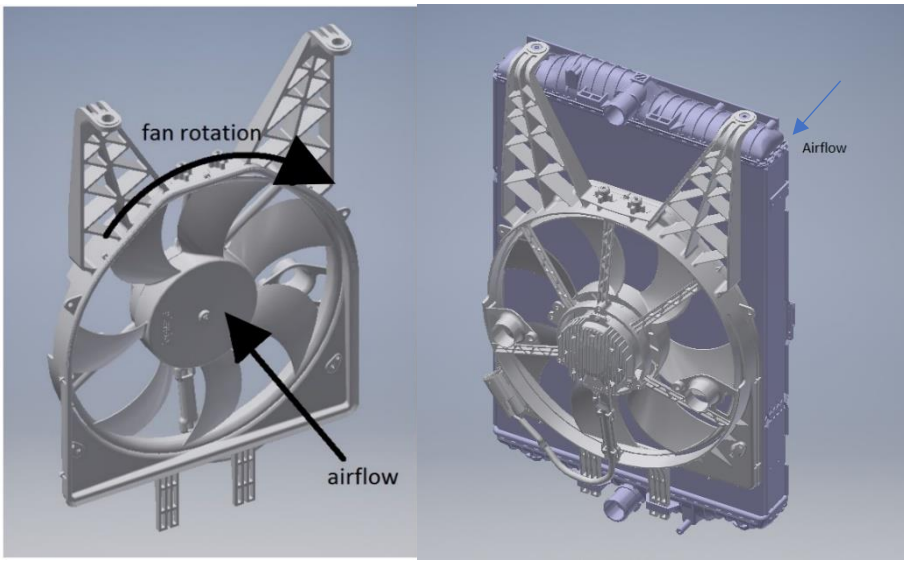

Figure 4-15: 15V McLaren fan and schematic

As seen from Figure 4-16, there was not much change seen with the airside pressure drop with the increase of air velocity for the given coolant flow rates. The heat rejection showed differing results, with a steady increase observed for higher air velocities. These results would need to be compared with heat rejection data for when no fan was used in the setup to get an accurate analysis.

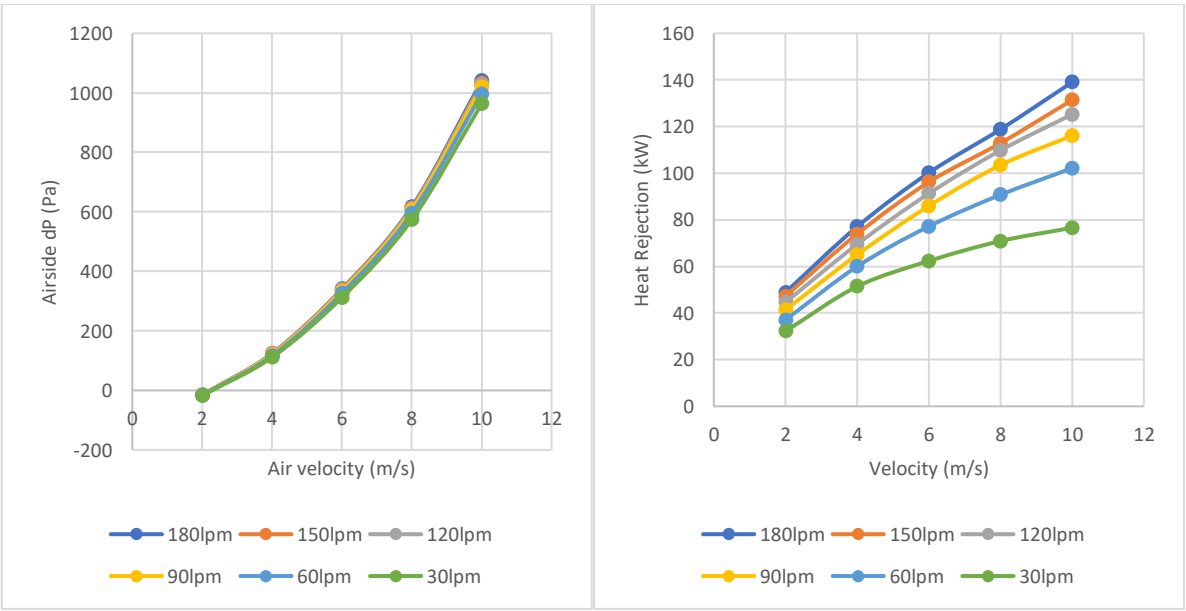

Figure 4-16: Airside dP and Heat Rejection with 13.6V fan

The following data was obtained; Table 3-5 was referred to when comparing data points for the two datasets.

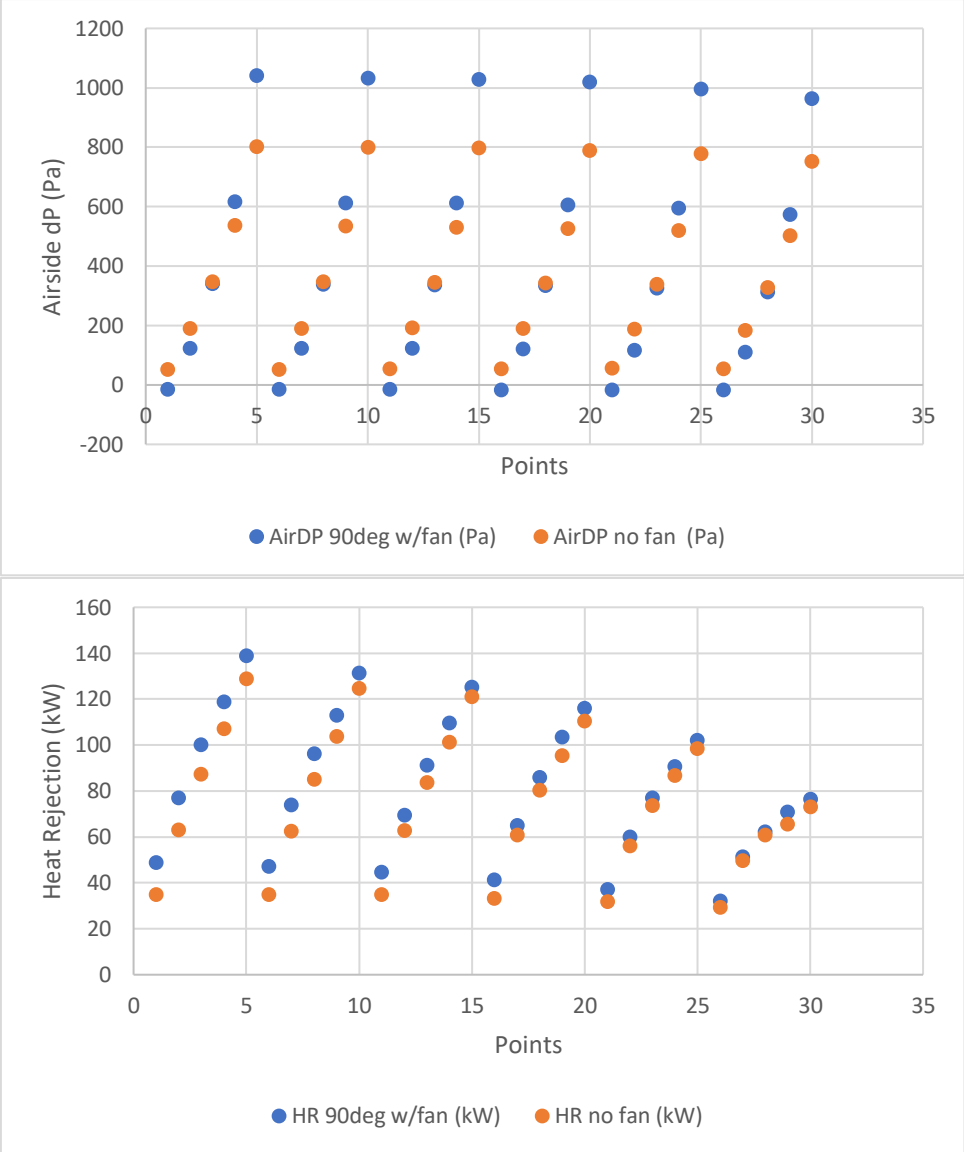

Figure 4-17: Fan heat rejection data comparison

Although the heat rejection data showed a definite increase when a fan was used, the airside pressure showed that it started contributing to decreased heat rejection after an air velocity of 6m/s was reached.

The heat rejection was also measured when the fan was turned off (0V). This was compared to the case when 13.6V was passed through the fan. It was expected to act as a blockage for each air velocity in the 0V case. Further testing could include adding digital anemometers to the setup to measure fan speed; this could help determine the fan speed for the 0V case, which would determine the aerodynamic performance. Due to health and safety concerns, this was not possible for the current setup.

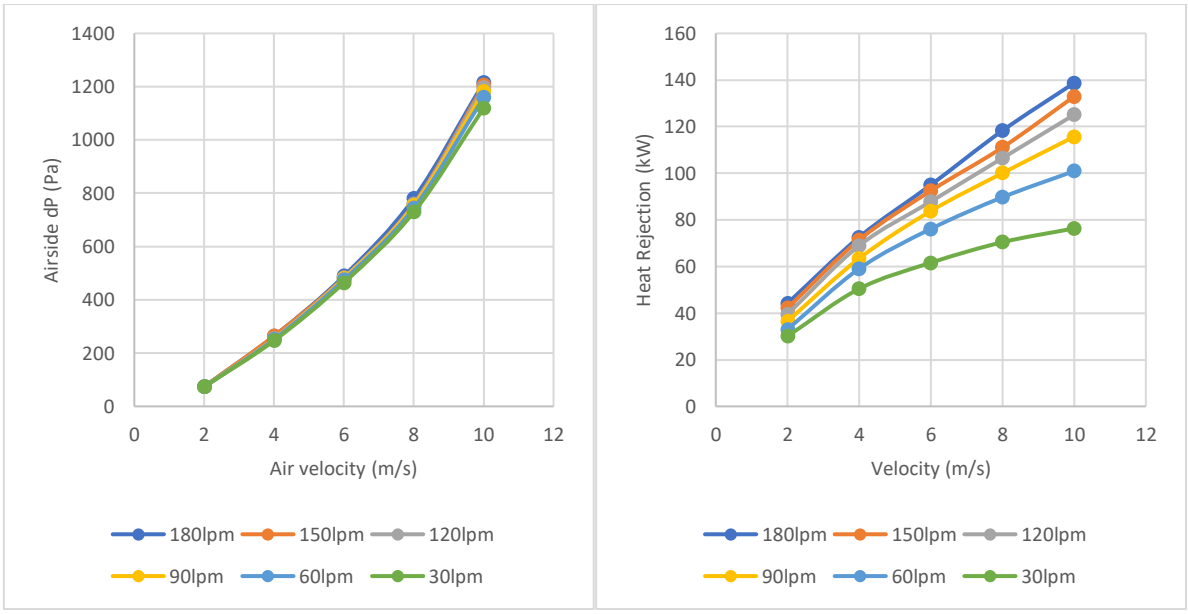

Figure 4-18: 0V fan Airside dP and Heat Rejection

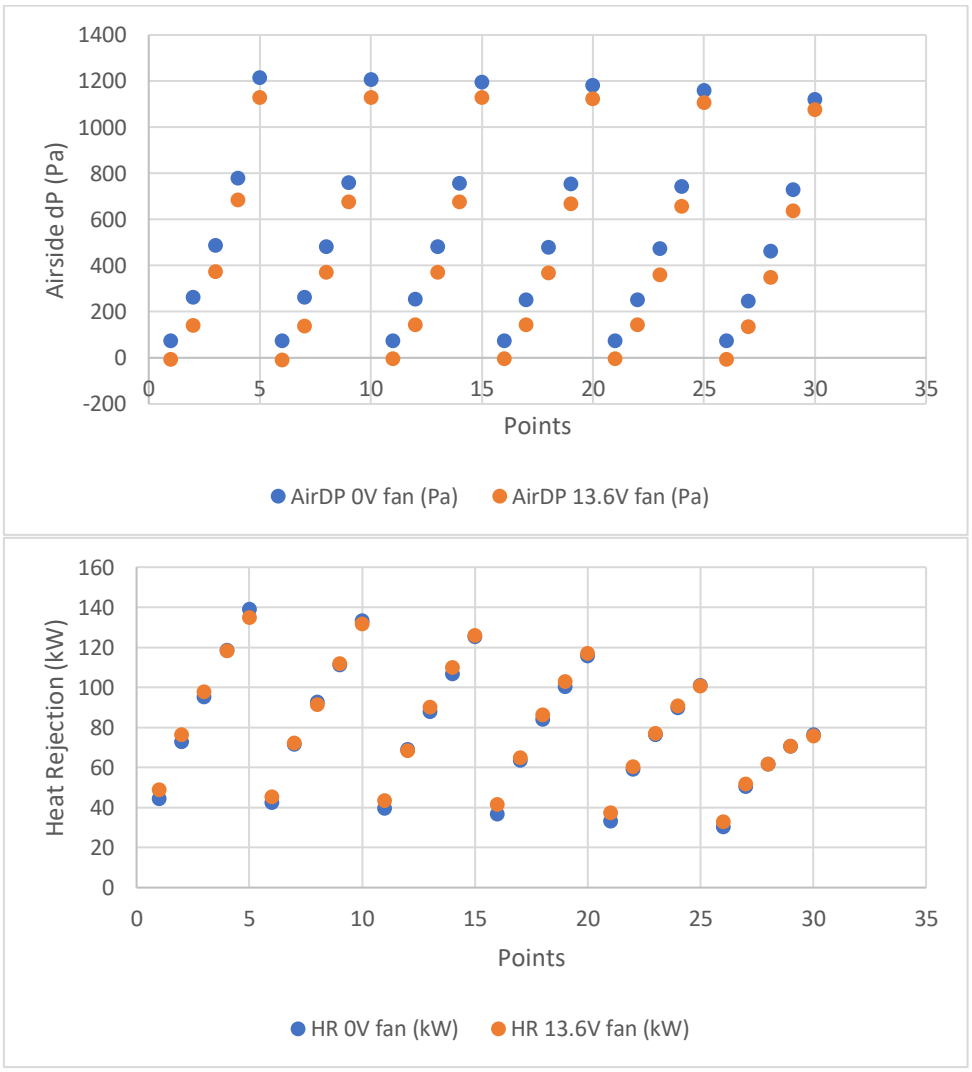

Figure 4-19: Comparison of Heat rejection Data- 0V fan and 13.6V fan

As expected, there was a definite drop observed in the pressure loss when the fan was switched on; this would indicate that the 0V fan acted like a blockage when compared to the fan with a 13.6V voltage passing through it. The average difference in heat rejection was 2.7kW for the higher flow rates between 150-180lpm, 2.4kW for 90-120lpm and 1.3kW for lower flow rates from 30-60lpm; further analysis is provided in the next section. This will prove beneficial as in setups such as McLaren's, a constant voltage is not supplied to the radiator fan and based on the load, the radiator fan can turn itself on. Hence, it is not detrimental to turn off the fan for the low load conditions as the heat rejection provided is nominal.

4.4.1.2 Delta HR Plots – Fan Testing

To aid in comparison and analyse the results, delta plots (Figure 4-20) were created, which plotted the difference in heat rejection against the air velocity. Differences were plotted as the fan was put through 13.6V, and 0V were compared against a baseline case where no fan was present.

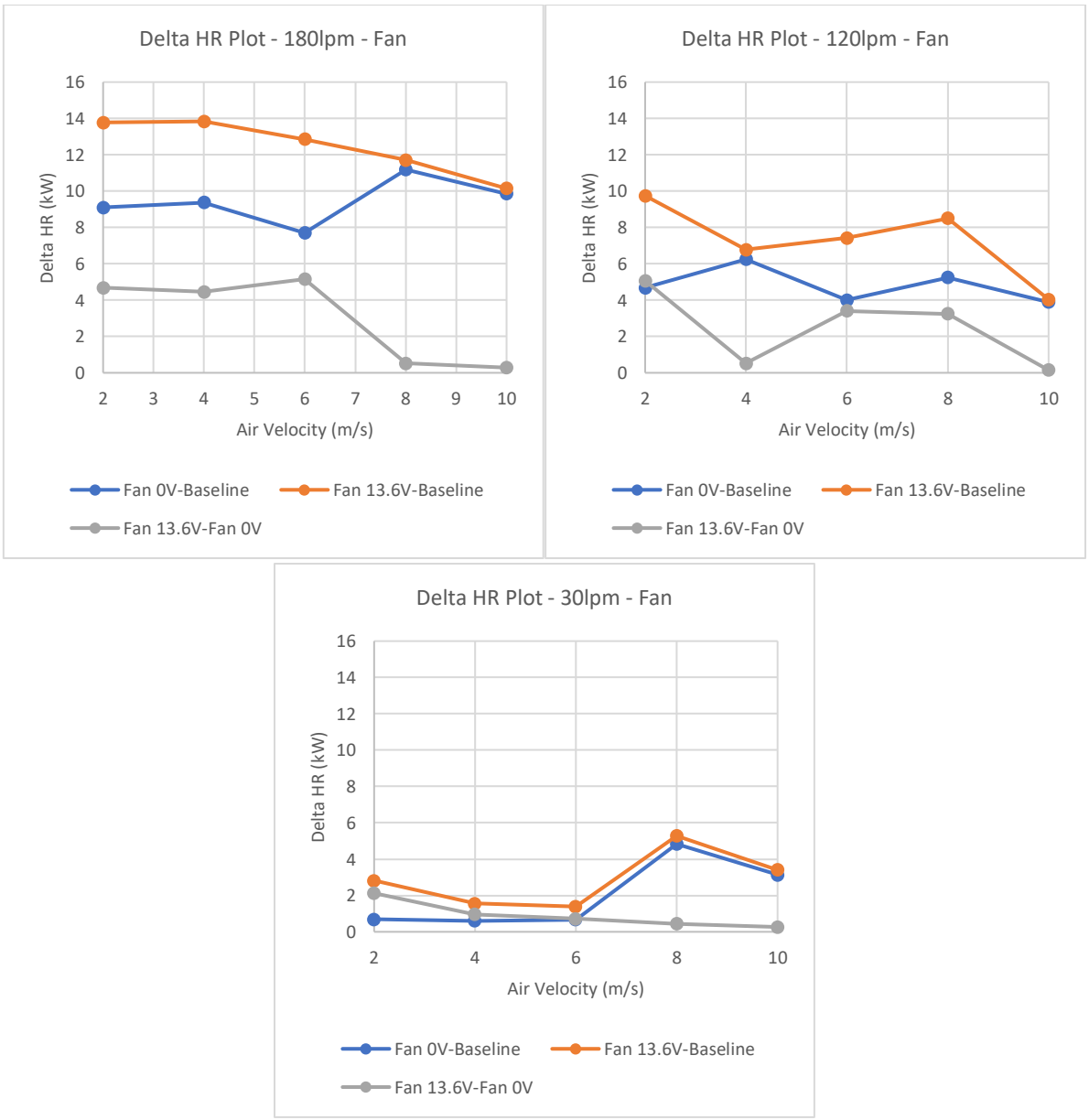

Figure 4-20: Comparison of Heat rejection Data- 0V fan and 13.6V fan

It was seen that for a coolant flow rate of 30lpm, for air velocities of greater than 6m/s, a fan at 13.6V and the fan at 0V showed heat rejection improvements when compared to the baseline case. However, the fan showed an average increase of 0.9kW when comparing the 13.6V case with the 0V case. Similar trends were observed for the 120lpm and 180lpm cases, with average increases of 3.0kW and 2.5kW seen for the improved heat rejection of the fan when put through a 13.6V compared to the fan when put through 0V. Trends were also observed where with increasing air velocity, the heat rejection improvements provided by the 13.6V fan case were almost identical to those provided by the 0V fan case. This was most visible at the 10m/s case; this could have been due to the fact that the 13.6V supplied to the fan was not enough. Further testing of the fan described previously could also give insight into the aerodynamics and heat rejection of the rig.

4.4.1.3 Blockage Testing

As mentioned previously, this testing considered a blockage with an open area of 70-80% to simulate ram air passing through an engine bay. The heat rejection and airside pressure drop were measured. The effects of the blockage 0.5m and 1m upstream of the radiator were then considered. A fan was also added to study the effects of the non-uniformities on the system.

Based on the configurations studied in the literature review and dimensions of standard Mercedes, Audi and Mazda vehicles[11], we can expect bonnet sizes to vary from 1-1.5m. Although specific dimensions for radiator placement are not readily available, we can expect the length upstream of the radiator to be <1m. Hence, blockages of 0.5m and 1m were chosen for the study. Blockages of <0.5m were not considered as they were expected to further disrupt the flow (will be discussed in limitations).

4.4.1.3.1 0.5m blockage testing

A blockage was introduced 0.5m upstream of the radiator in a number of locations (as described in Table 3-4), and the results were analysed and compared. Firstly, the blockage covered the lower half (285mm) of the radiator, and the heat rejection was measured for the configuration. The schematic is depicted in Figure 4-21, and the results are shown in Figure 4-22.

[11] Obtained from manuals and parts dimensions for the vehicles and general sources such as Ingram, A., 2022. Audi A4 sizes, dimensions & legroom guide. [online] carwow.co.uk. Available at: <https://www.carwow.co.uk/blog/audi-a4-dimensions-0364>.

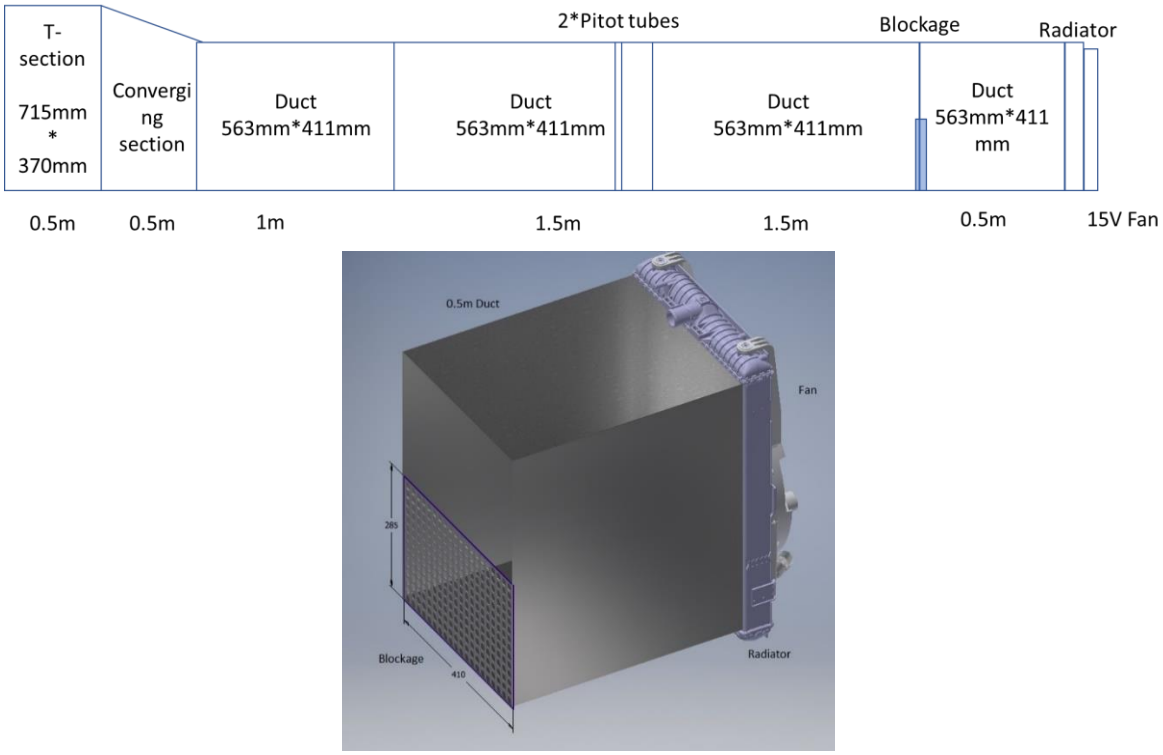

Figure 4-21: 0.5m Blockage Schematic

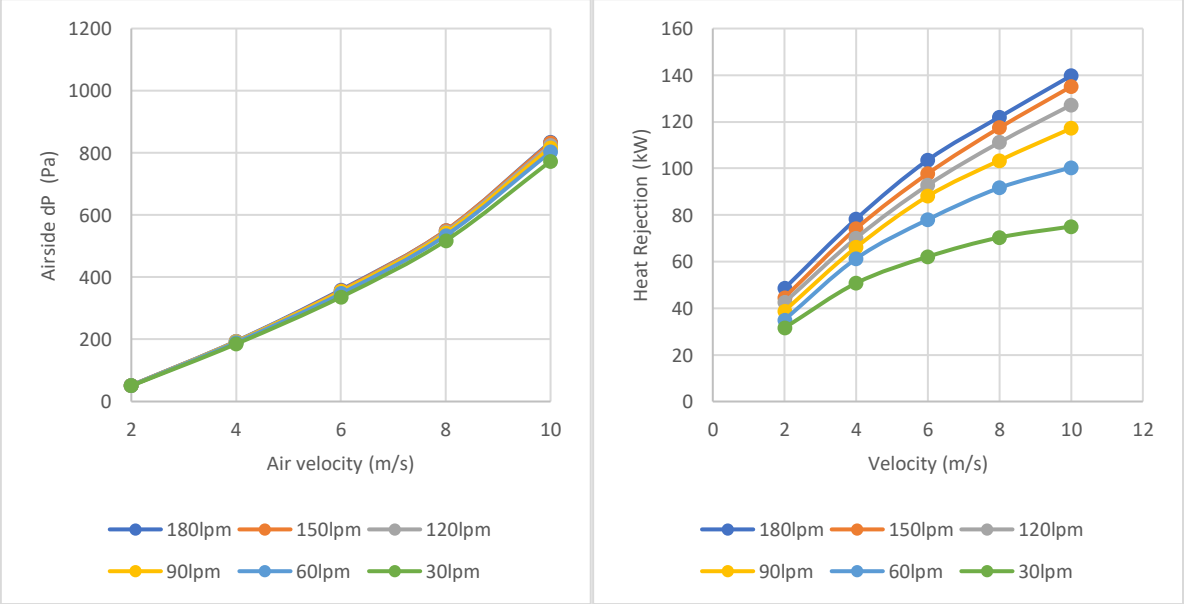

Figure 4-22: Airside dP and Heat Rejection for a 0.5m Lower Half Blockage (no fan case)

Next, to ascertain if the blockage would affect the heat rejection if it were in the upper half, the same blockage was placed 0.5m upstream of the radiator whilst it covered the upper 285mm of the face of the radiator (Figure 4-23). The results were plotted in Figure 4-24. Comparisons of the two cases (Figure 4-25) with the baseline case have been made with Delta HR plots.

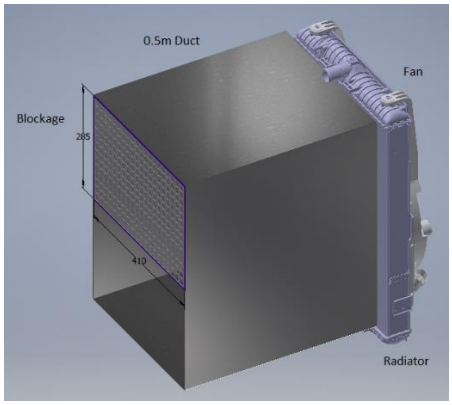

Figure 4-23: Upper-half Blockage Schematic

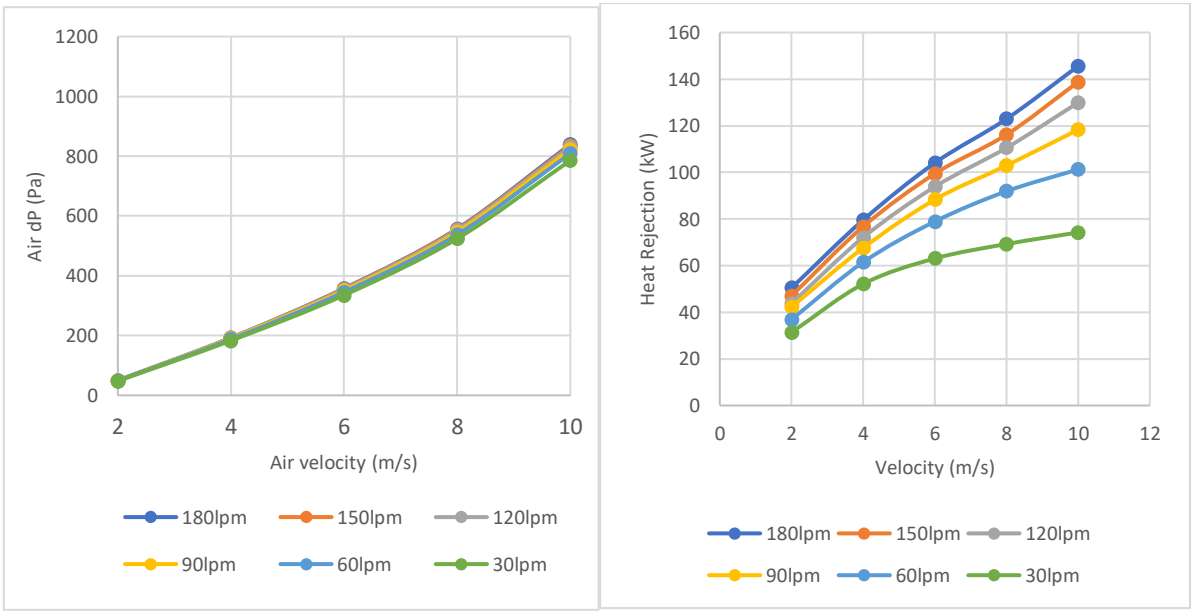

Figure 4-24: Airside dP and Heat Rejection for a 0.5m Upper Half Blockage (no fan case)

To simulate real driving conditions, the 13.6V fan was used again.

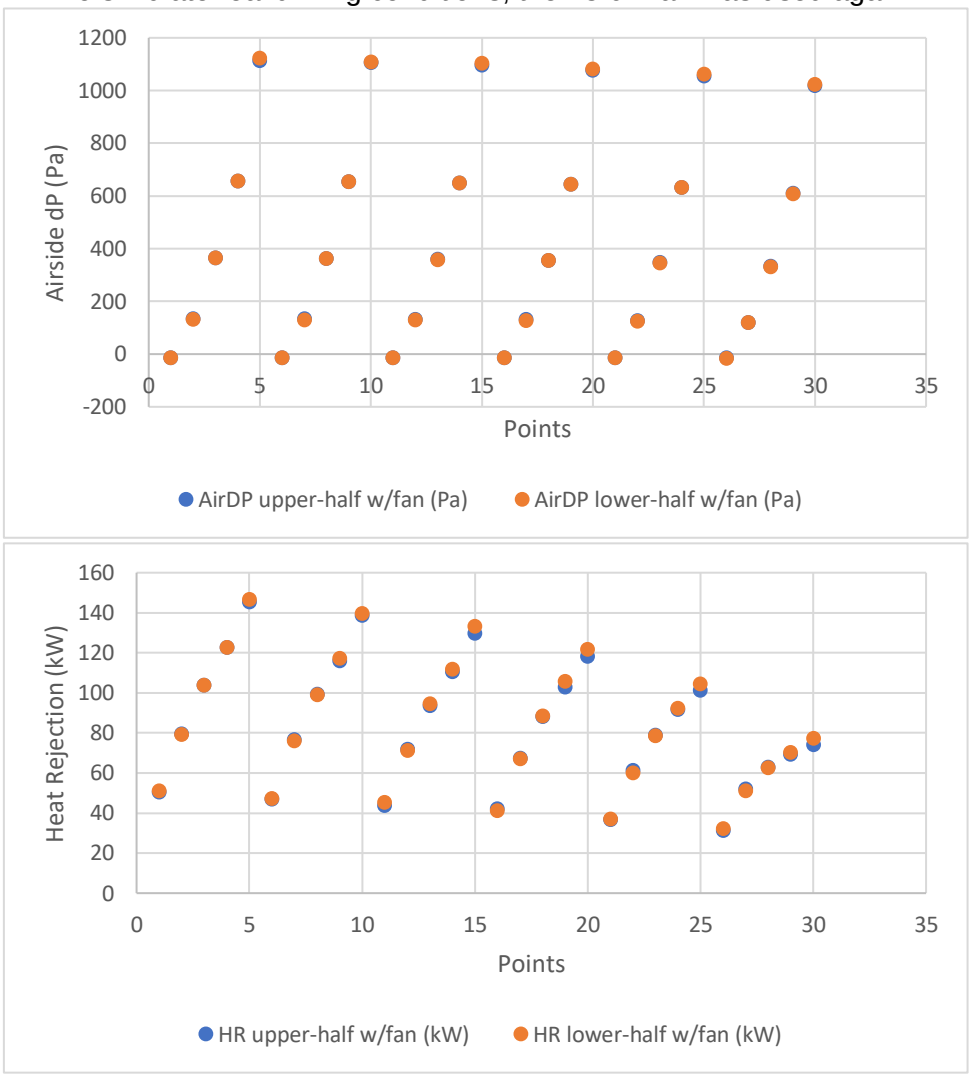

Figure 4-25: Heat rejection comparison for Upper and Lower Half Blockages

4.4.1.3.2 Delta HR Plots – 0.5m blockage

The Delta HR Plots (Figure 4-26) do show that the 0.5m blockage, 13.6V fan provided from an average increase in heat rejection of a 3.1kW(for 30lpm)-16.4kW(for 180lpm) when compared to the baseline case.

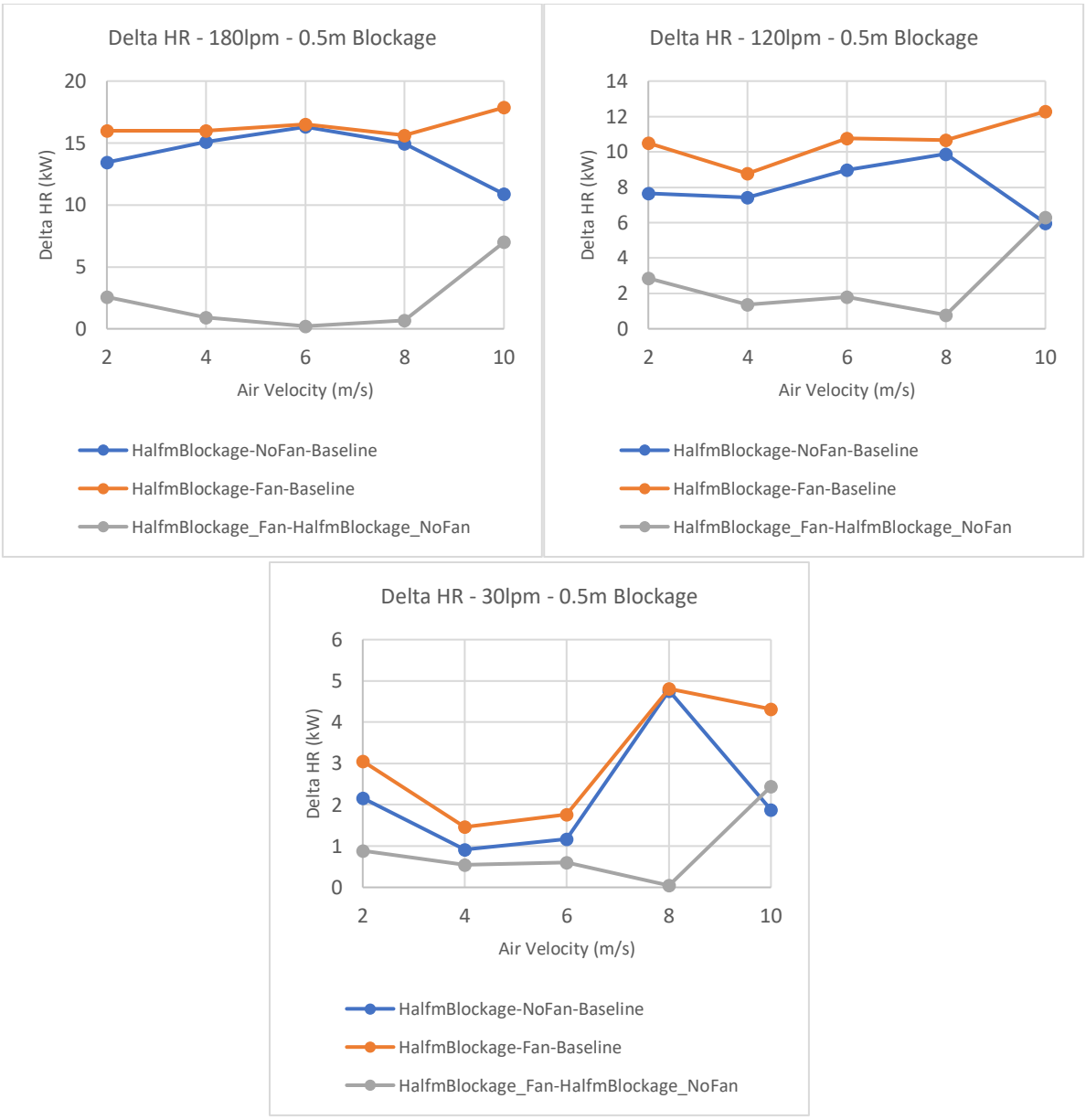

Figure 4-26: Delta HR Plots - 0.5m Blockage

The 0.5m blockage, no fan case also showed an increase in the heat rejection, ranging from 2.1kW(for 30lpm) to14.1kW(for 180lpm). The presence of a fan was very noticeable for a higher air velocity of 10m/s case, with an average increase of 4.9kW seen over the no-fan case in all three cases. Compared to the baseline cases, the increase in heat rejection in both cases could have possibly been due to the accelerated airflow over the blockage. As the blockage has an open area of 70-80%, this could have had an effect on the heat rejection. Limitations for the section have been discussed later and could provide avenues for future testing (discussed in future work).

4.4.1.3.3 1m blockage testing

The next series of tests were conducted with a blockage located 1m upstream of the radiator. The schematic is seen in Figure 4-27.

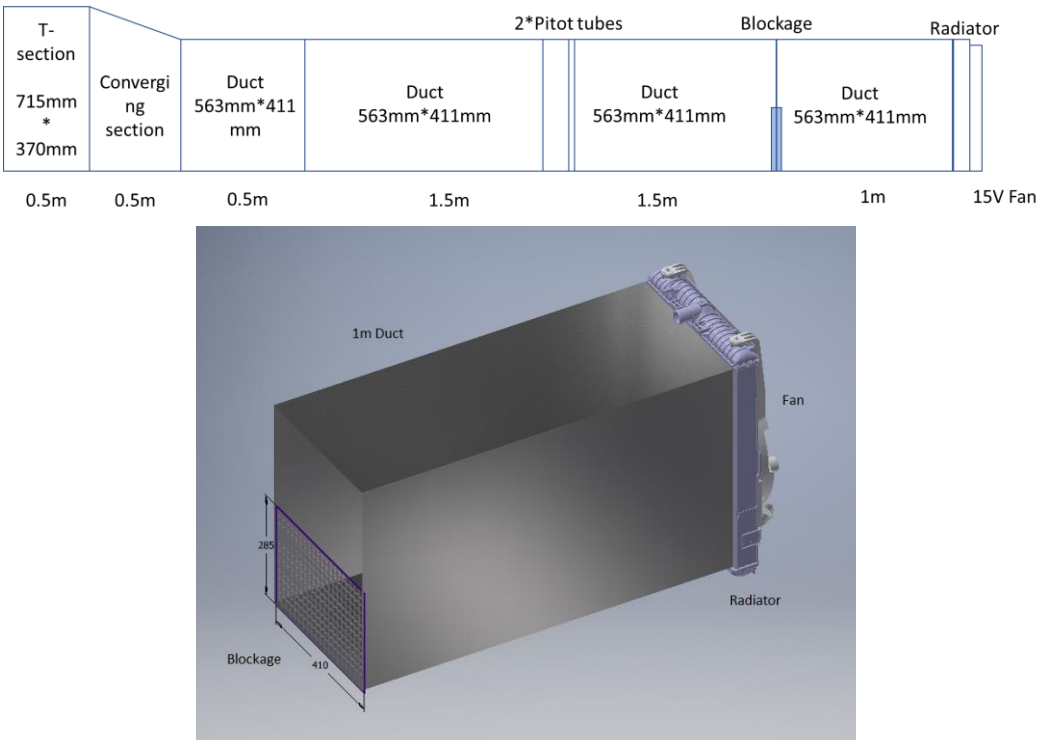

Figure 4-27: 1m Blockage Schematic

The airside pressure drop and heat rejection were analysed for the setup, depicted in Figure 4-28 (no fan) and Figure 4-29 (with 13.6V fan).

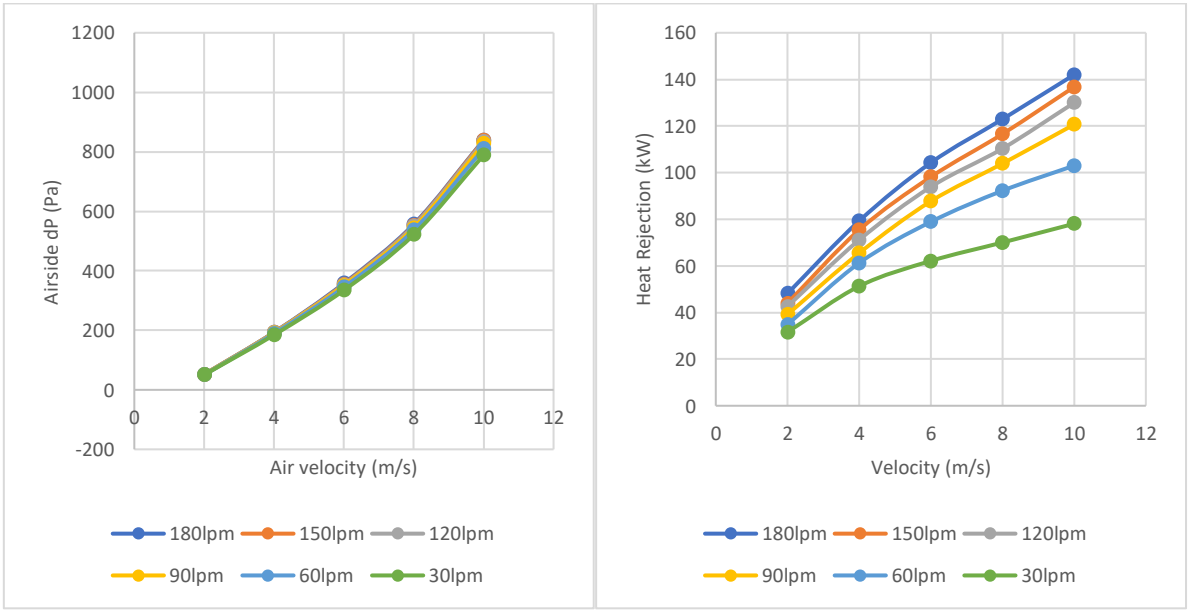

Figure 4-28: Airside dP and Heat Rejection for 1m blockage w/o fan

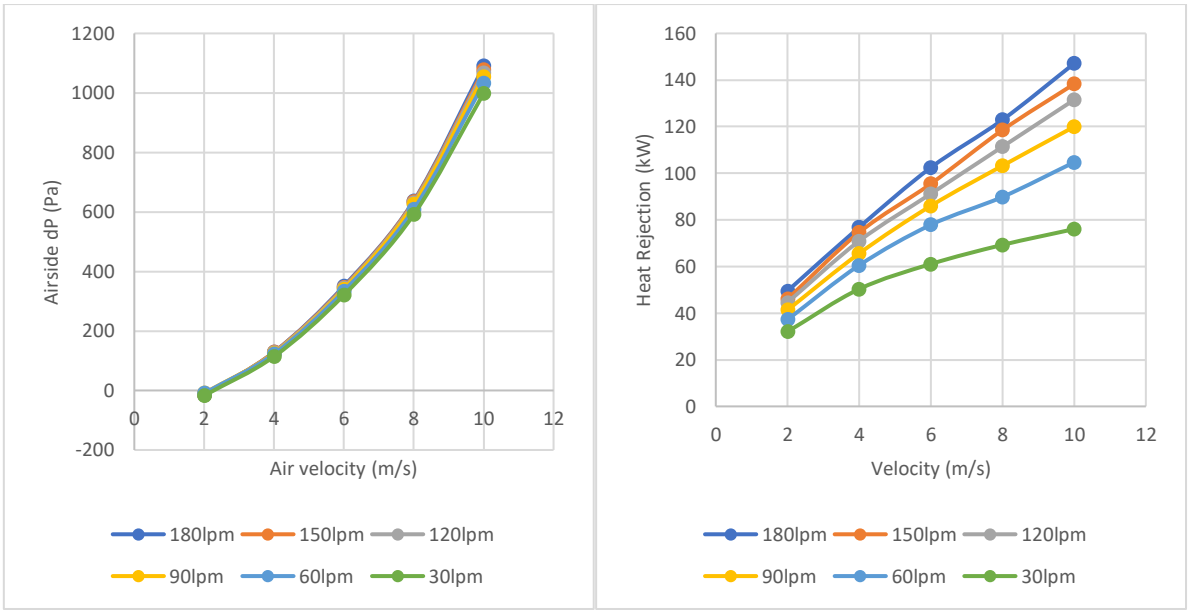

Figure 4-29: Airside dP and Heat Rejection for 1m blockage w/fan

The heat rejection data showed similar curves, and they were compared against each other with delta HR plots where differences between the heat rejection and baseline curves were plotted.

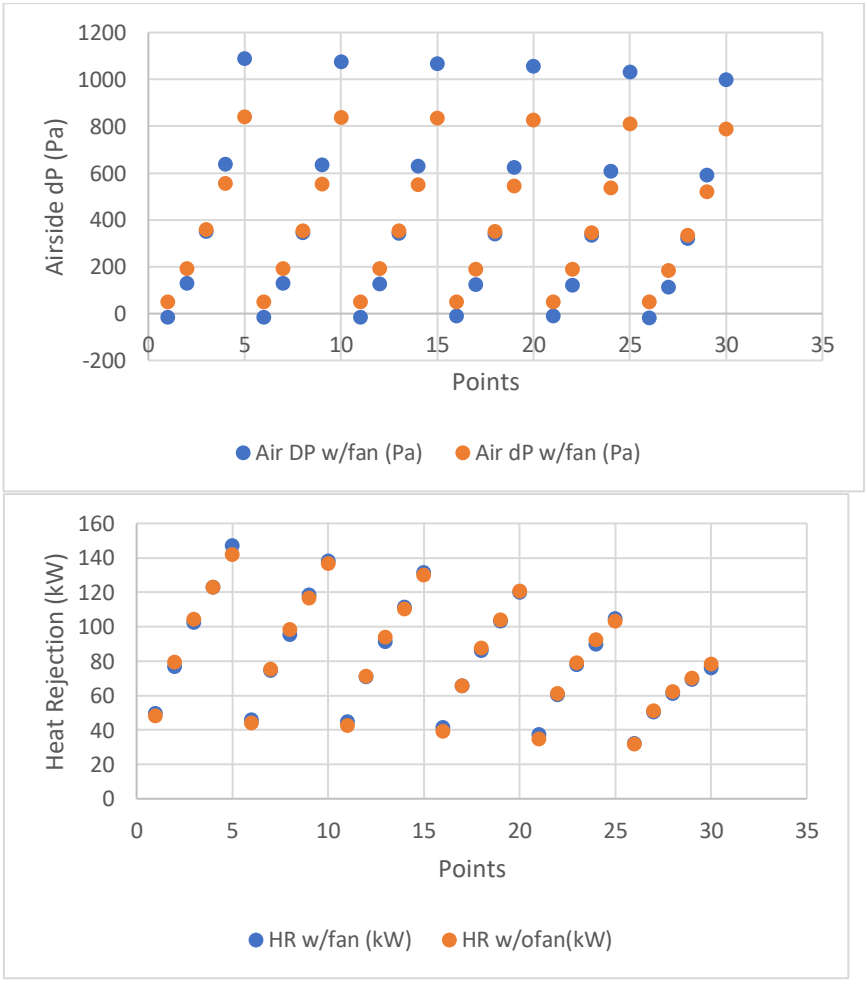

Figure 4-30: Heat rejection Comparison for 1m blockage with and without fan

It was observed that the fan started acting as a blockage at air velocities of 6m/s and higher. A definite pressure drop was observed, and a trend was observed in the heat rejection data wherein the heat rejection was higher or almost equal without a fan until an air velocity of 6m/s was reached. The fan provided better heat rejection at higher air velocities. Delta plots were then plotted to get a better understanding of the data.

4.4.1.3.4 Delta HR Plots – 1m Blockage

From Figure 4-31, when comparing the 1m blockage, 13.6V fan with the baseline case, it was found that the average heat rejection for 30lpm was 1.9kW more than that of the baseline case, whereas the average heat rejection for 180lpm was 15.4kW more than that of the baseline case. The same averaged heat rejection for the 1m blockage, no fan case was in excess of 2.8kW(for 30lpm)-15kW(for 180lpm) compared to the baseline case. The effects of the fan could be observed for the 10m/s air velocity case, as a fan showed an average increase of 4.5kW in heat rejection.

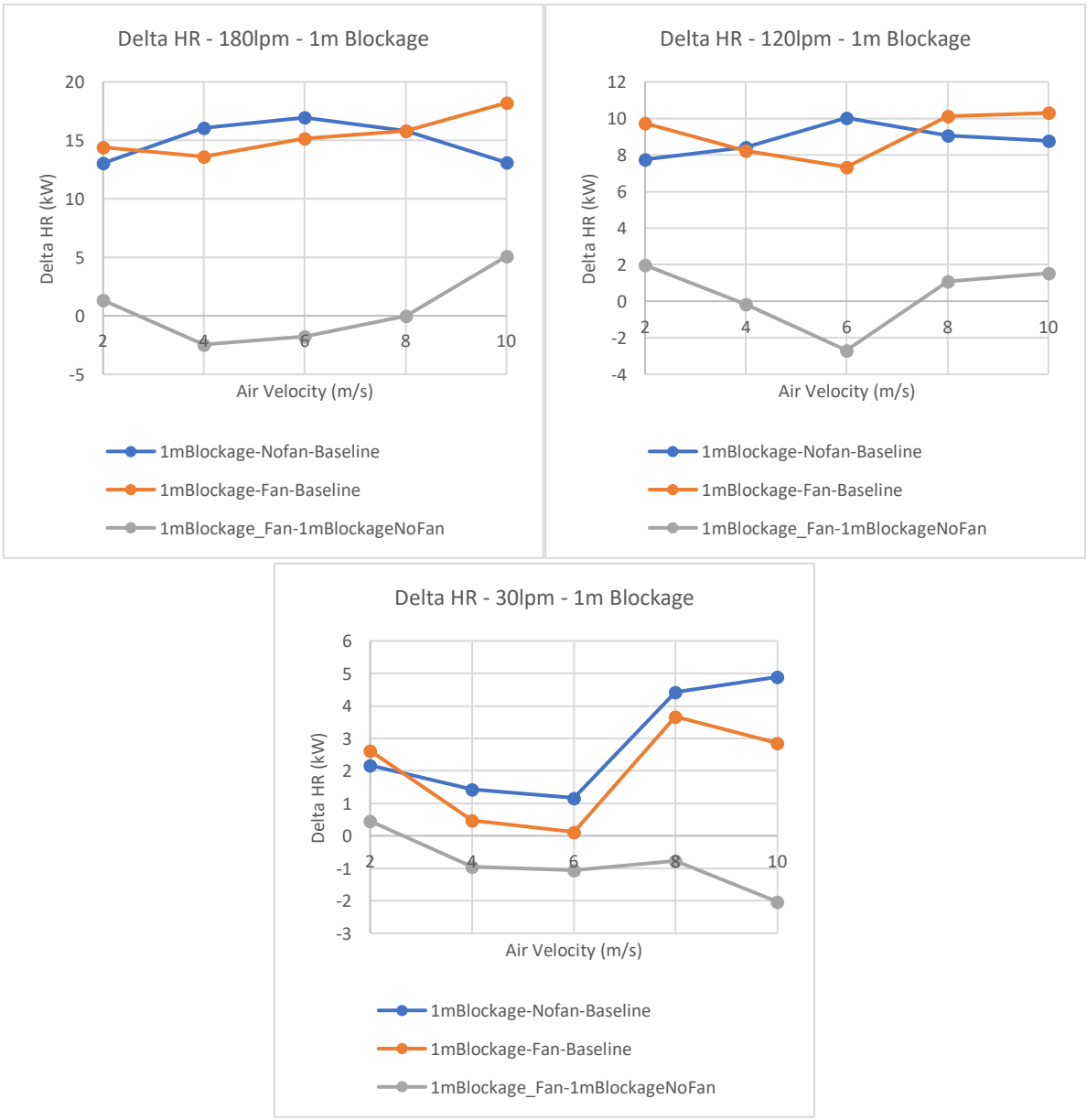

Figure 4-31: Delta HR Plots - 1m Blockage

The heat rejection increase was higher than the 0.5m blockage case (without the fan in both cases). This would imply that a 1m blockage with no blockage provided better heat rejection. However, with the fan, this changed as 0.5m blockage showed better heat rejection with the fan on when compared to the 1m blockage case.

Further testing could involve studying the geometry of the fan and CFD analysis of the same to investigate the cause for the change when the fan is in place.

4.4.2 35° testing

Heat Rejection tests were conducted with a converging section to test heat rejection for a 35° incidence angle for the radiator. As mentioned previously, this angle was chosen as when placed in front of a wheel, a radiator would likely be at that angle in a car.

4.4.2.1 Fan Testing

The same fan was placed at the back of the radiator, and a 13.6V voltage was passed through it (Figure 4-32). The heat rejection results were obtained and compared against the case when a fan was not used (Figure 4-33).

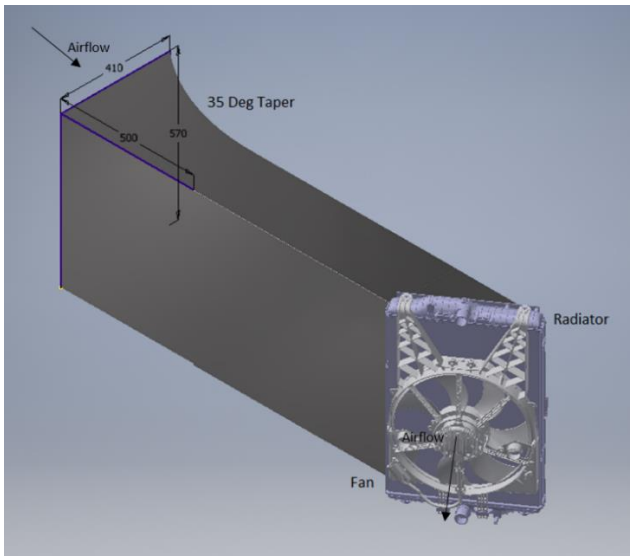

Figure 4-32: 35° Configuration Schematic

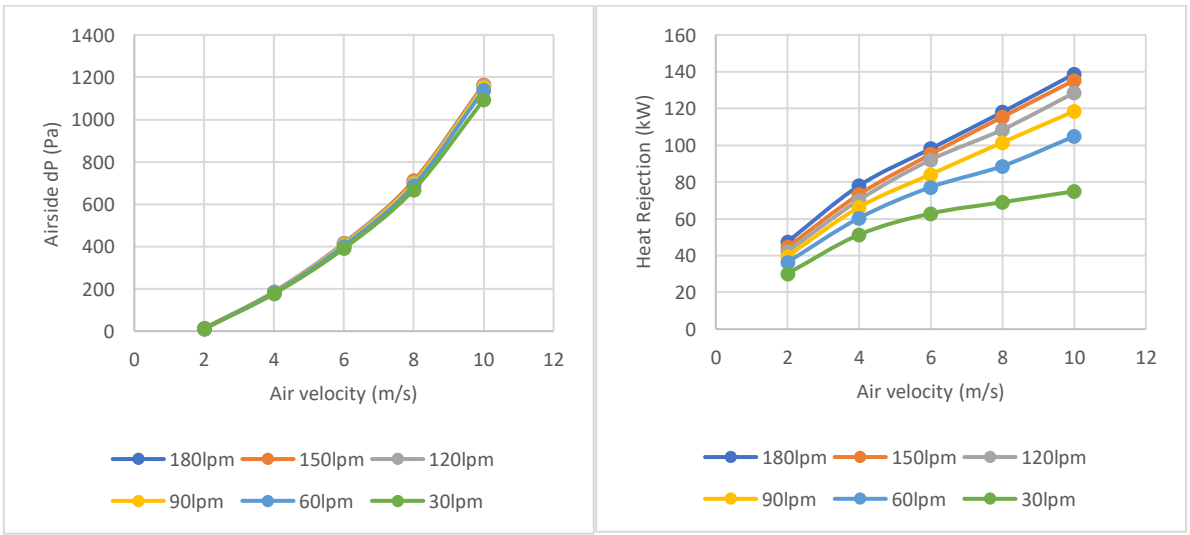

Figure 4-33: Airside dP and Heat Rejection for 35deg AOI and 13.6V fan

The heat rejection curves followed similar trends observed in the previous cases. Coolant flow rates showed an improvement of 85% in heat rejection when the 30lpm-180lpm cases were compared; however, not much change was observed with the airside dP as less than a 5% change was observed between the two extreme cases (30-180lpm).

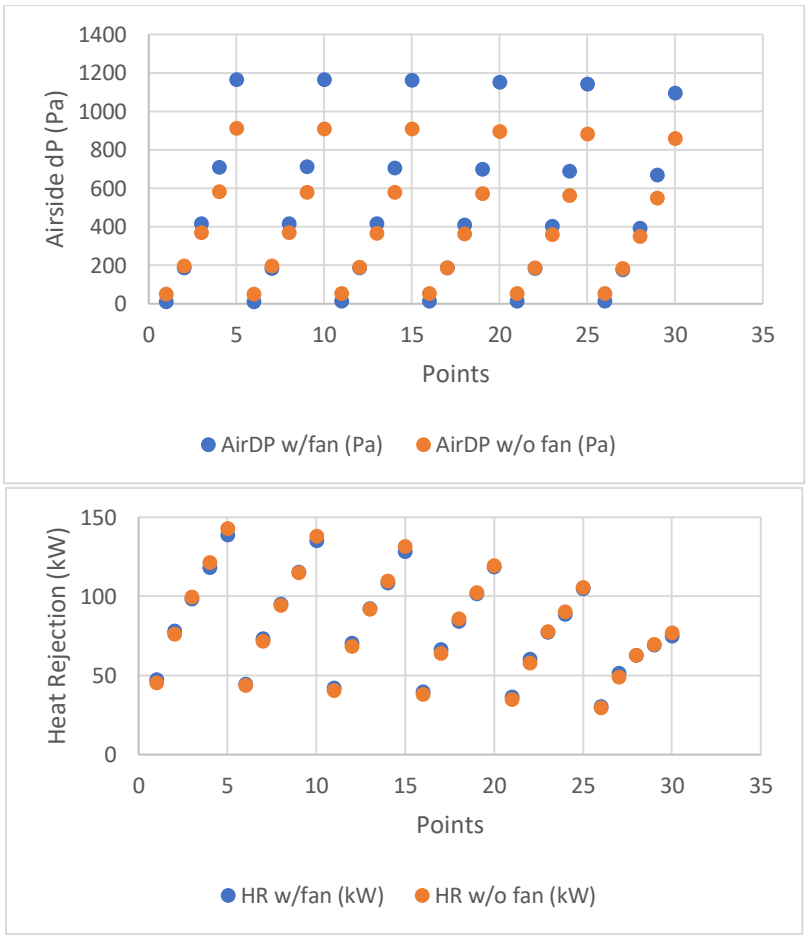

Figure 4-34: Heat rejection comparison for 35 deg AOI with and without 13.6V fan

As can be seen from Figure 4-34, a definite drop in pressure was observed right before an air velocity of 6m/s was reached. This would be the point at which the fan would start acting as a blockage. The same can be seen in the heat rejection comparisons as the heat rejection for the 2m/s and 4m/s air velocities were higher for the 13.6V fan case, whereas for higher flow velocities, it was lower.

4.4.2.2 0.5m Blockage Testing

As mentioned previously, a 0.5m blockage was used in a similar upstream configuration (Figure 4-35). Airside pressure drop and heat rejection were measured, and the results were compared with and without a 13.6V fan (Figure 4-36).

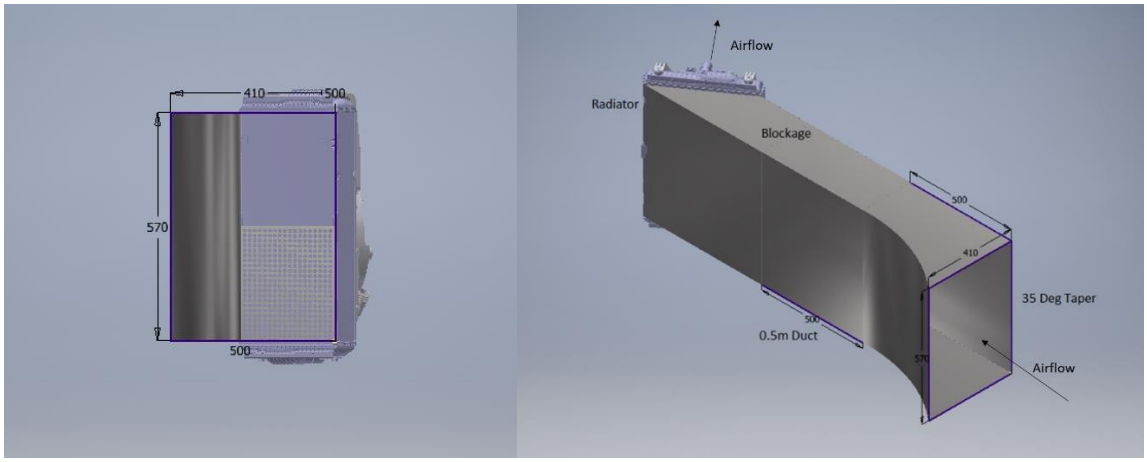

Figure 4-35: 35° 0.5m blockage schematic

The results showed a similar trend to the case with a fan. The fan acted as a blockage on velocities of upwards of 6m/s, and this was echoed as a definite pressure drop and decrease in heat rejection was observed for those higher velocities.

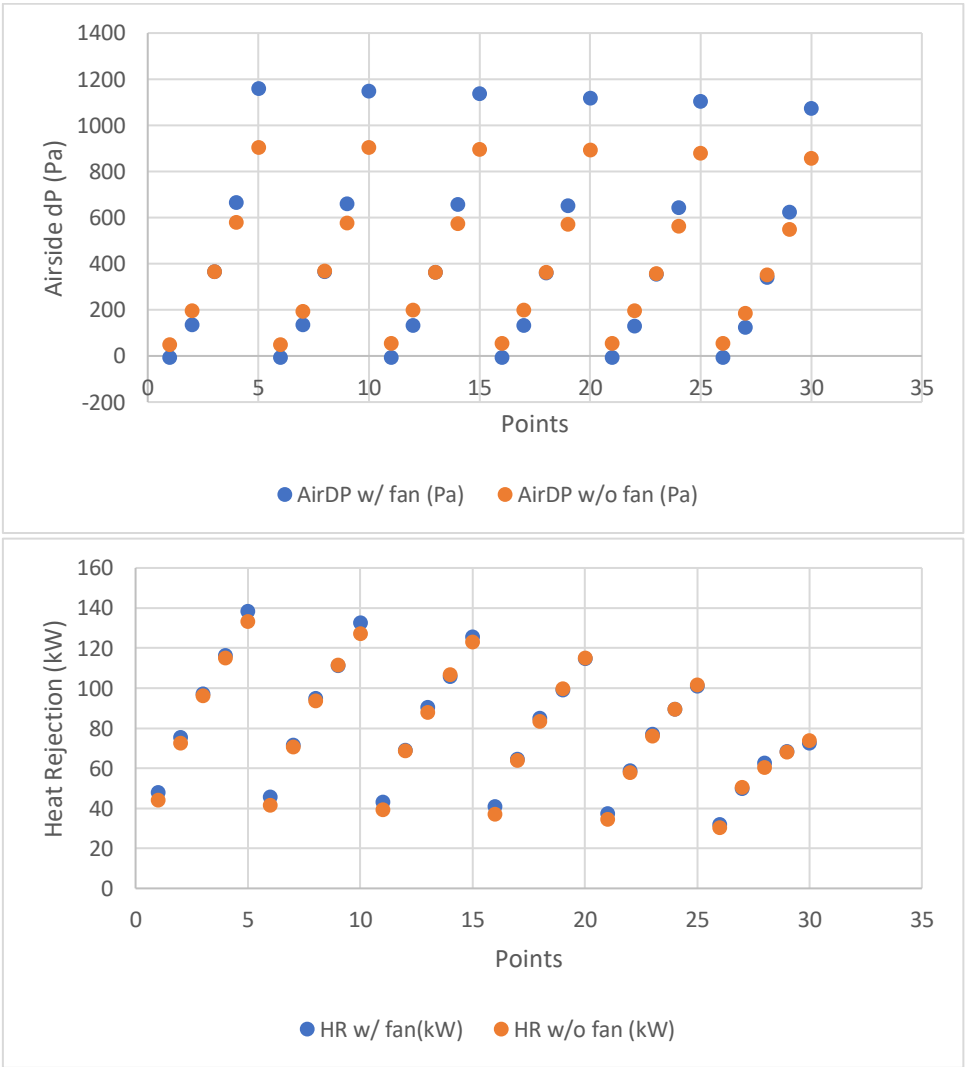

Figure 4-36: Heat rejection Comparison for 35deg AOI 0.5m blockage with and without a 13.6V fan

4.4.2.3 Delta HR – 35° 0.5m Blockage

When compared to the 35-degree Heat Rejection plots (Figure 4-37), a 0.5m blockage without a fan showed a decrease of 0.8kW(30lpm)-4.7kW(180lpm), whereas the fan brought the decrease down to 1.1kW(30lpm)-1.9kW(180lpm). Although the fan provided an average of 0.4kW (for 30lpm)-2.9kW (for 180lpm), a blockage significantly affected the heat rejection. This was more pronounced in this case compared to the 90 degree-baseline case. A possible reason could be that the 35-degree taper slightly accelerated the flow. Additionally, the flow was concentrated over a smaller area now meant that a blockage had a more significant effect on heat rejection.

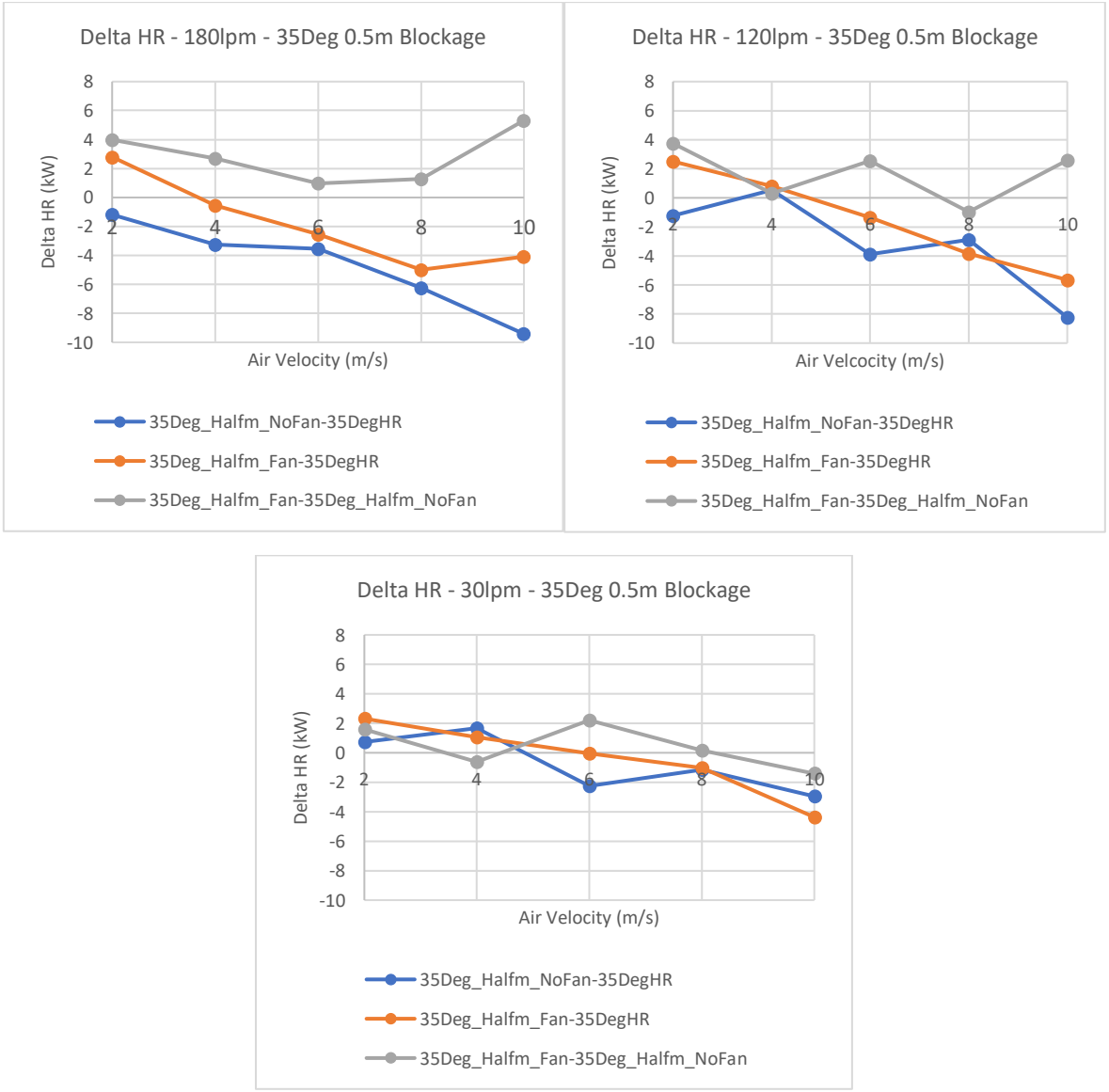

Figure 4-37: Delta HR Plots - 35° 0.5m Blockage

4.4.2.4 1m Blockage Testing

Similar to the 0.5m case, a 1m blockage was used upstream of the radiator (Figure 4-38). Airside pressure drop and heat rejection were measured, and the results were compared with and without a 13.6V fan (Figure 4-39).

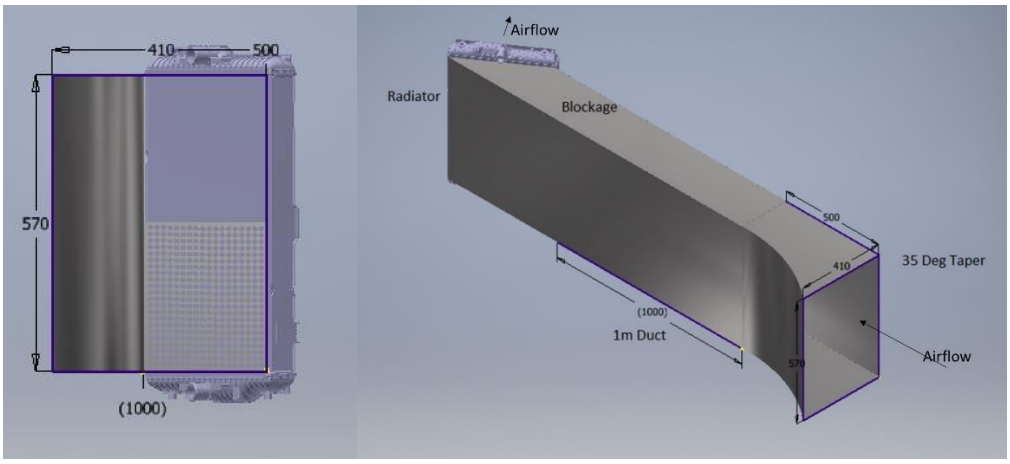

Figure 4-38: 35° 1m Blockage Schematic

The fan was observed to act as a blockage over 4m/s air flow velocities as a definite increase in pressure loss and decrease in heat rejection was seen thereafter. This was seen to be lower than in previous cases. This could have been due to the angle of the bend and the acceleration of flow velocity along it. Further testing would be needed to ascertain the cause.

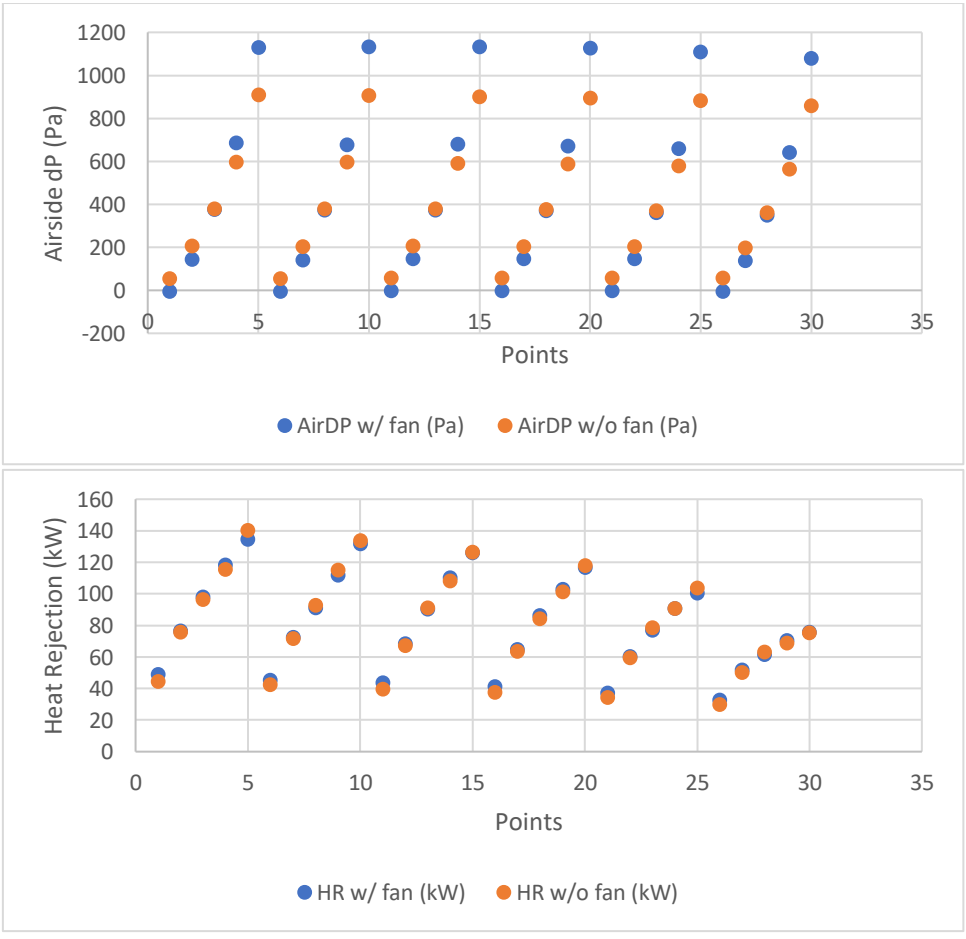

Figure 4-39: Heat rejection comparison for 35deg AOI 1m blockage with and without a fan

4.4.2.5 Delta HR Plots – 35° 1m Blockage Testing

Similar to the 35° 0.5m blockage case, the 35° 1m blockage case followed comparable trends in heat rejection (Figure 4-40). A 1m blockage without a fan showed an averaged decrease of up to 2.7kW (for 180lpm) compared to the 35° case with no blockage/no fan case. With a 13.6V fan, this decrease of up to 1.9kW (for 180lpm). Again, this showed that a blockage had an adverse effect on heat rejection, possibly due to flow blocked over a smaller, more concentrated area. Further testing would involve the fan and specific CFD dynamics of the setup to be examined.

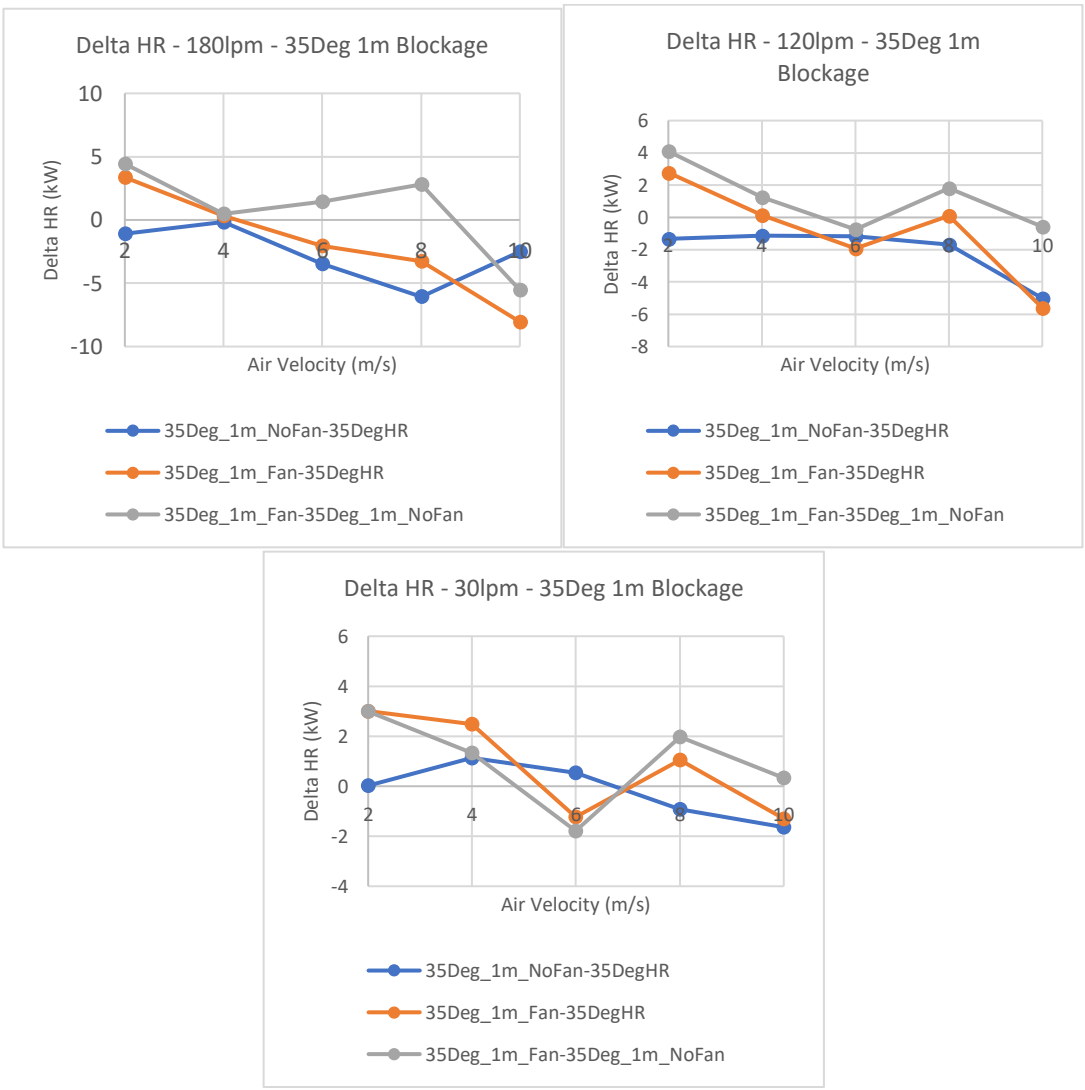

Figure 4-40: Delta HR Plots - 35° 1m Blockage

4.5 Limitations of the rig and results

Limitations of the current rig were based on its modular design and non-uniform flow. They are listed as follows.

- CFD studies, including turbulence sensitivity testing of blockages, would have been beneficial in explaining certain phenomena. However, the biggest impediment to this was the airflow coming out of the centrifugal pump. The non-uniformity of the flow at the pump outlet was pronounced and could not be accurately predicted as the rig lacked the capability to measure air velocity at the outlet. Additionally, due to the modular nature of the rig, each of the 14 test cases would involve changing the rig, which would involve changing the rig length, elements upstream and downstream of the radiator, and location of blockages/fan. As the turbulence intensity is unknown, each case would have to be plotted for varying turbulence intensities. Hence, to correctly assess the effects of blockages on turbulence intensity, several physical experiments and CFD simulations would need to be carried out. This was not possible within the given scope of the study.
- Since there were two distinct systems for cooling and heating the ambient air temperature in the test facility, control of the ambient air temperature could have been better.
- Only one high-temperature radiator was provided for this study. Hence, the cross-sectional analysis could not have been performed better to understand the physical characteristics of the high-temperature radiator.
- The modular nature of the rig meant that the airflow measured in the rig often changed measurement locations. This would mean that the required length for the averaging pitot tubes was not always met, and tapered sections in the rig might have also accelerated the flow. Hence, the accuracy of the air velocity measurements might have been off by a certain degree which would have been hard to predict.

4.6 Uncertainty Analysis

As mentioned in the methodology, a cumulative error attributed to the measurement sensors is 2%. However, given how the heating and cooling system functioned, the largest error while measuring the heat rejection was estimated to be 5%. The ambient temperature varied because of the hot air being ejected from the outlet in the atmosphere. At the higher air velocities, temperatures of around 80-90°C, this equated to an increase of 1.5°C in ambient temperature, which contributed to the 5% error in heat rejection measurement.

5 Conclusion and Future Work

A small-scale wind tunnel and cooling circuit were constructed. Baseline, angled, blockage and fan testing were carried out to quantify the heat rejection of a high-temperature radiator in different configurations. Error in heat rejection was predicted to be 5% at the point of the highest error in ambient temperature caused due to high air velocity being ejected from the radiator; given the different sensors used in the rig, this was unavoidable yet acceptable. Conclusions regarding the following were observed:

1 The LTR was modelled using the ε-NTU model. Due to limitations in data, an NTU of 3 was assumed, which correctly predicted the heat rejection with a 4% margin. This provided a base for further testing and only gave a brief overview of the topic. Future testing could include conducting steady-state tests, which could then be used to predict the thermal transients of the system accurately. This result ensured that objectives 1.1.6 and 1.1.7 were met.

2 A modular and mobile rig was constructed, and the effects of air velocity and coolant flow rates were studied. The air velocity significantly affected the heat rejection, whilst the coolant flow rate effect was much smaller. Higher coolant flow rates showed that the heat rejection was 19% higher for an air velocity of 2m/s when comparing the 180lpm case to the 30lpm case. However, this was 76% higher for the 10m/s case. The average heat rejection at 180lpm only showed an overall improvement of 51% over that of the 30lpm case. This is possibly due to the radiator's large effective surface area, which enhances the heat rejection rate. Therefore, a higher air velocity meant a higher rate of heat transfer and a higher heat transfer coefficient. Objective 1.1.1 was thus met.

3 Comparisons made for the 15°,25° and 35° cases showed that the 15° and 25° cases did not show much improvement in heat rejection; however, the 35° degree case showed significant improvements over the baseline case in terms of heat rejection. For the 180lpm, the 35° case showed an improvement of about 14kW for air velocities of the 8m/s and 10m/s cases. A possible reason for the enhancement of heat rejection in only the 35° case would be the additional direct convection caused by the inner geometry of the radiator (louvres). This could provide a base for future testing if the cross-section and internal geometry are studied, ensuring that objectives 1.1.2 and 1.1.7 were met.

4 When comparing the 1m blockage, 13.6V fan with the baseline case, it was found that the average heat rejection for 180lpm was 15.4kW more than that of the baseline case. The same averaged heat rejection was in excess of 15kW(for 180lpm) for the 1m blockages, with no fan case compared to the baseline case. The effects of the fan were pronounced for the 10m/s air velocity case, as a fan showed an average increase of 4.5kW in heat rejection. The same heat rejection for a 0.5m blockage was 14.1kW without a fan at 180lpm and 16.4kW with a 13.6V fan. Hence, a 1m blockage without a fan provided better heat rejection. However, with a 13.6V fan, this changed as 0.5m blockage showed better heat rejection with the fan on when compared to the 1m blockage case.
   Further testing could involve studying the geometry of fan and CFD analysis of the same to investigate the cause for the change when the fan is in place. As stated in the thesis, a blockage of an open area of 70-80% was chosen, which could be attributed to the heat rejection increase. Therefore, objectives 1.1.3 and 1.1.5 were met while providing a basis for objective 1.1.7.

5 Fan operation generally improved the heat rejection; however, it acted as a blockage after a certain air velocity was reached in certain instances. For the 90° case, the fan showed an average increase of 0.9kW when comparing the 13.6V case with the 0V

case. Similar trends were observed for the 120lpm and 180lpm cases, with average increases of 3.0kW and 2.5kW seen for the improved heat rejection. The fan generally showed an increase in heat rejection performance as for the higher flow rates (150-180lpm), an average increase of 3kW was observed. The fan did not show much change at 8m/s and 10m/s when comparing the fan at 13.6V and the fan at 0V cases. This could imply that the fan acted as a blockage for air velocities of over 6m/s, which may explain the pressure drops observed beyond the air velocity of 6m/s. Objective 1.1.4 was, therefore, met.

6 Since the 35° case accelerated the airflow over a smaller area, the adverse effects of the blockage were more pronounced. While the 35°, 1m blockage case saw a heat rejection decrease of 2.7kW, this was brought down to 1.9kW when a fan was used. Like the 0.5m blockage case, heat rejection decreased from 4.7kW (no fan) to 1.9kW (with 13.6V fan). As determined in the literature review and industry research, similar angular configurations are most commonly used in automobiles. Hence, studying these effects is essential to characterise thermal heat rejection systems. Further CFD analysis would enable this hypothesis to develop further. Therefore, the effects of a combination of the configurations were studied, thereby adding to objective 1.1.5.

Therefore, this study quantified the heat performance for high-performance vehicles with different angular and non-uniform configurations. This was done by studying the effects of angles of incidence, blockages, fan, and combined configurations for the 90° and 35° cases, on high-performance (high coolant flow rate and air velocity) thermal heat rejection systems.

5.1 Future Work

Future work on the rig, addressed in objective 1.1.7, could include the following.

- Use of an auxiliary 15kW heater to control the temperature within the rig itself. This would negate the effects of the two distinct heating and cooling systems and allow better ambient temperature control.
- Improving air flow, possibly by building a closed loop wind tunnel which would allow for a more uniform airflow distribution over the working section/face of the radiator.
- Performing CFD analysis to get an idea of the turbulence intensity of airflow that would allow for studying the effects of turbulence intensity on blockages and understanding why certain setups yield higher heat rejection rates.
- Cross-sectional analysis, which would involve cutting the radiator in half and analysing the physical characteristics of the radiator, such as fin dimensions. This could help characterise certain heat rejection graphs.
- Testing and modelling the Low-Temperature Radiator, simulated Water- Charged Air Cooler (WCAC) circuit. Using the lumped capacitance model would also allow for considering the effects of thermal inertia
- For the 35° blockage cases, the effects of the fan and CFD performance of the blockage could be studied to understand why a radiator fan improved heat rejection in the 0.5m blockage case.

Therefore, a comprehensive overview of the High-Temperature Radiator system was undertaken, and heat rejection and airside dP were plotted. The Low-Temperature Radiator system was also modelled using the ε-NTU model. This provided a base for future testing, including considerations such as CFD analysis and better thermal and airflow control.

6 References

1. Will F, Boretti A. A new method to warm up lubricating oil to improve the fuel efficiency during cold start. SAE technical paper 2011-01-0318; 2011.
2. Samhaber C, Wimmer A, Loibner E. Modeling of engine warm-up with integration of vehicle and engine cycle simulation. SAE technical paper 2001-01-1697; 2001.
3. Roberts, A., Brooks, R. and Shipway, P., 2014. Internal combustion engine cold-start efficiency: A review of the problem, causes and potential solutions. Energy Conversion and Management, 82, pp.327-350.
4. Sanguesa, J., Torres-Sanz, V., Garrido, P., Martinez, F. and Marquez-Barja, J., 2021. A Review on Electric Vehicles: Technologies and Challenges. Smart Cities, 4(1), pp.372-404.
5. IEA (2010), "World Energy Outlook 2010", IEA, Paris https://www.iea.org/reports/world-energy-outlook-2010
6. Kim, K., Choi, K., Kim, Y., Lee, K. and Lee, K., 2010. Feasibility study on a novel cooling technique using a phase change material in an automotive engine. Energy, 35(1), pp.478-484.
7. Bhaskaran, R. and Collins, L., n.d. Introduction to CFD Basics. [online] Dragonfly.tam.cornell.edu. Available at: https://dragonfly.tam.cornell.edu/teaching/mae5230-cfd-intro-notes.pdf
8. Bahrami, M., n.d. Forced Convection Heat Transfer. [online] Sfu.ca. Available at: https://www.sfu.ca/~mbahrami/ENSC%20388/Notes/Forced%20Convection.pdf
9. Kanefsky, P., Nelson, V. and Ranger, M., 1999. A Systems Engineering Approach to Engine Cooling Design. SAE Technical Paper Series,.
10. Mehta, R., & Bradshaw, P. (1979). Design rules for small low speed wind tunnels. The Aeronautical Journal (1968), 83(827), 443-453.
11. Grc.nasa.gov. 2020. Closed Return Wind Tunnel. [online] Available at: <https://www.grc.nasa.gov/WWW/K-12/airplane/tuncret.html> [Accessed 1 April 2020].
12. Grc.nasa.gov. 2020. Open Return Wind Tunnel. [online] Available at: <https://www.grc.nasa.gov/WWW/K-12/airplane/tunoret.html> [Accessed 1 April 2020].
13. The European Parliament and of the Council, 2019. Regulation (EU) 2019/631 Of The European Parliament And Of The Council. Official Journal of the European Union.
14. Hu, X., Zheng, Y., Howey, D., Perez, H., Foley, A. and Pecht, M., 2020. Battery warm-up methodologies at subzero temperatures for automotive applications: Recent advances and perspectives. Progress in Energy and Combustion Science, 77, p.100806.
15. 2014. I12 Powertrain- Technical Training and Product Information. BMW Service.
16. 2020. Tesla Model 3 Teardown And Benchmarking Study. Munro Associates.
17. 2015. Toyota Mirai Dismantling Manual. Toyota Motor Corporation.
18. 2009. Toyota Prius Repair Manual. Toyota Motor Corporation.
19. 2012. Toyota Prius Repair Manual. Toyota Motor Corporation.
20. Zhang, G. & Kandlikar, S. G. (2011), A critical review of cooling techniques in proton exchange membrane fuel cell stacks. DOI: 10.1016/2011.11.010. Department of Mechanical Engineering, Rochester Institute of Technology. Published: November 2011.
21. Pischinger, M., Tomazic, D., Wittek, K., Esch, H., Köhler, E. and Baehr, M., 2012. A Low NVH Range-Extender Application with a Small V-2 Engine - Based on a New Vibration Compensation System. SAE Technical Paper Series,.

22. Pang, H. and Brace, C., 2004. Review of engine cooling technologies for modern engines. Proceedings of the Institution of Mechanical Engineers, Part D: Journal of Automobile Engineering, 218(11), pp.1209-1215.
23. Leighton, D., 2015. Combined Fluid Loop Thermal Management for Electric Drive Vehicle Range Improvement. SAE International Journal of Passenger Cars - Mechanical Systems, 8(2), pp.711-720.
24. US EPA. 2021. Dynamometer Drive Schedules | US EPA. [online] Available at: <https://www.epa.gov/vehicle-and-fuel-emissions-testing/dynamometer-drive-schedules>
25. Carroll, J., Alzorgan, M., Page, C. and Mayyas, A., 2016. Active Battery Thermal Management within Electric and Plug-In Hybrid Electric Vehicles. SAE Technical Paper Series,.
26. Gorman, J., Carideo, M., Sparrow, E. and Abraham, J., 2015. Heat transfer and pressure drop comparison of louver- and plain-finned heat exchangers where one fluid passes through flattened tubes. Case Studies in Thermal Engineering, 5, pp.122-126
27. Yangjun, Z., Minggao, O., Jianxi, L., Zhao, Z. and Yongjun, W., 2003. Mathematical Modeling of Vehicle Fuel Cell Power System Thermal Management. SAE Technical Paper Series,.
28. Stephens, B., Novoselac, A. and Siegel, J., 2010. The Effects of Filtration on Pressure Drop and Energy Consumption in Residential HVAC Systems (RP-1299). HVAC&R Research, 16(3), pp.273-294.
29. Węcel, D., Chmielniak, T. and Kotowicz, J., 2008. Experimental and numerical investigations of the averaging Pitot tube and analysis of installation effects on the flow coefficient. Flow Measurement and Instrumentation, 19(5), pp.301-306.
30. Boyes, W., 2011. Instrumentation Reference Book. Amsterdam: Butterworth-Heinemann/Elsevier.
31. Viquerat, A., 2006. A Continuous Wave Doppler Radar System For Collision Avoidance Applications. B.Eng. University of Sydney.
32. 2008. ISO 3966:2008 Measurement Of Fluid Flow In Closed Conduits - Velocity Area Method Using Pitot Static Tubes =. 2nd ed. Geneva: ISO.
33. Sattarzadeh, S., Kalpakli, A. and Örlü, R., 2013. Hot-Wire Calibration at Low Velocities: Revisiting the Vortex Shedding Method. Advances in Mechanical Engineering, 5, p.241726. Örlü
34. Nickels, T., Marusic, I., Hafez, S., Hutchins, N. and Chong, M., 2007. Some predictions of the attached eddy model for a high Reynolds number boundary layer. Philosophical Transactions of the Royal Society A: Mathematical, Physical and Engineering Sciences, 365(1852), pp.807-822.
35. Hutchins, N. and Marusic, I., 2007. Evidence of very long meandering features in the logarithmic region of turbulent boundary layers. Journal of Fluid Mechanics, 579, pp.1-28.
36. Russo, G., 2011. Aerodynamic Measurements From Physical Principles To Turnkey Instrumentation. 1st ed. Woodhead Publishing Limited.
37. Dept.aoe.vt.edu. n.d. HOT-WIRE AND HOT-FILM ANEMOMETRY. [online] Available at: <http://www.dept.aoe.vt.edu/~simpson/aoe4154/hotwirelab.pdf> [Accessed 1 March 2020].
38. Dehghan, M. and Kazemi, M., 2012. Analytical and Experimental Investigation About Heat Transfer of Hot-Wire Anemometry. An Overview of Heat Transfer Phenomena,.
39. Bhuiyan, A. and Islam, A., 2016. Thermal and hydraulic performance of finned-tube heat exchangers under different flow ranges: A review on modeling and experiment. International Journal of Heat and Mass Transfer, 101, pp.38-59.

40. Zhan, C., Duan, Z., Zhao, X., Smith, S., Jin, H. and Riffat, S., 2011. Comparative study of the performance of the M-cycle counter-flow and cross-flow heat exchangers for indirect evaporative cooling – Paving the path toward sustainable cooling of buildings. Energy, 36(12), pp.6790-6805.
41. Zhan, C., Zhao, X., Smith, S. and Riffat, S., 2011. Numerical study of a M-cycle cross-flow heat exchanger for indirect evaporative cooling. Building and Environment, 46(3), pp.657-668.
42. Tertipis, D. and Rogdakis, E., 2015. Maisotsenko cycle: technology overview and energy-saving potential in cooling systems. Energy and Emission Control Technologies, p.15.
43. Erbay, L., Doğan, B. and Öztürk, M., 2017. Comprehensive Study Of Heat Exchangers With Louvered Fins, IntechOpen.
44. Martin, H., 1996. A theoretical approach to predict the performance of chevron-type plate heat exchangers. Chemical Engineering and Processing: Process Intensification, 35(4), pp.301-310.
45. McNab, C., Atkinson, K., Heikal, M. and Taylor, N., 1998. Numerical Modelling Of Heat Transfer And Fluid Flow Over Herringbone Corrugated Fins, Proceedings For The International Heat Transfer Conference. Assembly for International Heat Transfer Conference, pp.119-124.
46. Bergman, T., Lavine, A. and Incropera, F., 2011. Fundamentals Of Heat And Mass Transfer. 7th ed. John Wiley & Sons.
47. Achaichia, A. and Cowell, T., 1988. Heat transfer and pressure drop characteristics of flat tube and louvered plate fin surfaces. Experimental Thermal and Fluid Science, 1(2), pp.147-157
48. Henriksson L., Dahl E., Gullberg P., Löfdahl L., CFD Method and Simulations on a Section of a Detailed Multi-Louvered Fin Where the Incoming Air is Directed at 90◦ and 30◦ Relative to the Compact Heat-Exchanger, SAE Paper 2013-01-2417, SAE Commercial Vehicle Engineering Congress, 2013.
49. Larsson L., Dahl E., Gullberg P., Contet A., Skåre T., Löfdahl L., CFD Simulation and Experimental Investigation of Pressure-Drop Through 90◦ and 30◦ Angled Compact Heat-Exchangers Relative to the Oncoming Airflow, VTMS11, 2013
50. Nuntaphan, A., Vithayasai, S., Kiatsiriroat, T. and Wang, C., 2007. Effect of inclination angle on free convection thermal performance of louvre finned heat exchanger. International Journal of Heat and Mass Transfer, 50(1-2), pp.361-366.
51. Sadeghianjahromi, A., Kheradmand, S. and Nemati, H., 2018. Developed correlations for heat transfer and flow friction characteristics of louvred finned tube heat exchangers. International Journal of Thermal Sciences, 129, pp.135-144.
52. Baker, C., Johnson, T., Flynn, D., Hemida, H., Quinn, A., Soper, D. and Sterling, M., 2019. Computational techniques. Train Aerodynamics, pp.53-71.
53. Webb, R. and Trauger, P., 1991. How structure in the louvred fin heat exchanger geometry. Experimental Thermal and Fluid Science, 4(2), pp.205-217.
54. Gifford, N., Savory, E. and Martinuzzi, R., 2007. Experimental Study of Automotive Cooling Fan Aerodynamics. SAE Technical Paper Series.
55. Baniasadi, E., Aydin, M., Dincer, I. and Naterer, G., 2013. Computational Aerodynamic Study of Automotive Cooling Fan in Blocked Conditions. Engineering Applications of Computational Fluid Mechanics, 7(1), pp.66-73.
56. Datta, S., Das, P. and Mukhopadhyay, S., 2014. Obstructed airflow through the condenser of an automotive air conditioner – Effects on the condenser and the overall performance of the system. Applied Thermal Engineering, 70(1), pp.925-934.

57. Subramaniyan, B. and Rajaraman, R., 2015. Numerical Investigation on Airflow Distribution of Automotive Radiator. International Review of Mechanical Engineering (IREME), 9(4), p.417.
58. Choi, Jong & Payne, Vance & Domanski, Piotr. (2003). Effects of Non-Uniform Refrigerant and Air Flow Distributions on Finned Tube Evaporator Performance.
59. Mao, J., Chen, H., Jia, H., Wang, Y. and Hu, H., 2013. Effect of air-side flow maldistribution on thermal–hydraulic performance of the multi-louvered fin and tube heat exchanger. International Journal of Thermal Sciences, 73, pp.46-57.
60. Kim, J., Kim, K., Ha, S. and Kim, M., 2016. Grille design for passenger car to improve aerodynamic and cooling performance using CFD technique. International Journal of Automotive Technology, 17(6), pp.967-976.
61. Incropera, F., 2006. Fundamentals Of Heat And Mass Transfer. 6th ed. New York: John Wiley & Sons.
62. Cengel, Y., 2003. Heat Transfer. 2nd ed. Boston: McGraw-Hill.
63. Shen, K., Zhang, Z., Zhang, Z. and Yang, Y., 2017. Investigation of effect on cross-flow heat exchanger with air flow non-uniformity under low Reynolds number. Advances in Mechanical Engineering, 9(7), p.168781401770808.
64. Gnielinski V. New equation for heat and mass transfer in turbulent pipe and channel flow. Int Chem Eng 1976; 16: 359–368.
65. Ezgi, C., 2017. Basic Design Methods of Heat Exchanger. IntechOpen.